Investigation of Low Frequency Electromagnetic Waves for Long-range Lightning Location

Liu, Zhongjian

Award date:
2017

Awarding institution:
University of Bath

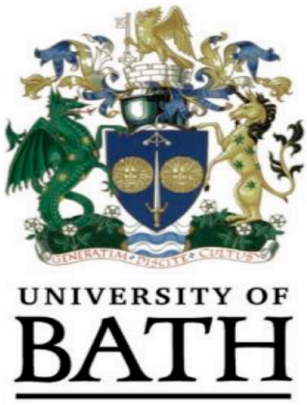

Investigation of Low Frequency Electromagnetic Waves for Long-range Lightning Location

By

Zhongjian Liu

BEng, MSc

This thesis is submitted for the degree of

Doctor of Philosophy

in

The Department of
Electronic and Electrical Engineering
University of Bath

September 2017

Signature:…… Date:……

Abstract

Lightning is the strongest natural electromagnetic radiation source, emitting electromagnetic energy in the frequency range from ~4 Hz to ~300 MHz or more. The location of lightning is calculated based on the received electromagnetic waves. The received electromagnetic waves, or lightning sferics, propagate from the lightning radiation source to the receiver along the ground path and reflections by the ionosphere named sky waves. Particularly for a long-baseline (>400 km) lightning receiver array, the received electromagnetic waves are usually a mixture of the ground wave and sky waves, which easily introduce a certain level of location uncertainty. Lightning sferics and the wave propagation velocity are analysed in order to mitigate the interference from long distance wave propagation. The complex lightning sferics are calculated by the Hilbert transform, which provides additional information regarding the instantaneous phase and frequency. The time differences calculated from the instantaneous phases are closer to the phase delay time introduced by the speed of light when compared to other possible signal processing methods. It is also found that the instantaneous frequencies at maximum amplitudes in the waveform bank are distance dependent, which has a potential application, i.e., to determine the distance between the lightning location and the receiver. The radio waves from two submarine communication transmitters at 20.9 kHz and 23.4 kHz exhibit phase propagation velocities that are ~0.51% slower and ~0.64% faster than the speed of light as a result of sky wave contributions and ground effects. Therefore, a novel technique with a variable phase propagation velocity is implemented for the first time using arrival time differences. The lightning locations inferred from variable velocities improve the accuracy of locations inferred from a fixed velocity by ~0.89–1.06 km when compared to the lightning locations reported by the UK MetOffice. The velocity map inferred from the calculated phase propagation velocities reflects the impact of sky waves and ground effects on the calculation of lightning locations as a result of the network configuration. Overall, the wave propagation issues are mitigated by analysis of the complex waveform and the variable phase propagation velocity. Finally, three interferometric methods, 2D lightning mapping, cross-correlation with a short time

window, and lightning locations inferred from each sample, are proposed here in order to take advantage of the greater number of samples and information from the recordings.

Acknowledgements

Firstly, I would like to express my sincere and deepest gratitude to my dear supervisor, Dr. Martin Fullekrug, for his invaluable encouragement, guidance and support throughout the duration of my research. He taught me the skills required for independent research and knowledge for my life. I am sincerely grateful to be a member of his research team, where I had an exciting and fascinating research time.

Secondly, I am indebted to the University of Bath, Chinese Scholarship Council and UK MetOffice, who jointly provide financial support for my research. I want to thank Dr. Dirk Klugmann and Dr. Ivan Astin for inspiration and encouragement toward this research project. I also wish to thank Dr. Serge Soula, Dr. Jean-Louis Pincon, Dr. Stephane Gaffet, and their teams for hosting the instruments for my research.

I would like to thank my previous colleague, Dr. Andrew Mezentsev, for sharing his knowledge and advice. I am also thankful to my dear colleague, Mr Kuang Liang Koh, for his assistance and all his wonderful discussions. Many thanks are due to Dr Nathan Smith, Dr. Jacqueline Sugier, and Dr. Sven-Erik Enno for their help and collaboration during my PhD.

I would like to express my sincere appreciation to my dear friends in Bath, including Dr. Maomao Zhang, Miss. Yihan Li, Dr. Bo Lian, Dr. Dongmin Yu, Mr. Da Huo, Mr. Minghao Xu, Dr. Huiming Zhang, Dr. Jiangning Gao, Dr. Zexin Chen, Dr. Andrew Moss, Dr. Neil Hindley, Dr. Corwin Wright, and Dr. Ran Li, for their support. Last but not least, I would like to take this opportunity to express my ultimate gratitude to my parents, and my thanks for understanding and supporting my career choice.

Contents

List of Figures

List of Acronyms

ABI	Advanced Baseline Imager
ATD	Arrival Time Differences
DE	Detection Efficiency
EOS	Earth Observing System
EUCLID	European Cooperation for Lightning Detection
FFT	Fast Fourier Transform
GLD360	Global Lightning Dataset
GLM	Geostationary Lightning Mapper
GOES	Geostationary Operational Environmental Satellite
HF	High Frequency (3–30 MHz)
IR	Impulse Response
ISS	International Space Station
LF	Low Frequency (30–300 kHz)
LINET	Lightning Detection NETwork
LIS	Lightning Imaging Sensor
LLP	Lightning Location and Protection, Inc.
LORAN	LOng RAnge Navigation
LMA	Lightning Mapping Array
MDF	Magnetic Direction Finding
MF	Medium Frequency (300–3000 kHz)

NASA	National Aeronautics and Space Administration
NLDN	National Lightning Detection Network
OTD	Optical Transient Detector
RMS	Root Mean Square
SAFIR	Surveillance et Alerte Foudre par Interférométrie Radioélectrique
SNR	Signal to Noise Ratio
TOGA	Time Of Group Arrival
TRMM	Tropical Rainfall Measuring Mission
VHF	Very High Frequency (30–300 MHz)
VLF	Very Low Frequency (3–30 kHz)
WWLLN	World Wide Lightning Location Network

Chapter 1 Introduction

1.1 Background

Lightning and thunder are common weather phenomena and have both been respected and feared by humans throughout history. It was present on earth before human life evolved, and it may have been crucial to the evolution of life on this planet. In 1752, Franklin's kite experiment demonstrated that clouds are electrically charged and that lightning is the discharge between the clouds and the ground. Lightning is the strongest natural source of electromagnetic radiation in the atmosphere. A number of techniques from spectroscopy to photography and many other new techniques are being used to further the understanding of these phenomena [*e.g. Schonland, 1964; Uman, 1971; Rakov and Uman, 2003*].

Lightning can be defined as a transient electric discharge in air with a high current. The whole length of lightning is observed to be a few kilometres. The whole lightning discharge channel is composed of plasma. Its peak temperature is typically 30,000 K, which is about five times higher than the temperature of the sun's surface. A 'lightning flash' is always determined as a lightning discharge whether it strikes the ground or not. The 'lightning strike' means the lightning that involves an object on the ground or in the atmosphere. The lightning is the transient electric discharge between the clouds or the ground in two forms: cloud-to-cloud lightning, and cloud-to-ground lightning [*Rakov and Uman, 2003*].

Cloud-to-cloud lightning has a discharge path between different parts of clouds. Inter-cloud lightning happens between two different clouds. Intra-cloud lightning happens between different regions of electric potential within one cloud. Over 50% of all lightning is intra-cloud lightning. The cloud-to-cloud lightning has less effect on human life, but is important in the atmosphere. The cloud-to-ground lightning always refers to a lightning stroke. Each stroke has the following process: a downward leader and an upward return

stroke, which has an extremely high voltage and current, and probably a relatively low level continuing current after the return stroke (Section 2.1). The continuing current is the most damaging part of lightning, because the continuing high current and heat may easily cause a forest or building fire. The stepped leader initiates the lightning. As a result, the cloud-to-cloud lightning is divided into four kinds depending on the property and direction of the stepped leader, as shown in Figure 1.1.

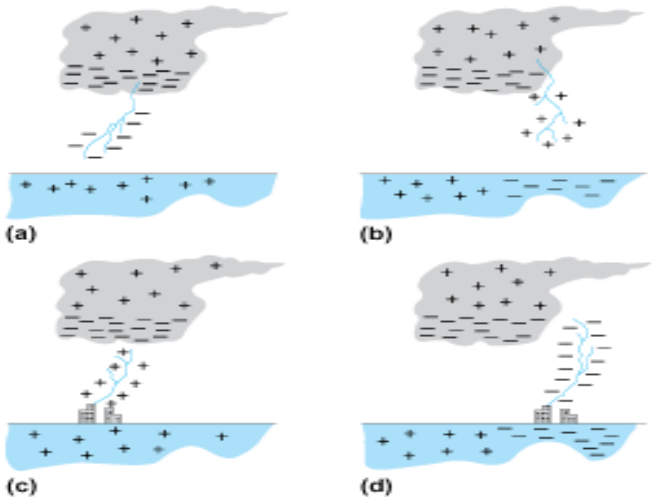

Figure 1.1 Categorization of cloud-to-ground lightning

Negative downward lightning (Figure.1.1, a) is the most common cloud-to-ground lightning, which accounts for over 90% of global cloud-to-ground lightning. A downward moving negatively charged leader initiates this type of lightning. The least common lightning is the negative upward lightning (Figure.1.1, d), which is initiated by an upward moving negatively charged leader. The discharge channel can be formed between the ground with the lowering of a positive cloud, or with a downward moving positively charged leader.

The transferred charge and peak current of positive lightning is stronger than normal negative lightning. Positive lightning normally has the highest current and largest electrical discharge. It mostly occurs during the cold season and in the dissipating stage of any thunderstorm. Ten percent or less of global cloud-to-ground lightning is the downward positive lightning flash (Figure.1.1, b). The upward positive lightning

(Figure.1.1, c) always occurs from tall buildings or mountain tops during a summer thunderstorm, which is initiated by an upward moving positive leader.

Natural weather phenomena tend to have both positive and negative effects. Lightning had a positive effect on human evolution by inspiring people to discover fire [*Rakov and Uman, 2003*]. The hot temperature and ionization around discharge channels produces chemicals including fixed nitrogen, which helps improve crop yields [*Fowler et al., 2013*]. As part of the global environmental balance, lightning maintains the electric field between the atmosphere and the ground of earth [*e.g. Noxon, 1976; Levine et al., 1984; Uman, 1974*]. One negative effect of lightning is the powerful destruction it can cause. It has caused death and injury to people and animals, and has also ignited forest fires. It leads to the strike of airplanes on average once a year, tall buildings and some sensitive electronic components in power systems and communication systems. Over 30% of all electric power line failures are lightning related [*e.g. Cooper, 1980, Rakov, 2013*]. It is a disaster if lightning strikes an unprotected object.

1.2 Aim and Objectives

In order to prevent lightning damage and to investigate more knowledge about lightning, the development of lightning location systems is crucial. Early detection of lightning discharges gives people an alert to protect assets from powerful lightning, because most thunderstorms generate many lightning strikes within a nearby area. Depending on the distance between lightning receivers, existing lightning location systems are divided into: short-baseline (<100 km), median–baseline (100–400 km), long-baseline (400–1000 km) and extreme-long-baseline (>1000 km). They operate at different frequency ranges, and lightning is located by analysing the electromagnetic waves received at different receivers. Received electromagnetic waves propagate from the lightning radiation source to the receiver. Wave propagation is complicated, and consists of the wave propagated along the ground path (ground wave), and the ionosphere reflected wave (sky wave). Especially for a long-baseline lightning receiver array, received electromagnetic waves are usually a mixture of ground waves and sky waves, which easily introduces a certain level of location uncertainty if they are treated as a pulse signal propagated in a vacuum. The term

'long-range lightning location' represents the lightning location inferred from a long-baseline lightning receiver array. As a result, the main aim of this research is to investigate the electromagnetic waves for mitigation of the interference from ground and sky waves, especially for long-baseline receiver arrays.

Two main interference sources associated with long distance electromagnetic wave propagation are the received lightning waveforms and the wave propagation velocity. The received lightning waveforms are variable due to attenuation, ground conductivity and the proportion of ground waves and sky waves. The average lightning waveforms at different distances are calculated to characterize the electromagnetic wave propagation (Chapter 5). The corresponding wave propagation velocity is also variable because of the frequency ranges, ground conductivity, and ionosphere conditions. Details of the wave propagation velocity are discussed in Chapter 6.

There are three popular methods commonly used in ground-based lightning location systems: Magnetic Direction Finding (MDF) [*e.g., Horner, 1954, 1957; Krider et al., 1976*], Arrival Time Differences (ATD) [*e.g., Lee, 1986; Fullekrug et al., 2000; Dowden et al., 2002*], and interferometry [*e.g., Mardiana et al., 1997; Mazur et al., 1997; Stock et al., 2010; Rison et al., 2016*] (Section 2.3). The application of these methods is driven by the development of novel technology. The MDF technique was upgraded to ATD as a supplementary by the availability of GPS timing [*Cummins et al., 1998*]. The interferometric method was recently developed for Very High Frequency (VHF) and Low Frequency (LF) near-field radio waves as a result of the advancement of digital processing technology [*e.g., Lyu et al., 2014; Stock et al., 2015*]. Most long-baseline lightning location systems use the ATD method. In order to achieve this main aim, an experimental long-baseline receiver array was deployed in Western Europe for this research (Chapter 3), and the ATD method was developed as the fundamental location calculation algorithm for this receiver array (Chapter 4). The benefit of developing the interferometry technique is to use more samples and information from the original recording rather than just using a time stamp for the calculation of time differences. As a result, an attempt is made to apply the interferometry method to this long-baseline lightning receiver array (Chapter 7).

1.3 Outline of Thesis

The chapters of this thesis are organised as below.

Chapter 2 introduces basic knowledge about lightning physics, and reviews the different methods of space-based and ground-based lightning location systems. A better understanding of lightning processes and lightning electromagnetic signatures provides an overview of the research objectives. Some of the described lightning location methods are used with the following experimental lightning receiver array through this thesis.

Chapter 3 describes the deployment of the experimental lightning receiver array and the recorded data. This long-baseline receiver array consists of four novel LF radio receivers separated by 400–500 km in Western Europe. High quality data is presented.

Chapter 4 explains the detailed steps of using the ATD algorithm in this experimental network. The application of ATD algorithms is reviewed. A detailed description of the whole methodology contributes to a better understanding of the research aim and lightning location systems.

Chapter 5 introduces the analysis of the instantaneous phase and frequency inferred from complex waveforms for the characterization of lightning sferics. A complex waveform bank and a spectral waveform bank have been produced from lightning sferics. Sub-sampling time accuracy has been achieved using the instantaneous phase of complex lightning waveforms. It is found that the inferred instantaneous frequencies at maximum amplitude are distance dependent. This work will be published in journal *Radio Science*.

Chapter 6 is the analysis of lightning electromagnetic wave propagation velocity. It is found that the phase propagation velocity can be slower or faster than the speed of light for two VLF transmissions. Therefore, a novel technique with a variable phase propagation velocity is implemented for the first time using the ATD method, and the result is improved by comparisons with locations reported by the UK MetOffice. The velocity map is produced over central France, based on the calculated phase propagation velocities, which reflects the impact of sky waves and ground effects on the calculation of

lightning locations as a result of the network configuration. This work has been published in journal *Radio Science* in 2016.

Chapter 7 presents the application of the interferometry technique in the long-baseline receiver array. Three methods, 2D lightning mapping, cross-correlation with a short time window, and lightning location for each sample, are proposed here in order to take advantage of the greater number of samples and information from the recordings.

Chapter 8 concludes this thesis with a summary of the contributions and suggestions regarding future investigation.

Chapter 2 Lightning and Lightning Location Systems

2.1 Lightning Physics

2.1.1 Lightning Processes

As described in chapter 1, lightning activities are classified into cloud-to-cloud lightning, and cloud-to-ground lightning. Most of the time, cloud-to-ground lightning causes more damage. In terms of transferring charge to the ground, several modes are proposed for lightning discharge. Here we discuss the physical processes of cloud-to-ground lightning events. A better understanding of lightning physical processes can contribute to more precise lightning location.

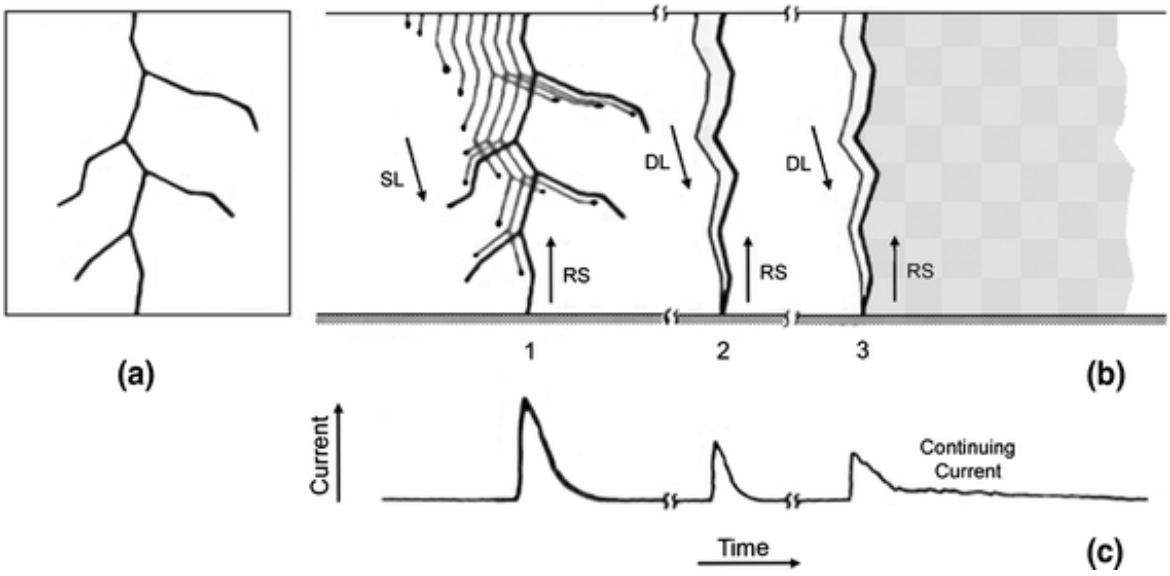

Figure 2.1 The luminosity of a three-stroke flash and corresponding current at the channel base. a. Still camera image; b. streak camera image; and c. channel base current. SL is stepped leader, DL is dart leader, and RS is return stroke. Taken from Rakov (2013).

As described in chapter 1, ninety percent or more of global cloud-to-ground lightning is negative downward lightning. This type of lightning effectively transports negative charge to the ground, as discussed here. Many negative flash contains 3–5 strokes, with 26 strokes being observed in extreme cases, but the flash multiplicity is ~2 stroke per flash. Half of these lightning discharges strike the ground at different points, kilometres apart. A sketch of the three-stoke case is drawn in Figure 2.1.

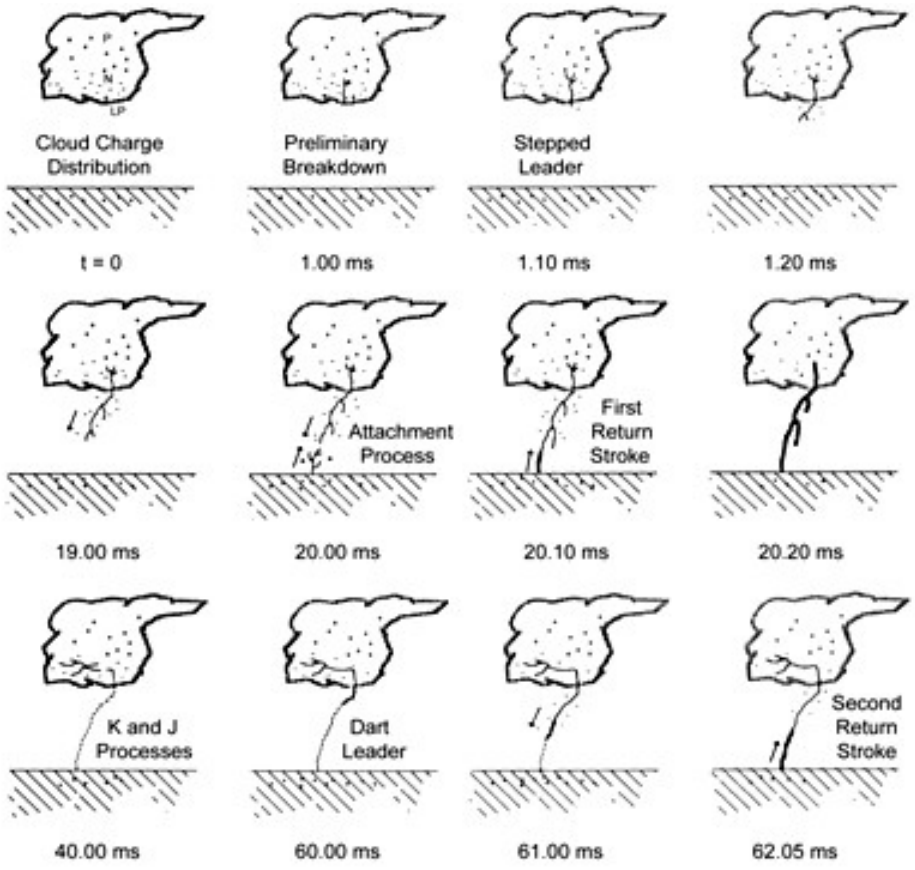

Figure 2.2 Drawing illustrating various processes of a two-stroke negative lightning flash. Taken from Rakov and Uman (2003).

In Figure 2.1, time advances from left to right, though the time scale is not continuous. These strokes are normally separated by tens of milliseconds. This figure is simplified with two major lightning processes: a downward-moving process, termed a leader, and an upward-moving process, termed a return stroke. The leader creates a conduction path and distributes negative charge from the cloud to the ground. The return stroke traverses the path from the ground to the cloud and neutralizes the negative charge of the leader.

Therefore, the leader and return stroke compose an effective negative charge transport from the cloud to the ground. As seen in Figure 2.1b, the leaders of different strokes are slightly different. The leader that initiates the first return stroke appears as an intermittent process, named a stepped leader, and then leaders of subsequent strokes follow the preconditioned path, named dart leaders. A drawing illustrating various processes is shown in Figure 2.2.

The detailed lightning processes of negative lightning are presented in detail in Figure 2.1 and Figure 2.2. As shown in Figure 2.3, dart-leader-return stoke sequences are an effective negative charge transport from the cloud to the ground. The lightning continuing current is normally tens to hundreds of amperes over hundreds of milliseconds. The continuing current can be understood as a quasi-stationary arc between the cloud and ground. Lightning M-components can be understood as the perturbations in the continuing current and its associated luminosity, appearing to be a superposition of two waves propagating in opposite directions. Overall, there are three possible modes of charge transfer in this type of lightning: dart-leader-return stroke sequences, continuing current, and M-components (Figure 2.3).

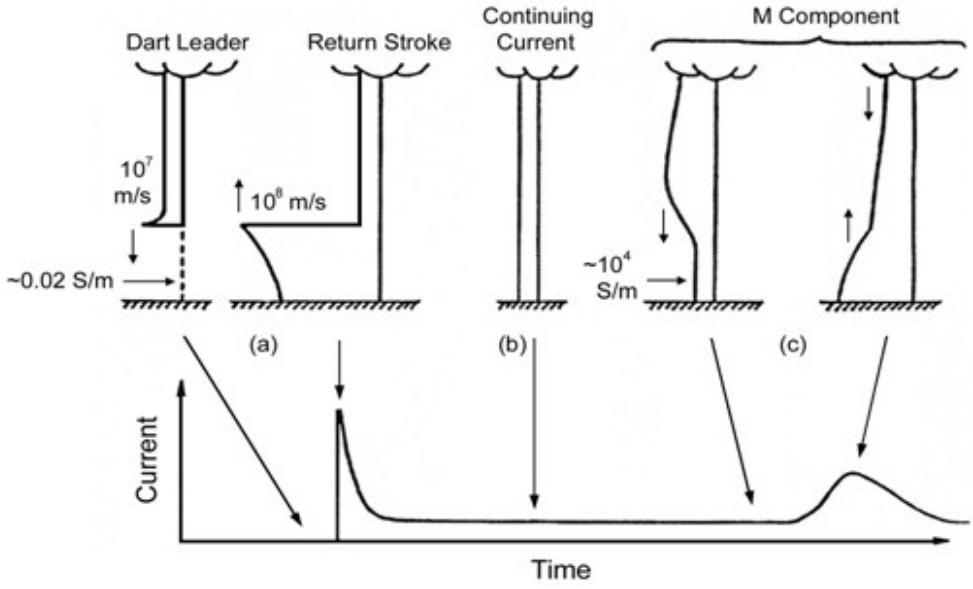

Figure 2.3 Schematic representation of lightning current and the three modes of charge transfer in negative lightning subsequent strokes. Taken from Rakov et al. (2001).

2.1.2 Lightning Electromagnetic Signature

Many processes of both cloud-to-cloud lightning and cloud-to-ground lightning produce electromagnetic signatures in the range from a few hertz (long continuing currents) to 10^{20} Hz (hard X-rays) [*Rakov, 2008*]. Cummer et al. *(2005, 2011)* observed that terrestrial gamma-ray flashes emit gamma ray emissions associated with lightning. The peak electromagnetic radiation from lightning is expected to be about 10 kHz, decreasing with increasing frequency [*e.g., Cummins and Murphy, 2009; Fullekrug et al., 2013*]. Most identifiable lightning radiation signatures are summarized in Table 2.1, as recorded at the ground [*Rakov, 1999*].

Different lightning processes produce electromagnetic signatures at different frequency ranges [*e.g., Nag et al., 2015*]. For example, energy with a wide range from Very Low Frequency (VLF), e.g. 3–30 kHz, to Medium Frequency (MF), e.g. 300–3000 kHz, are produced by lightning return strokes. This type of signal is normally propagated through ground and earth-ionosphere waveguides, and is captured by a ground-based lightning location system. Lightning signals at High Frequency (HF), e.g. 3–30 MHz, and Very High Frequency (VHF), e.g. 30–300 MHz, are normally produced by leader processes and cloud-to-cloud lightning. This frequency range can be used for short-baseline lightning location systems. The signal near the infrared/optical (30–3000 THz) can be observed by space-based lightning detection systems, which are produced by hot current-carrying channels. Lightning-produced electromagnetic signatures can thus be used for lightning location from space and at the ground over different frequency ranges.

Table 2.1 Characterization of wideband electric field pulses associated with various lightning processes

Type of pulses	Dominant polarity	Typical total pulse duration, μs	Time interval between pulses, μs	Comments
Return stroke in negative ground flashes	Positive	30–90 (zero-crossing time)	60×10^3	3–5 pulses per flash and ~2 in average

Stepped leader in negative ground flashes	Positive	1–2	15–25	Within 200 μs just prior to a return stroke
Dart-stepped leader in negative ground flashes	Positive	1–2	6–8	Within 200 μs just prior to a return stroke
Initial breakdown in negative ground flashes	Positive	20–40	70–130	milliseconds to some tens of milliseconds before the first return stroke
Initial breakdown in cloud flashes	Negative	50–80	600–800	The largest pulses in a flash
Regular pulse burst in both cloud and negative ground flashes	Both polarities are about equally probable	1–2	5–7	Occur later in a flash; 20–40 pulses per burst
Compact intracloud discharge (narrow bipolar event)	Both polarities occur with negative being more frequent	10–30	–	Typically not preceded or followed by any other lightning process within hundreds of milliseconds

Taken from Rakov *(1999)*.

2.2 Space-based Lightning Location

Lightning can not only damage instrumentation and the lives of humans and animals, but also poses a threat to the normal operation of spacecraft and aircraft. Lightning has caused accidents for the National Aeronautics and Space Administration (NASA). For instance, vital spacecraft electronics were knocked out by lightning which struck during the launch of the Apollo 12 mission in 1969 [*e.g. Finke, 2007*]. Many lightning forecast instruments in space have been developed by a number of research institutes (e.g. NASA) in order to avoid the negative impact of lightning. Figure 2.4 shows the scene observed by one of these instruments.

Figure 2.4 Image of lightning observed from above the clouds (red circle). Taken from Anderson (2011).

2.2.1 Lightning Investigation by High-altitude Instruments

The closer lightning is observed, the more detailed the data which can be obtained. Since lightning is normally unpredictable, scientists have developed methods to create lightning discharge under controlled conditions. Rockets, spacecraft and high-altitude airplanes are usually used as high-altitude instruments.

In order to investigate lightning from close-up, many researchers focus on the measurements in the cloud. In order to obtain more detailed data, a small sounding rocket is used, especially during lightning occurrence. The principle of a sounding rocket is similar to Franklin's kite. The key part of the kite is the electronic sensor, which can measure the electrical charge of the cloud in a thunderstorm. However, sounding rockets have been replaced by high-altitude airplanes with the development of technology that can overcome the effect of water droplets in the cloud, which affects the electrical measurement due to the water conductivity [*e.g. Christian, et al., 1998*].

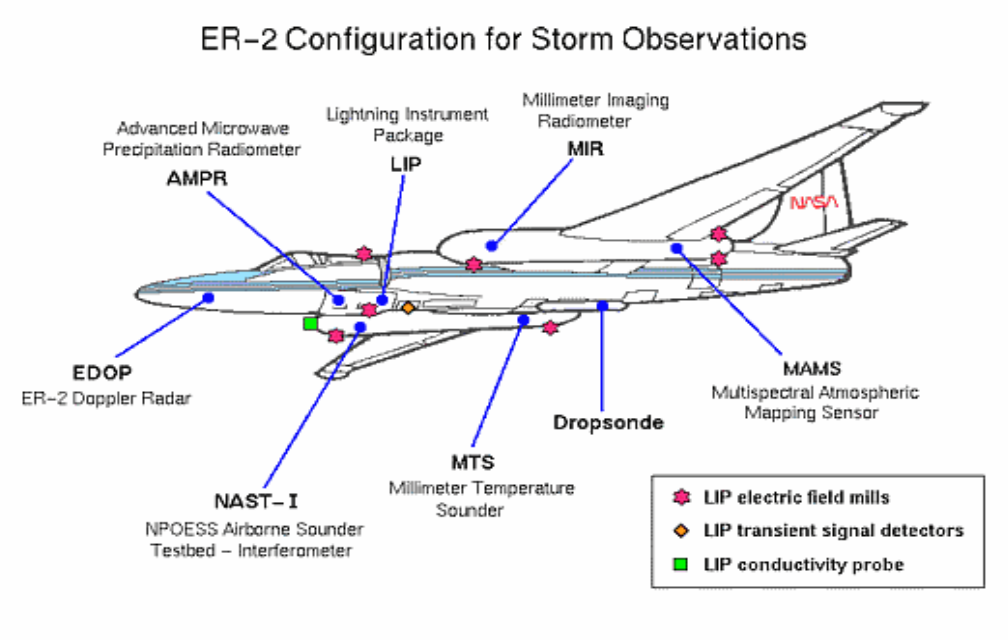

Figure 2.5 The configuration of ER-2. Taken from Christian and McCook (1998)

The ER-2 and U-2 high-altitude airplanes are two high-altitude plans that carry instruments to make optical measurements from space. High-altitude airplanes have promoted research into the optical and electrical features of lightning discharges in the cloud, proving a number of assumptive theories. Severe thunderstorms can be observed by the ER-2, shown in Figure 2.5, using multiple sensors, including visible spectrometers, lasers, microwave scanner, infrared and electric field antennas, which can obtain key data from the lightning.

2.2.2 Lightning Detection by Satellite

Observation by satellites can prove the development of science and technology. Satellite lightning observation uses optical sensors and high-speed cameras operating from low-earth orbit focusing on the top of the cloud. For example, Optical Transient Detector (OTD) was launched into low earth orbit on April 1995 on the Orbview-1 (formerly Microlab-1) spacecraft, and Lightning Imaging Sensor (LIS) is aboard NASA's Earth Observing System (EOS) Tropical Rainfall Measuring Mission (TRMM) satellite and International Space Station (ISS), which records the time of occurrence of a lightning event, measures the radiant energy and estimates the location. For another example, the

Geostationary Operational Environmental Satellite (GOES) system is a fundamental and huge environmental satellite network. GOES-1 was launched in 1974, and GOES-15 has already been developed. Monitoring and forecasting weather is the main function of this environmental satellite network [*Goodman, et al., 2013*]. The Geostationary Operational Environmental Satellite R-series (GOES-R) has been developed and launched following the existing GOES network.

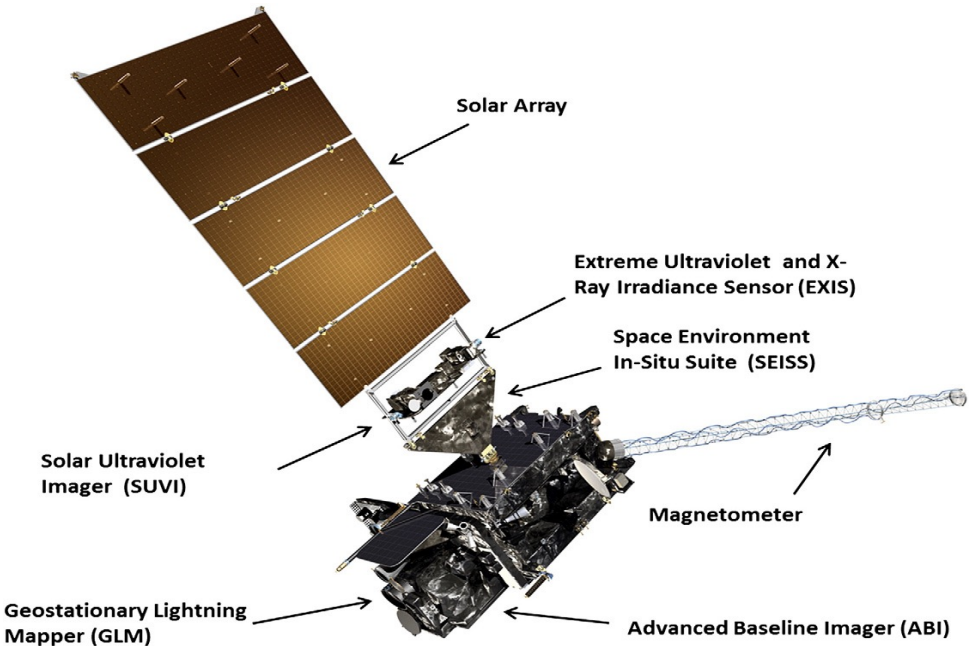

Figure 2.6 The GOES-R spacecraft and instruments. Taken from Goodman et al. (2013)

Figure 2.6 presents the 3-axis stabilized GOES-R spacecraft and instruments, which are composed of instruments, an auxiliary communication payload, and the launch vehicle and spacecraft bus. The Geostationary Lightning Mapper (GLM) and the 16-channel Advanced Baseline Imager (ABI) can promote the function of total lightning detection of GOES-R. The GLM is able to monitor and detect the activity of thunderstorms very well. GLM maps lightning activity continuously so that aircraft can be kept safe and efficient when crossing the clouds. Using ABI and other instruments, GOES-R is able to make the forecast and warning system for lightning more efficient and accurate.

2.3 Ground-based Lightning Location

Electric and magnetic field fluctuations can be generated by physical processes in cloud-to-ground lightning and cloud-to-cloud lightning. Lightning in the thunderstorm gives radiation with a significant electromagnetic wave (1 Hz–300 MHz). The frequency spectrum's peak value is ~5–10 kHz at the distance of about 50 km from the lightning. Lightning detection and location can use visible transient emissions, electromagnetic radiation, and acoustic signals from a lightning discharge. The first return stroke emits the largest current value of the electromagnetic wave. The flash magnitude and polarity can be detected over a long distance by analysing data from the first return stroke [*e.g. Rakov and Uman, 2003; Rakov, 2013*].

In the past, flash counters could be used to determine the density of lightning strikes. This method cannot work over a wide range or distinguish between different lightning types. Electromagnetic radiofrequency techniques which are useful for detecting lightning mainly include Magnetic Direction Finding (MDF), interferometry, and Arrival Time Differences (ATD). The most important information derived from these three techniques is the wavelength (λ) and frequency (f) of the radiation detected. The wavelength, as a crucial part of the lightning channel length, varies inversely with the frequency (f) [*e.g. Ibrahim and Ghazali, 2012*].

The detection efficiency can be influenced by seven factors: the distance between the thunderstorm and the network, the waveform strength, the unique features of the thunderstorm, the network configuration, sensor status, local sensor interference, and geography. The fact that many researchers contribute essential novel results in the field of lightning location indicates that the improvement of lightning location system accuracy and detection efficiency is an important and active research area [*e.g., Rodger et al., 2004; Said et al., 2010; Diendorfer et al., 2009; Mallick et al., 2014; Wang et al., 2016; Sun et al., 2016*].

2.3.1 Magnetic Direction Finding

The magnetic direction finding theory locates lightning by identifying the direction of the point of the strike. The electromagnetic fields are measured by the magnetic direction finding system from a lightning flash. Waves can be detected in the wideband MDF network in two vertical and orthogonal loops, which are used to detect the current induced by the radiated magnetic fields of lightning orientated to north-south and east-west. The strength of the magnetic field by the cosine of the angle between the loop and the direction from the lightning leads to the difference between the voltage signals measured using two loop antennas. As a result, the direction of the station can be determined by comparing and calculating the voltage difference between the two-loop antennas. Therefore, one lightning strike can be located using two MDF devices [*e.g. Sonnadara, et al., 2001*].

The return stroke of cloud-to-ground lightning leads to a dramatic rise in voltage after the stepped leader reaches the ground. This kind of lightning can be distinguished from other lightning by magnetic direction finding. It can be assumed that the electromagnetic fluctuation in the raw data of the MDF sensors within 25 ms is from the same lightning. Within 400 km, the system efficiency of MDF can reach up to 80% [*e.g. Sonnadara, et al., 1999*].

Three major errors of the MDF technique are: random errors, systematic errors, and site errors. The typical random error of this system is within 0.5° azimuthal angle. The systematic error is related to the environment of the antennas, and can be reduced by 2° azimuthal angle with comparison to prior data. The site error has an influence on the accurate angle from the loops, caused by huge conductive objects near the sensor. This site error can be estimated by determining a correction function for each MDF or by using redundant locations, and can be eliminated by determining the parameters of a sinusoidal correction function using a least squares analysis [*e.g. Ortega, 2007*].

Figure 2.7 Commercial MDF sensor used for the National Lightning Detection Network. Taken from Anderson (2011).

Figure 2.7 presents a commercial MDF used for the National Lightning Detection Network from the company Lightning Location and Protection, Inc. (LLP). Several errors in lightning detection are resolved by the MDF computers and network which are used for processing the data and errors. The MDFs from LLP were not used for the US National Lightning Detection Network until it was reorganized in 1989 [*e.g. Orville, 1991, 2008*].

2.3.2 Arrival Time Differences

The electromagnetic field signals of a given portion of the lightning arrive at separated sensors differently. The key to the ATD system is the time difference when sensing the arrival of the electric pulse at different stations. There are at least three stations in the ATD system. They are used to define intersecting hyperbolas that locate the lightning flash. The principle of the ATD technique using two receivers is shown in Figure 2.8. An ATD station consists of two antennas, with one receiving the electrical field produced by the lightning, and the other receiving the signal produced by geo-stationary satellites or a GPS system. Therefore, a station can not only generate information on lightning-generated electric fields but also provides the relative arrival time of peak amplitude [*e.g. Oetzel and Pierce, 1969; Dowden et al., 2002*]. The hyperbola of the possible stroke locations can be finalized by comparing the time that the peak values of the electric field arriving at two receivers.

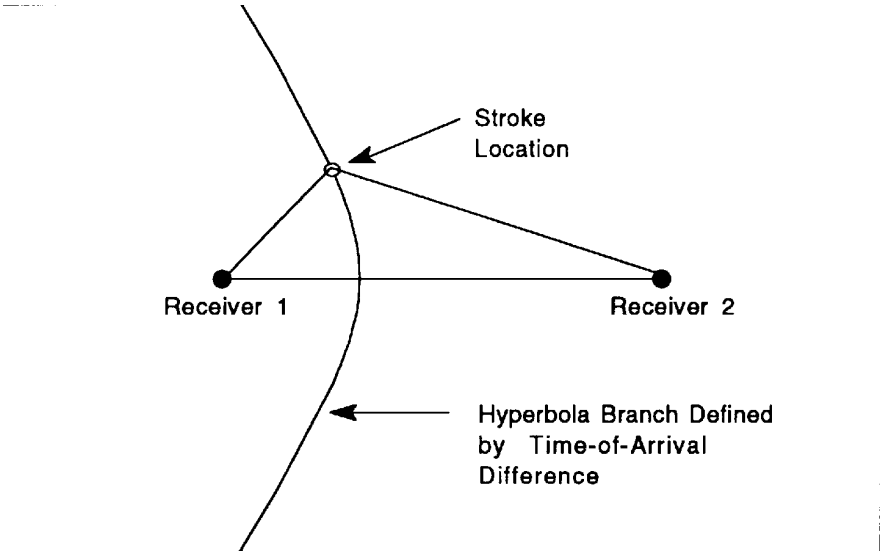

Figure 2.8 Detection of a lightning strike by two ATD receivers. Taken from Holle and Lopez (1993)

Since the lightning electromagnetic signature can be observed at different frequency ranges (see Section 2.1.2), the ATD system consists of three main types: very-short-baseline (tens to hundreds of metres), short-baseline (tens of kilometres), and long-baseline (hundreds to thousands of kilometres). The very-short-baseline and short-baseline always operate in the VHF and HF, normally in the ranges of about 30–300 MHz while the long-baseline systems always operate in VLF and LF, generally in the range of 3–300 kHz. The VHF radiation is associated with the process of air breakdown while the VLF signal is related to the current flow through existing lightning channels.

In the ATD system, there are two errors that affect the accuracy of lightning detection: propagation error and synchronization error. The propagation error is due to signal deformation, which means the signal propagating from the strike point to the antennas may be deformed. Since the ground conductivity is different during wave propagation, it is difficult to correct this error. There may be a few microseconds of error over propagation of tens of kilometres or a few hundreds of kilometres, depending on the difference in ground conductivity. The other error is synchronization error. The ATD system receives the signal produced by a GPS system or geo-stationary satellites almost at the same time. The synchronization error means that there may be error in the clock signals to the order of 2 μs due to the movements of the telecommunication satellites [*e.g. Chen and Du, 2011*].

The ATD technique has been used most widely for lightning detection systems in recent years. Some of these systems will be discussed in Section 2.3.4. The long- baseline ATD technique is also the fundamental algorithm for this PhD.

2.3.3 Interferometry

Due to the fact that lightning also emits noise-like bursts of electromagnetic radiation which last 10–100 μs, it is difficult for the ATD technique to identify the different individual pulses in some circumstances. Since the interferometer gives measurements of the phase difference between the noise-like bursts corresponding to narrowband signals, identification of the individual pulses can be avoided. There are at least two antennas several metres apart as the simplest interferometers, connected to a narrowband filter. After outputs from the two receivers are received, the phase detector generates the phase difference in proportional voltage. The ATD detectors determine the location of the flash by comparing the time difference, while the interferometers determine the direction to the VHF source by comparing the phase difference. At least three receiving antennas and two orthogonal baselines are needed to detect the source's azimuth and elevation. Two or more synchronized interferometers separated by more than 10 km are needed to locate the source in three dimensions, and each of them act as a direction finder (Figure 2.9).

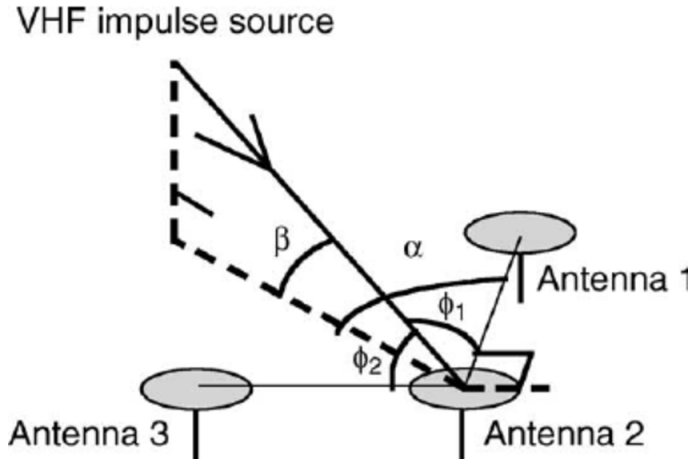

Figure 2.9 VHF impulse source location in three-dimensions by an interferometer site. Taken from Morimoto et al. (2005)

Narrow-band interferometers show significant achievement in explaining the progression of cloud-to-cloud and cloud-to-ground lightning, and imaging the lightning channel in two dimensions [*Maridiana et al., 2002*]. By making two or more synchronized interferometers 10 km apart, the lightning source can be located in three dimensions. The SAFIR (Surveillance et Alerte Foudre par Interférométrie Radioélectrique), as a commercial lightning interferometer system, is used for locating lightning radiation sources in three dimensions. The SAFIR, working as a VHF direction finder, normally has three stations 10–100 km apart [*e.g. Richard et al., 1986, 1988*].

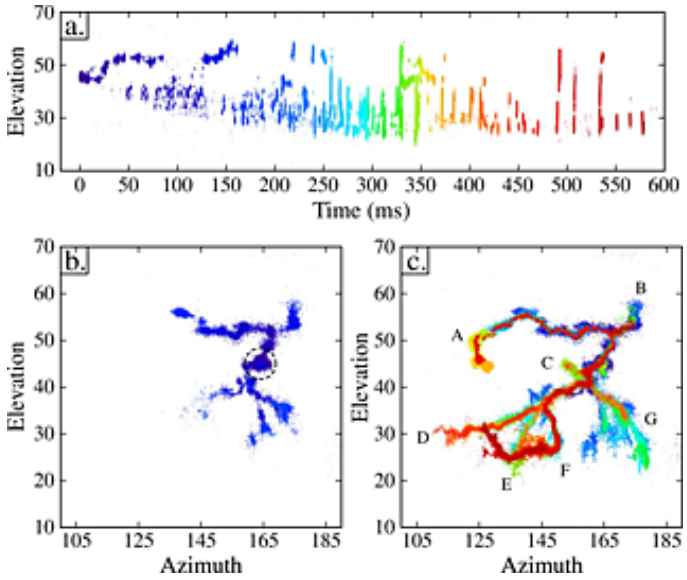

Figure 2.10 The interferometry observations of a bilevel intra-cloud flash 8–10 km distant from the interferometer site. (a) Elevation angle versus time, (b) azimuth versus elevation angle during the first 200 ms, (c) azimuth versus elevation angle for entire flash. Taken from Stock et al.(2014)

As a result of the advancement of digital processing technology and affordable electronics, more research towards using broadband interferometry using LF signals have been developed [*e.g. Akita et al., 2011; Sun et al., 2013; Stock, et al., 2014*]. 50000–80000 radiation sources are located for a typical lightning flash by the VHF broadband digital interferometer developed by Osaka University [*Stock, et al., 2014*]. The measurements from 20–80 MHz provide angular uncertainty less than 1° and time resolution better than 1 μs using a generalized cross-correlation algorithm. The

interferometer observations are combined with a 3D Lightning Mapping Array (LMA) to produce a quasi 3D map of lightning activity.

Mazur et al. *(1997)* compared the output result from a VHF ATD system and a VHF interferometry system, indicating that the result of the interferometry system seems to be discrete while that of the ATD system looks continuous during the lightning. The ATD system is good at dealing with impulsive radiation, while the interferometer system does well in locating long-duration noise-like radiation bursts. Since the observation of these two location systems covers different aspects of lightning discharge, the two techniques can be combined together when used in lightning research. Lyu et al. (*2014*) attempted to apply the interferometric cross-correlation technique combined with the ATD technique to an LF near-field array. This array of five stations can detect the signal from stepped and dart leaders and intra-cloud lightning. This result illustrates that the electromagnetic signatures from weak lightning processes can be detected in LF. It also proves the possibility of applying the combination of ATD and interferometry to a VLF lightning location system. This innovative method is the final aim of this thesis.

2.3.4 Examples of Lightning Location Systems

Due to the damage caused by lightning events, all continents and most of the oceans are covered by multiple lightning location systems. Some of them are operated by governmental meteorological institutes, and some of them are run by commercial companies. According to the different service aims, these systems are operated with different baseline and different frequency ranges. As discussed in Section 2.1.2, the network baseline decreases with a higher operation frequency range, but is more sensitive to the weak pulses. Some typical lightning location systems are briefly reviewed below.

The World Wide Lightning Location Network (WWLLN) and Global Lightning Dataset (GLD360) are two well-known ground-based global VLF lightning location systems (Figure 2.11). The WWLLN has employed 57 sensors (6–18 kHz) on all continents since March 2012, each thousands kilometres apart [*e.g. Rodger et al., 2004, 2005*], named the extreme-long-baseline network. The Time Of Group Arrival method (TOGA) is used so that 10 sensors can cover lightning location globally [*Dowden et al., 2002*]. The cloud-to-

ground lightning Detection Efficiency (DE) increased from 3.88% in 2006–2007 to 10.3% in 2008–2009, and 35% of lightning events stronger than 130 kA throughout the contiguous United States, with respect to the lightning location as reported by the National Lightning Detection Network (NLDN) [*e.g. Abarca et al., 2010; Hutchins et al., 2012a*]. GLD360 uses both ATD and MDF techniques in conjunction with a lightning waveform recognition algorithm [*e.g. Said et al., 2010*]. The cloud-to-ground lightning DE was 86–92% with a median location error of 10.8 km with reference to NLDN data [*Demetriades et al., 2010*], but the DE was 16% and mean location error was 12.5 km when compared to data from the Brazilian lightning detection network [*Naccarato et al., 2010*]. It illuminates that the disadvantage of a global lightning location system is the difficulty in covering all the weak lightning events.

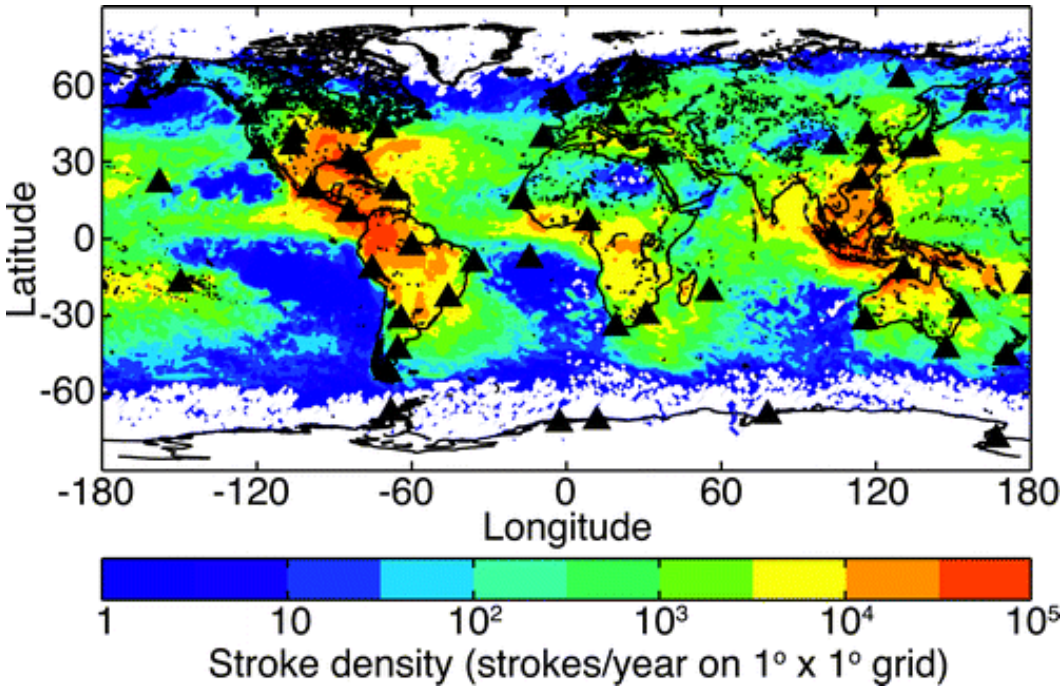

Figure 2.11 The annual global stroke density based on the WWLLN continuous monitoring. Taken from Hutchins et al. (2012b)

A short-baseline lightning location network can locate nearby lightning very precisely in three dimensions. One of the most typical short-baseline lightning location systems is the LMA, which can locate pulses from different lightning processes. The New Mexico LMA network consists of 10–15 sensors separated by 15–20 km, which receive electromagnetic

waves at 60–66 MHz [*Rison et al., 1999; Thomas et al., 2004*]. The network has been validated using a sounding balloon carrying a VHF transmitter as a known lightning simulator. The location error is less than 100 m for 3D lightning location. As a result, most networks are compared with the LMA result as the 'ground truth' [*e.g. Enno et al., 2016*].

The medium (<400 km) and long (>400 km) baseline lightning location systems consist of sensors separated by hundreds of kilometres. This kind of network is most common in VLF/LF for a country or a continent, such as NLDN, Lightning Detection NETwork (LINET), European Cooperation for Lightning Detection (EUCLID), UK MetOffice ATDnet. Few exceptional median baseline networks can service globally but with many sensors, such as, Earth Networks Total Lightning Network (ENTLN) that consist of over 1200 broadband sensors [*e.g. Mallick et al., 2013; Zhu et al., 2016*]. NLDN is one of the earliest digital lightning location systems, which consist of more than 100 stations separated by 300–350 km and covering the whole US [*e.g. Rakov and Uman, 2003; Orville, 2008; Cummins and Murphy, 2009*]. The MDF technique was employed at the beginning, and the ATD technique was combined later. Both cloud-to-cloud lightning and cloud-to-ground lightning can be located with high detection efficiency and location accuracy. The peak current of NLDN has been referenced to directly measure current at the triggered lightning channel base [*Nag et al., 2011*]. LINET employs ATD as the basic location method, and the MDF provides arrival-angle information for plausibility checking. Height information is calculated from the arrival time at the nearest reporting sensor, so that cloud-to-cloud lightning and cloud-to-ground lightning can be distinguished [*e.g. Betz et al., 2009*].

In summary, the MDF method has completely updated or replaced by ATD technique due to its large location error. The ATD technique is widely used in lightning location systems with different baseline because of the high GPS resolution. The results from different lightning location systems proves that network with smaller baseline has a higher detection efficiency and higher location accuracy, but covers smaller area with consistent receiver number. In order to balance these effects, a medium and long baseline lightning location system is proposed in this thesis. One of the most challenging aspects to improve performance in a long-baseline lightning location system is wave propagation.

The received electromagnetic waves are propagated through the ionosphere reflection for extreme-long-baseline networks, as the waves propagated along the ground, i.e. ground waves, are normally attenuated over such a long distance. The waves received from a closed short/medium baseline network are mainly ground waves, because the ionosphere reflected waves, i.e. sky waves, arrive with a long time delay, while the electromagnetic waves received from a long-baseline network are a mixture of both propagation modes. The detailed analysis of the receiving lightning waveform and wave propagation in a long-baseline lightning location system is discussed in Chapters 5 and 6. The interferometry technique has strong application for short baseline lightning location system, which reports accurate 3D lightning pulses from near field recording. The detailed proposal about the methods to apply interferometry technique in long baseline lightning location system is discussed in Chapter 7.

2.4 Lightning Protection

Lightning causes death and injury to people and animals, ignites forest fires, and also has led to the destruction of airplanes, tall buildings and some sensitive electronic components in power and communication systems. The amount and type of lightning damage depends on the properties of the lightning discharge and characteristics of the object. The main properties of lightning associated with producing damage are the current waveform and the radio frequency electromagnetic fields, which can be analyzed from the data recorded [*e.g. Rakov and Uman, 2003*].

The lightning current waveform has four significant characteristics that are important to producing damage: the peak current, the maximum rate of change of the current, the cumulative current, and the action integral. The peak current presents essential resistive impedance in certain circumstances. The maximum rate of change of the current represents the essential inductive impedance under some conditions. The cumulative current is the sum of the current over time, and always refers to the charge transfer. The action integral means the integral of the current square over time.

The electromagnetic field from the lightning is also evidence of lightning damage, because it has a connection to the lightning current and voltage. The two significant

properties of the electromagnetic field that are always associated with the destruction of electronic components are the peak values of the electric and magnetic field, and the maximum of change of these fields. These two values are very easy to detected using a lightning detection system, which can give the relative power of each lightning strike. The absolute energy of the lightning can be deduced by reference to a measured value from triggered lightning.

Lightning protection design is always divided into two aspects. The first area is diversion and shielding. This protects the structure and reduces the magnetic and electric field induced within the structure. The lightning current is diverted to the connected vertical lightning rods or down conductors to the ground terminal. The second aspect is the effect of currents and voltages on communication, electronic and power systems, which are mainly protected through surge protection. Some techniques and devices are used to minimize the damage caused by peak values: voltage crowbar devices, voltage clamps, circuit filters and isolating devices. Protection designs have been developed thoroughly in recent years.

Lightning detection for lightning protection is the application of this research. The early streamer emission system is based on the detection result, which launches an upward connecting leader early to avoid a direct connection between lightning and protected items. For some sensitive electronic devices, the temporary turnoff is an urgent method after it is known that there are some thunderstorms that will threaten the devices. The statistics of lightning detection can provide annual and monthly lightning distribution prediction, which can at least help to set the lightning protection standard. If the lightning detection system reports extremely hazardous thunderstorms, emergency evacuation will also be an alternative lightning protection plan.

Chapter 3 Instrument and Experiments

3.1 LF Radio Receiver

The newly developed wideband digital low-frequency radio receivers will be used for this PhD project. This kind of radio receiver can record the electrical field between 1 m altitude and the ground, as shown in Figure 3.1. It can record the electromagnetic wave over a large frequency range from ~4 Hz to ~400 kHz per microsecond. The highest time resolution achievable is ~12 ns by the GPS clock, and the amplitude resolution is ~ 35 μV. The device is powered by a battery, which can avoid the 50 Hz noise caused by AC power [*Fullekrug, 2010*]. This radio receiver was originally designed for sprite and lightning research [*e.g., Fullekrug et al., 2006; Fullekrug et al. 2014; Mezentsev et al., 2013; Soula et al., 2014*]. The high timing accuracy enables the array to locate lightning sources and to study the recorded radio signals with high temporal resolution.

Figure 3.1 The research device: the low-frequency radio receiver. Taken from Fullekrug (2010)

This instrument is made up of a data acquisition unit, a precise clock for timing the data acquisition, a vertical electric field sensor, an analogue signal conditioning circuit, a mass storage medium and a data processing unit. The radio receivers can be upgraded for

specific purposes. For example, the receivers can be developed into an interferometry network to map the low-frequency radio sky by synchronizing individual instruments.

A radio frequency survey is always conducted at the possible location before the instruments are fixed permanently. The radio frequency survey is a preliminary experimental test to detect the radio environment, which is focussed on nearby transmitters and power transmission lines to avoid their effects. The data recorded in the feasible location can be read the first time to determine the quality of the data. The location also needs to be considered in light of four aspects: people, animals, nearby power lines, and nearby transmitters. This is because human activity, animal activity or some transmitters affect the quality of electromagnetic wave detection.

The principle of recording data from this novel radio receiver is the same irrespective whether it is used permanently, or temporarily as part of the radio frequency survey. The sensor measures the electrical field over one meter measured between the flat plane antenna and the ground. The antenna is connected to the amplifier to make the data large enough to be visible. Then the data is transmitted to the computer through the data acquisition instrument, which can transfer the data and also combine the time signal from the GPS clock. The whole process is shown in Figure 3.2.

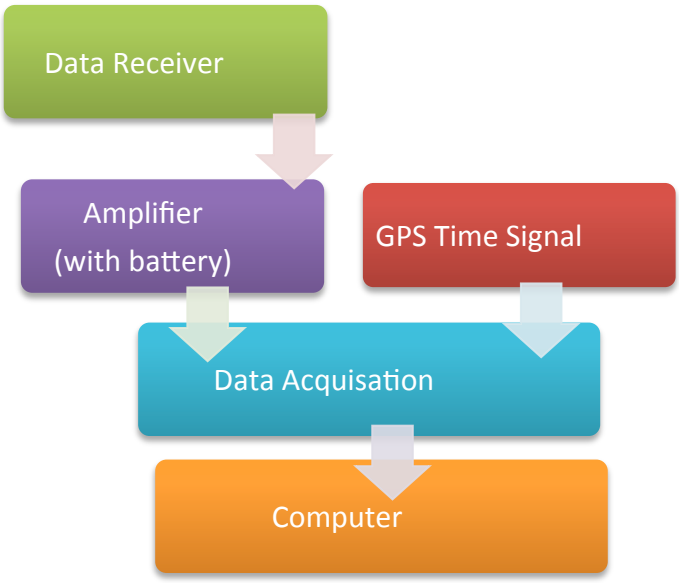

Figure 3.2 The processes of recording data.

The software used for the radio frequency survey is LabVIEW (Laboratory Virtual Instrumentation Engineering Workbench) from National Instruments, which can read the binary data in C language. The advantage of using this software in a radio frequency survey is that the measurement can be read whilst recording. The software used for the analysis of the lightning data afterwards is Matlab, which has the advantage of large size data processing.

3.2 Experimental Lightning Receiver Array Deployment

The purpose of this PhD project is to improve the performance of the long baseline lightning network. According to the cooperation with UK MetOffice ATDnet, the baseline of the experimental lightning receiver array is designed to be 400–500 km. The sensors of the network are required to be homogeneously distributed in order to locate lightning precisely. The sensitivity of the network is low, if the sensors are linearly deployed (Figure 3.3). The sensitivity map is calculated from the average of the arrival time change if the source location shifts 1° to north, south, east and west direction (latitude and longitude). In theory, the arrival time varies more for a 1° source shift if the sensitivity of the network is higher.

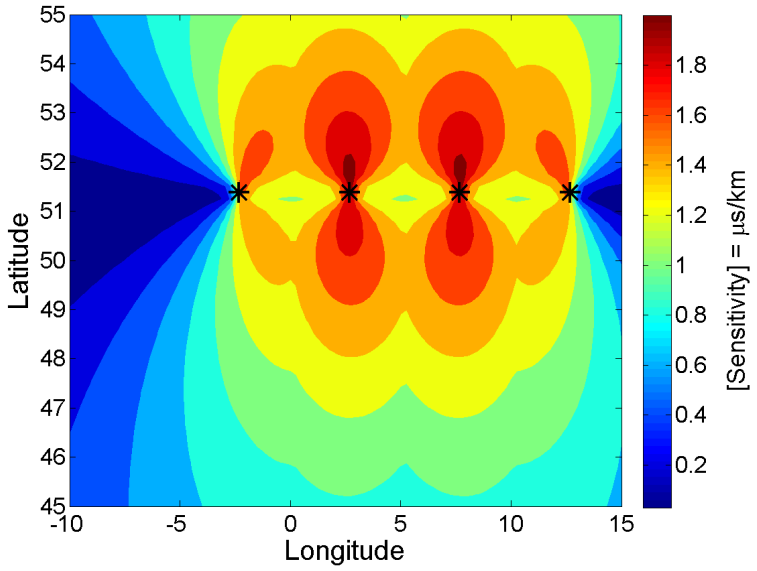

Figure 3.3 The sensitivity map of a four-station linear distributed network with resolution of 20 km.

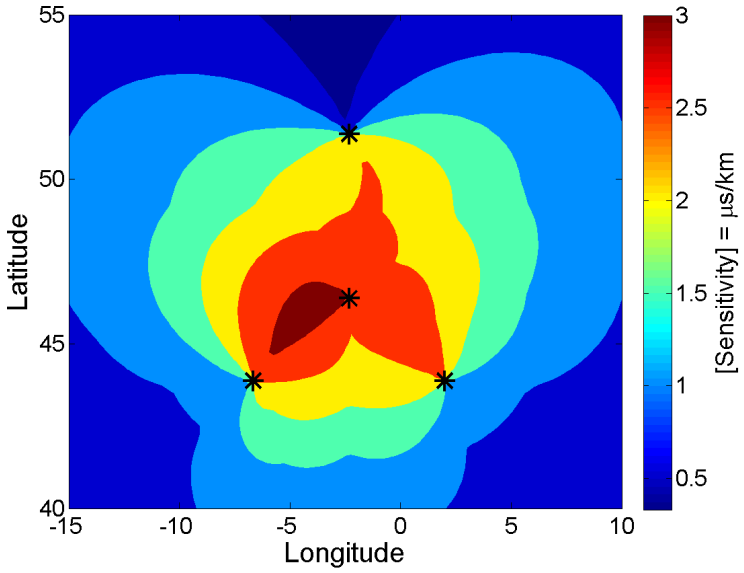

Figure 3.4 The sensitivity map of a four-station star distributed network with resolution of 20 km.

By comparing different network geometry with 4 sensors, such as, linear, square and star, it is found that the network sensitivity is much higher with a star geometry (Figure 3.4). The unsymmetrical sensitivity of this map may due to the different distances for the same latitude difference in different directions. With the practical consideration, such as, the availability of places to site the equipment, the four radio receivers used in this project are located in Bath (UK), Orleans (France), Lannemezan (France) and Rustrel (France). The map of the network is shown in Figure 3.5, where the yellow points are the device locations. The processing centre is the computer at the University of Bath, which receives the data from four stations each hour automatically. The low frequency electromagnetic waveform data from different sites can be analysed in different aspects for different purposes. In this thesis, the data from the different radio receivers can be compared to find the time differences and phase differences, which, by using the ATD technique and interferometry technique, can be used to locate lightning. This reliable device is thus popular in the atmospheric research area, and the sensors of the network may be increased in future. There are two more future stations that will be introduced into this network, which have already been installed at the red points on the map.

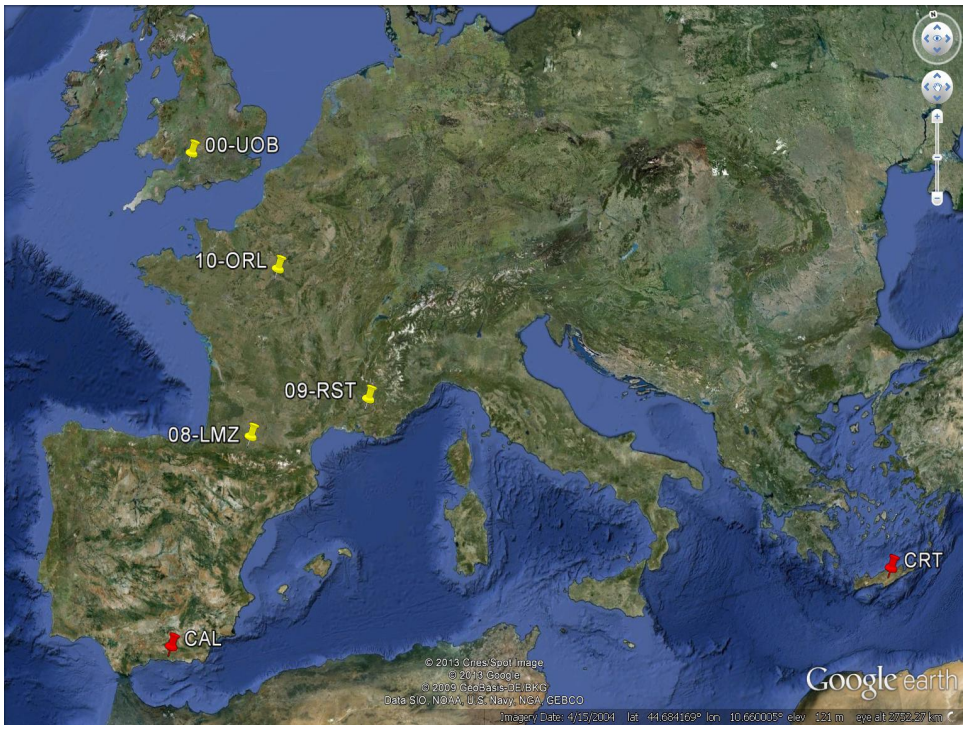

Figure 3.5 The network of radio receivers for sprite and lightning detection.

The sensitivity of the receiver network was tested to ensure the best experimental area (Figure 3.6). It illustrates that lightning events occurring in France can be located more accurately with the same level of time accuracy. As a result, most of the analysis in this PhD is based on data collected when thunderstorms occurred in France. In ideal circumstances, the sensitivity map can be transferred to a resolution map with known time accuracy. In this instance, the highest theoretical time resolution is ~12 ns, so that the best theoretical location resolution for this network is 4 m, i.e. $12\ ns/3\ (\mu s/km)$. However, the time resolution cannot achieve ~12 ns in most cases. The theoretical location resolution would be expected to be <400m, considering an error even 100 times larger.

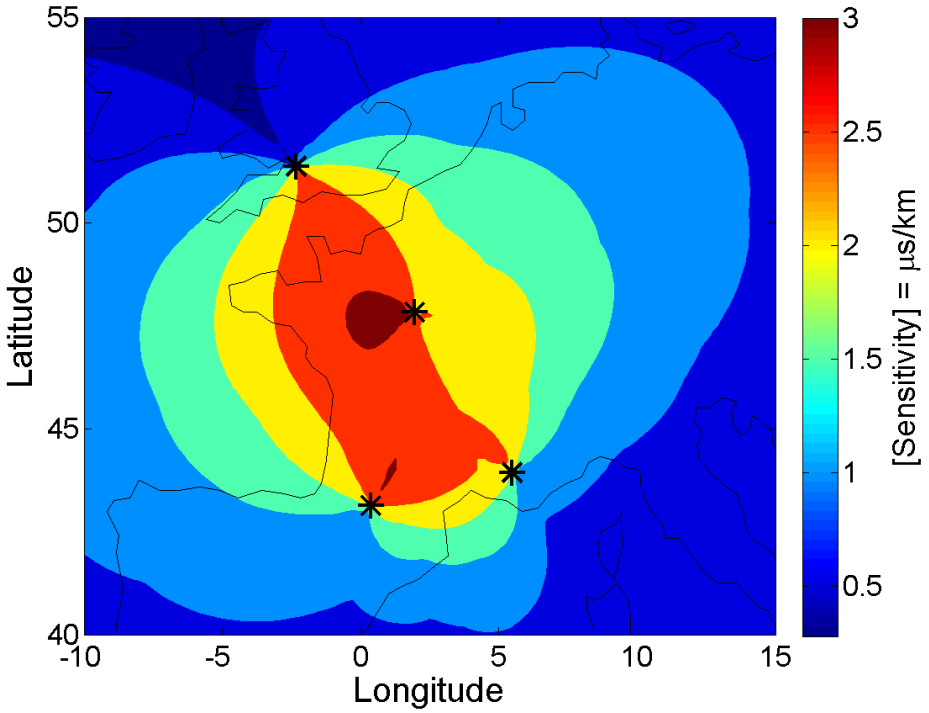

Figure 3.6 The sensitivity of the network deployment. France is the most sensitive area for this experimental lightning receiver array.

3.3 Recording and Simple Data Processing

A signal is a kind of physical phenomenon or information transmission function. Analogue signals and digital signals are the two expression functions of a signal. An analogue signal is a signal that has continuous time and amplitude. A digital signal is a signal that has discrete time and amplitude. A digital signal can be converted to the binary system, which is suitable for computer processing. In order to record the continuous analogue signals existing in the real world, digital signal processing is used to convert the signal into the digital domain by the novel radio receiver.

Two seconds of raw data with sampling frequency at 1 MHz as recorded by the radio receiver is shown in Figure 3.7. Each pulse represents one lightning event. More than 20 events can be easily observed during this two second period. More than one events initiate transient luminous phenomena in the middle and upper atmosphere, such as sprite. The observed sprite was triggered by a strong positive lightning event. According to the

observation, the lightning signal always has a large amplitude but for no longer than half a millisecond. Conversely, a sprite (1.002~1.004s) has a smaller amplitude but lasts for a few milliseconds. These characteristics can be observed directly from the data, and more information is extracted by more signal processing strategies.

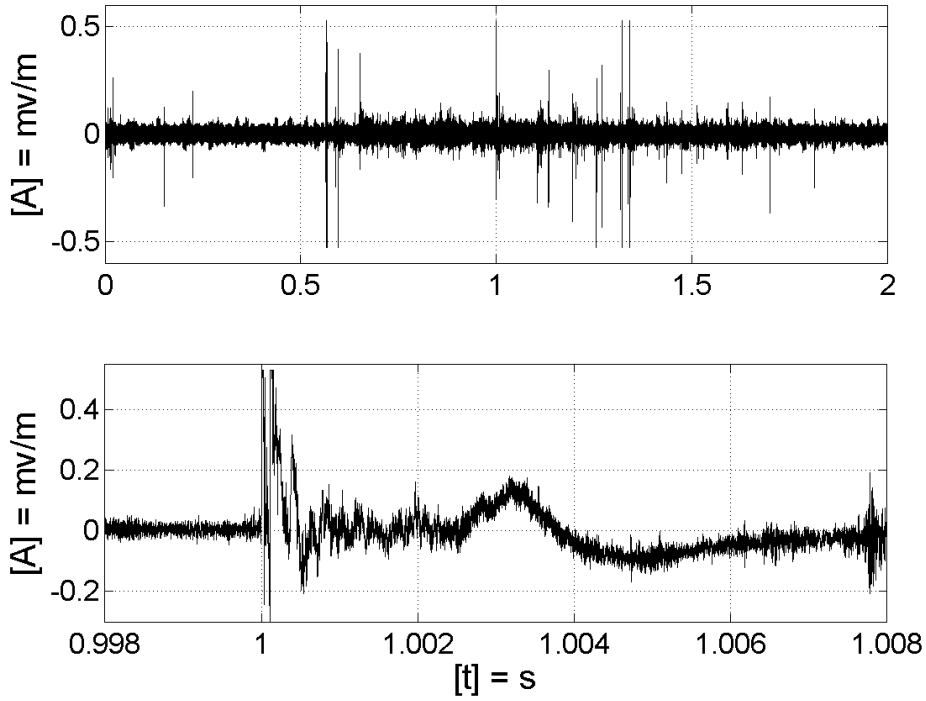

Figure 3.7 A 2-seconds raw data recorded by the LF radio receivers, including a sprite (~1.003s) triggered by a positive lightning (~1s).

3.3.1 Filtered Data

The instrument used in this project can receive electromagnetic waves from 4 Hz to 400 kHz. Most energy from lightning discharge is distributed in the 5–15 kHz range [*e.g. Fullekrug, 2013b*]. In order to extract the selected information from the raw data, a box filter can be applied over a certain frequency range to produce filtered data. The basic principle of the filter strategy is applying a Fast Fourier Transform (FFT), firstly to transfer the data into frequency domain, and then to set the data outside the selected frequency range to be zero while the data within the selected frequency range remains unaltered. The final result in the time domain is subsequently calculated by an Inverse Fourier Transform.

A frequency filter applied to the data between 5–15 kHz excludes the noise from other radio sources (Figure 3.8, top). More weak lightning events can then be observed. The intensity of lightning discharges differs, and the emitted electromagnetic waves attenuate with the distance as they propagate. A signal with a small amplitude may thus be emitted either by a weak lightning discharge or a very distant strong event. Therefore, the observed amplitudes of different lightning are diverse, and they cannot be directly inferred as an indicator of lightning intensity.

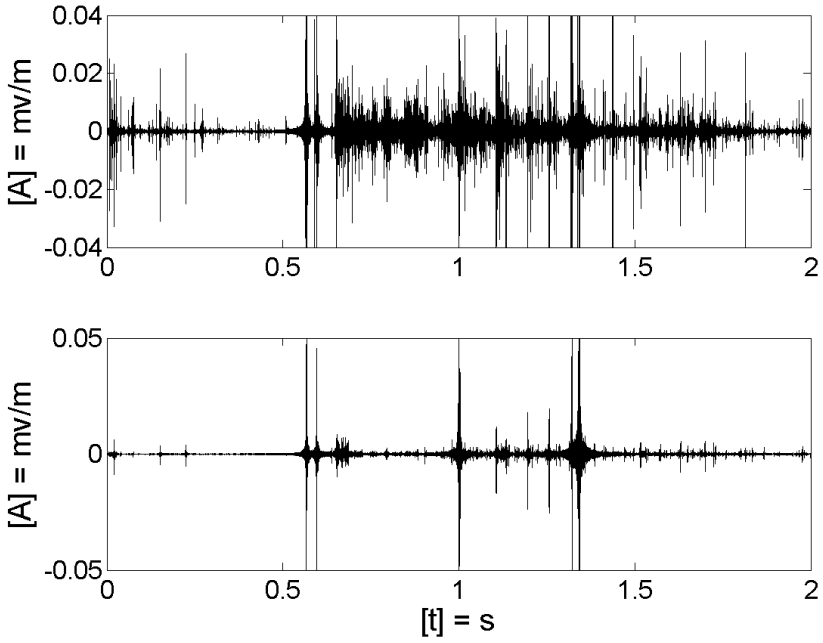

Figure3.8 Filtered signal of lightning and sprite sources from 5–15 kHz (top) and 500–1500 Hz (bottom).

Similar to the filtered data over the lightning frequency range, the Signal to Noise Ratio (SNR) of the data over sprite observation frequency range, i.e. 500–1500 Hz, is increased, which proves that no transmitter or other noise source is involved in this frequency range (Figure 3.8, bottom). The lightning data and sprite data can be compared in the time domain, which can show that sprites are always triggered by lightning. The lightning events that trigger sprites are mainly positive lightning, which always occurs a few milliseconds before sprites. The signal of some lightning or sprites may extend to other frequency ranges. For example, we can find some events show in both sets of filtered data.

The research in the frequency domain will help to understand this. The filtered data solves the low signal to noise ratio problem and simplifies the processing procedure for the lightning location calculation, which can be directly used in other lightning application research.

3.3.2 Spectrum and Dynamic Spectrum

The word 'spectrum' was first used in the optical area to describe the separated colours of light. Now, it is also used for an electromagnetic field to represent the amplitude or the phase information in the frequency domain. The Fourier Transform is the pivotal technique in generating the spectrum, which can convert the data from the time domain to the frequency domain. The Fast Fourier Transform is the practical tool for this application, which can reduce the time taken compared to the Discrete Fourier Transform.

The spectrum generated in this field includes the amplitude and phase information at each sampling frequency. In some situations the phase information can be ignored, which shows the amplitude at different frequencies. Sometimes the amplitude will be ignored, with the spectrum showing only the corresponding phase information in the frequency domain. Electromagnetic waves can be comprehended by different waves at each harmonic frequency. For each sinusoid wave, the amplitude and phase information can be extracted separately. The amplitude spectrum and phase spectrum are both important in lightning research. The following figure presents the amplitude spectrum to show the signal intensity at different frequencies.

Figure 3.9 shows the spectrum of a 2-second data, which presents the amplitude value from 1 Hz to 500 kHz. Due to the large difference between different frequencies, taking the logarithm to base 10 is a normal strategy to solve this problem. The pulses in the processed amplitude spectrum become obvious to select. Each of these frequency pulses represents one radio source, e.g. lightning, sprites, radio transmission, or local noise. Most of these pulses can be observed all the time, not only during these two seconds. Understanding these frequency performances is basic and important to analysing radio wave propagation.

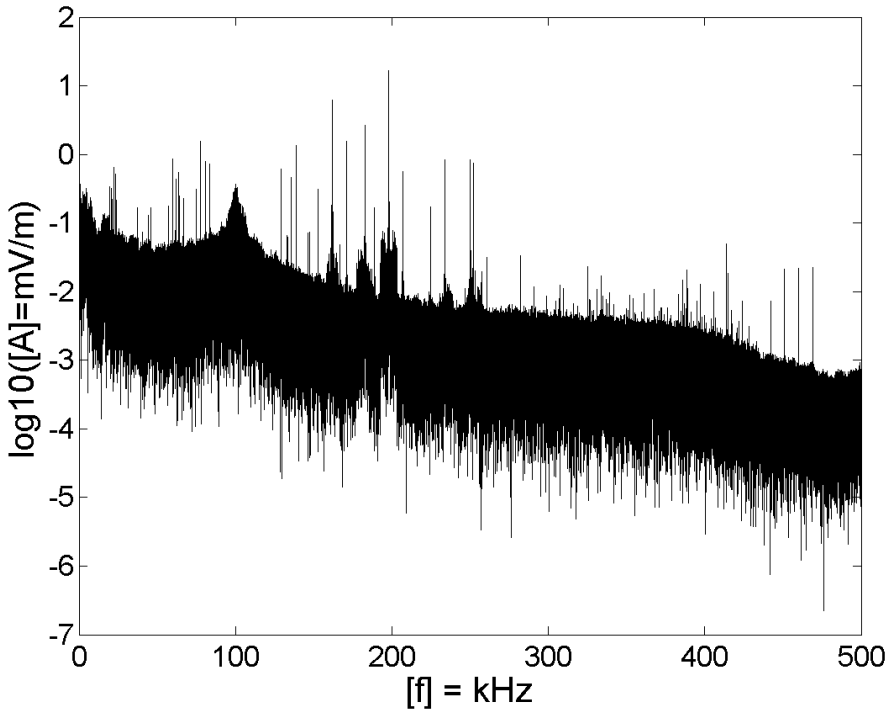

Figure 3.9 The spectrum of a 2-second data. The x-axis shows the sampling frequency and the y-axis shows the logarithm to base 10 of the amplitude.

Some narrow pulses are verified to broadcast transmission frequencies, for example, 198 kHz is the central frequency of BBC Radio Four, and 162 kHz is the central frequency of France International. The research device is a high quality radio receiver, which records data meticulously each microsecond. These data can be well retrieved and listened to through a signal processing strategy. The LORAN (LOng RAnge Navigation) system operates at around 100 kHz. This system is an old ground-based radio navigation system, which helps ships and airplanes to detect their location. Although GPS is the most common navigation technique now, the LORAN system still works as the alternative and ground-based backup for GPS. LORAN-C is the most recent version, developed in the 1970s. The working frequency is from 90 to 110 kHz. At present there are nine LORAN stations around the UK, which can be used in radio science.

Electromagnetic waves at high frequency are easy to attenuate, especially in salty water. As a result, submarine communication under water always takes place at a low frequency. The central frequency of several submarine communications transmissions is around 20

kHz, and most lightning energy is distributed at 5–15 kHz. As a result, the submarine communication frequency is very close to the lightning frequency range. Considering known operation regulations and known locations, research into submarine communications can contribute to the study of wave propagation issues of lightning signals (See Chapter 6).

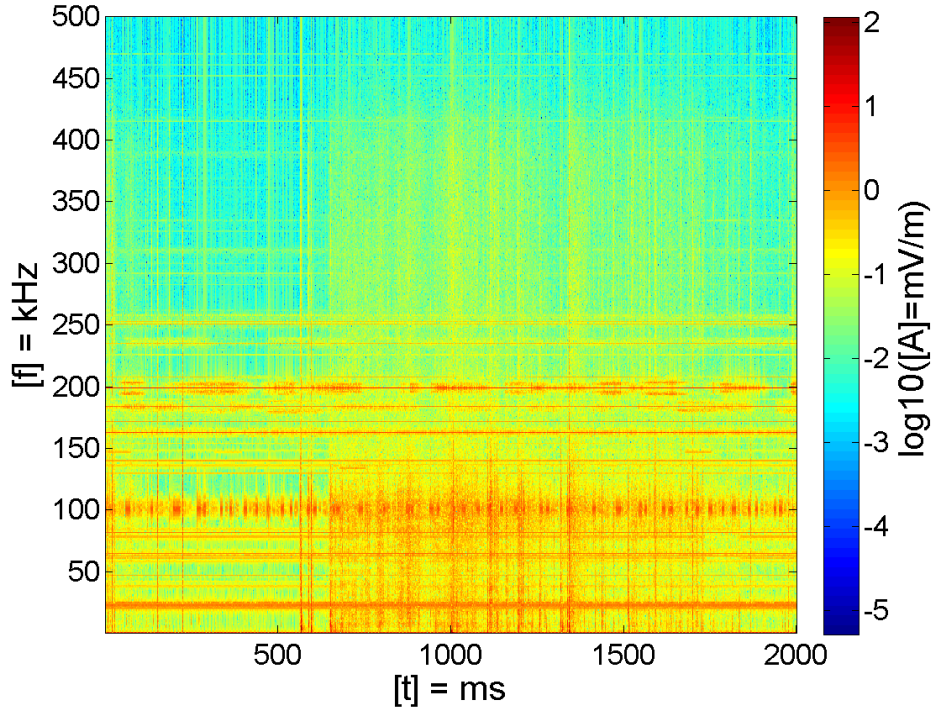

Figure 3.10 The dynamic spectrum of a 2-second data. The x-axis is the time domain. The y-axis is the frequency domain, and the colour is related to the logarithm to base 10 of the amplitude frequency.

The amplitude spectrum cannot present the frequency variance during recording, and so the dynamic spectrum is produced in both the time domain and the frequency domain (Figure 3.10). The two second period of data consists of two million samples. The first step is to reshape all the data into 2000 bins, each of which contains the data of one millisecond. The dynamic spectrum can be generated by Fourier Transferring this 2000*1000 matrix. The dynamic spectrum reduces the frequency resolution, but provides information about the frequency variance by time.

The frequency variance is obvious during recording. Reading the results horizontally, the waves from submarine communications, LORAN, and broadcast transmissions can be directly distinguished, which perform like Morse code. Reading the result vertically, the signals from some powerful lightning and sprites are obvious, for example at 0.7, 1.0 and 1.4 second. It corroborates the literature that strong lightning events produce electromagnetic signatures over a large frequency range (Section 2.1.2).

Chapter 4 Engineering Development of Experimental ATD Lightning Location Network

4.1 The Design Idea

As discussed in Chapter 2, most of the lightning location systems utilise the ATD technique. The principle of the ATD network is to use time differences to locate lightning, as described in the literature review. All of the commercial lightning location systems have their own unique calculation algorithm, but few of these systems publish their detailed program settings. As a result, a novel fundamental algorithm for lightning location using the ATD technique was developed for the experimental long baseline lightning receiver array. The design idea and the detailed processing steps are described below. The data recorded on 24th August 2013 at 20:12:05 has been used as the example to present the network performance. Several sprites and lightning events, especially three intense lightning events, were observed by human eyes and recorded within this three-second period of data. Three sprites triggered by the three most intense lightning are speculated to be dancing sprite.

The basic concept of an ATD lightning location network is to find the location that has the same arrival time differences to receivers as the measured time differences. A better understanding of the recording and possible arrival time differences is preliminary to designing the location calculation program. The raw data contains the full recorded information, but it is complicated to select useful information directly out of the noise (Figure 4.1).

In order from top to bottom, the data of the sky blue line was recorded by the receiver in Rustrel. The data for the red line was recorded by the receiver in Lannemezan. The data

from the green line was recorded by the receiver in Orleans, and the data from the blue line is recorded by the receiver in Bath. The signal to noise ratio of the recording from Rustrel station is the highest, because this station is located on a mountaintop. The noise of other three receivers seems larger because of the nearby human activities. Even so, the main objectives of this Chapter, the three strong events around 1 second, are clearly observed. In order to increase the signal to noise ratio and get the pure lightning information, the data from 5 kHz to 15 kHz is filtered for better observation (e.g. Figure 4.3, b).

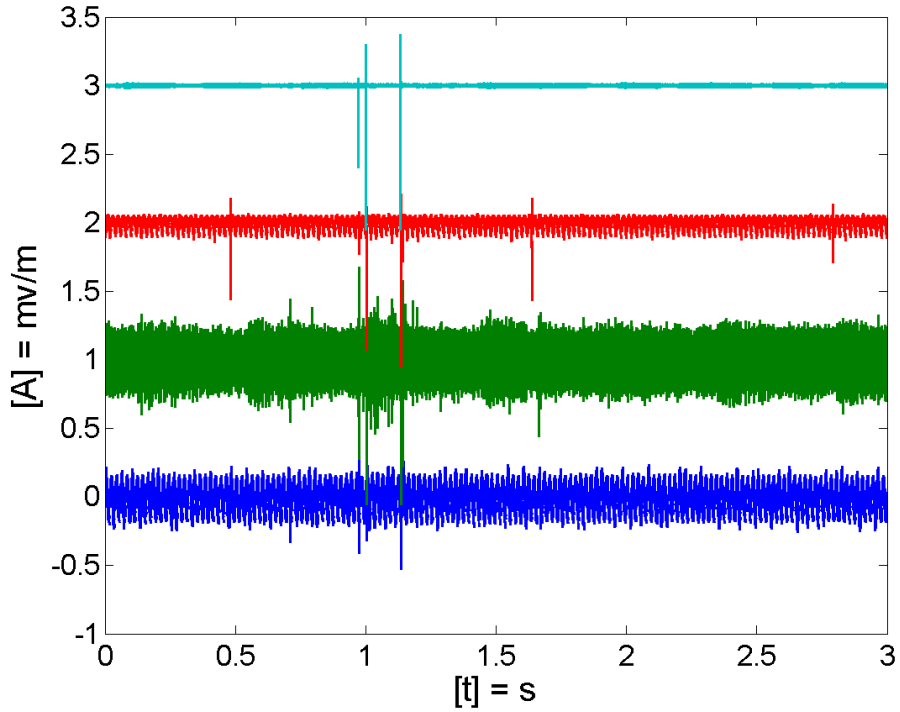

Figure 4.1 Three seconds of raw data recorded by the experimental lightning location network on 24rd August 2013 at 20:12:05.

The filtered data is much clearer than the raw data, and extracting lightning information is easier. The essential calculation of the ATD technique is to find the intersecting hyperbolas (Section 2.3.2), so determining hyperbolas between four stations is the minimum requirement. Most strong lightning discharges can be observed at all four stations, and can thus be located in this network. However, this experimental lightning location network is not available for lightning discharges only observed at fewer stations.

A lightning location network using the ATD technique carries out calculations based on the measured arrival time difference. As a result, the designed ATD programme can be divided into three steps (Figure 4.2). The first step is extracting the time stamp of events and detecting the valid time differences of the first return stroke. The second step is finding the best matching location to the measured time differences using an optimization method. The third step is evaluation of the network results using rigorous self-assessment and comparison with other operating lightning detection systems to determine the system error and to identify areas of improvement.

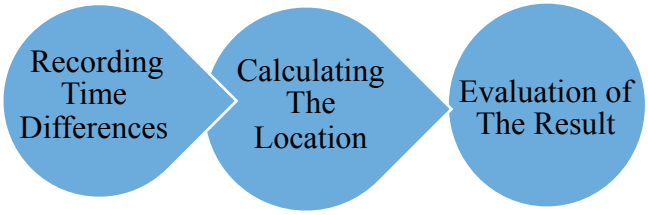

Figure 4.2 Developed ATD detection programme

4.2 Measurement of Arrival Time Differences

The lightning location is calculated based on the measured arrival time differences. There are two stages to extracting useful time differences from the recording. The first step is finding lightning events from a given amount of digital data and extracting the time stamp of it for retrieval. The second step is detecting the valid and accurate time differences from the retrieved lightning waveforms.

For the first stage, most lightning location systems set the amplitude thresholds, so that the signal above the threshold value is treated as the lightning events. However, some weak lightning or distant lightning fails to be detected if the signal to noise ratio is low. The threshold of phase coherency around the receivers is a novel and sensitive method for a short-baseline lightning receiver array [*Fullekrug, 2016*]. There is no reliable trigger algorithm for this experimental network, and the reported time by other networks has been used for most cases.

The second stage is to measure the valid and accurate time differences from lightning recordings. In ideal circumstances, the lightning recording is a strong pulse signal with certain time delay at different stations. In reality, the received electromagnetic recording may have unpredictable issues, such as wave transformation with propagation (discussed in detail in Chapter 5) and saturation, which limits the veracity of ATD detection. Signal processing strategies and time tracking methods are discussed and compared below in order to measure the most accurate time differences. The signal processing strategy means the method of processing the data to extract time more accurately and easily. The time tracking method means the way of measuring the arrival time differences from the processed data.

Four kinds of processed lightning data, raw data, filtered data, smoothed filtered data, and complex trace data, are compared using the example lightning shown in Figure 4.1 at 1 second (Figure 4.3). The raw data contains whole electromagnetic information from 4 Hz to 400 kHz, but is too noisy to extract time stamps from the low SNR. The filtered data is filtered from 5–15 kHz, where most of the energy of the lightning return stroke is distributed. The smoothed filtered data is produced by a moving average of the signal excluding some powerful transmitters, such as 100 kHz and 198 kHz, so that it is clearer than the raw data and contains more information than the filtered data. The complex trace data is the amplitude envelope of the complex lightning waveforms (See Chapter 5), for which it is extremely easily to define amplitude maxima.

The time tracking methods are methods for extracting time differences from the processed data. Three time tracking methods: maximum amplitude, zero crossing, and cross correlation, are discussed here. Maximum amplitude is normally a minimum value or maximum value, which is always associated with the first return stroke. The disadvantage of selecting the maximum amplitude is that the peak value sometimes causes saturation, which may result in error of a few microseconds. Zero crossing is selected from the zero crossing point before or after the maximum amplitude, which can avoid the saturation peaks. The zero crossing is normally associated with the initiation of stepped leaders or the rising of the return stroke, but this signature is easily affected by large noise. Cross correlation is an automatic method which uses the similarity of waveforms to detect time differences. It records the time shifted when waveforms get the best matching. However,

waveforms propagated from different distances are different, and noise outside the lightning period also contributes to the cross correlation result.

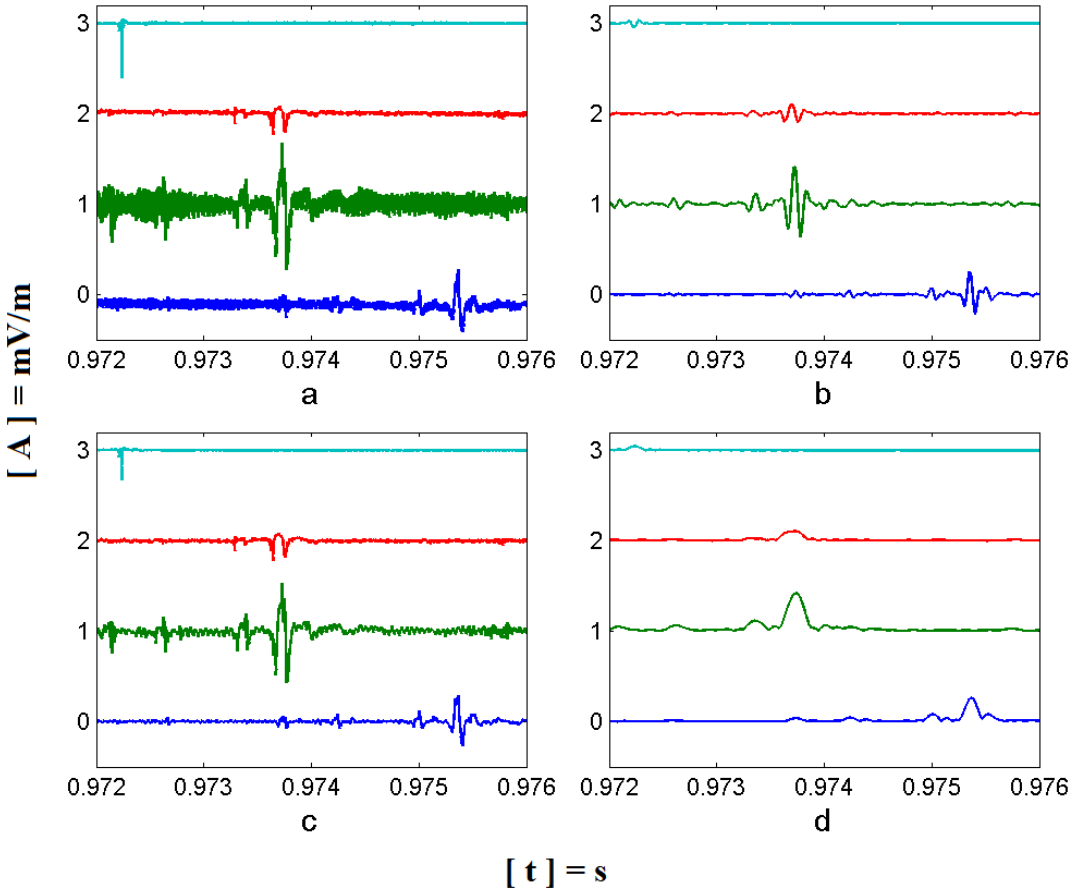

Figure 4.3 Four kinds of processed lightning data of the lightning at 0.97s. a. raw data; b. filtered data; c. smoothed filtered data; and d. complex trace data.

The combinations of different signal processing strategies and time tracking methods were tested and compared using three strong lightning events, as shown in Figure 4.1 at 0.97, 1.0, and 1.13 seconds (Table 4.1). The measured time differences are directly used to calculate lightning locations for comparison, which were also compared with locations reported by other lightning location systems, such as the UK MetOffice and Meteorage. This experimental lightning location network is simplified as 'UoB' in the table. The chi-square value (See Section 4.3), error distance (ΔX), and two error percentage (See Section 4.4) are the elements to represent the quality of the location calculation and the accuracy of the arrival time measurements.

Table 4.1 Comparison between the different methods of arrival time measurement.

24/08/2013 20:12:05.832715	Latitude °	Longitude °	X_{chi} μs^2	UoB-UKMO km	UoB-Meteorage km	UKMO-Meteorage km	P_{md} %	ΔX km	P_{sd} %
1Maximum amplitude & Raw data	44.0234	8.0255	2.3422	32.4267	-		2.15%	0.52	0.69%
1Maximum amplitude in Filtered data	44.0234	8.0255	2.3422	32.4267	-		2.15%	0.52	0.69%
1Zero Crossing & Filtered data	43.9337	8.3775	7.8697	2.5325			1.45%	1.03	0.25%
1Zero Crossing & Smoothed filtered data	43.9462	8.6337	20.2854	18.1368			5.60%	2.24	4.21%
1Cross correlation & Raw data	44.1415	7.0452	64.8225	111.778	-		15.12%	8.55	32.40%
1Cross correlation & Filtered data	44.1451	7.0178	133.968	114.006	-		17.65%	16.76	35.77%
1Cross correlation & Complex trace data	44.2695	6.834	24.8975	131.5866			9.00%	3.60	8%
Meteorage company	-	-	-	-	-	-			
UK MetOffice	43.9309	8.4088		R	-	-			
2Maximum amplitude & Raw data	44.7244	9.5575	11.6075	63.7526	11.0377		0.61%	1.46	0.03%
2Maximum amplitude & Filtered data	44.7244	9.5575	12.6075	63.7526	11.0377		0.61%	1.46	0.03%
2Zero Crossing & Filtered data	44.7584	9.4193	7.233	74.9306	22.047		0.36%	0.98	0.01%
2Zero Crossing & Smoothed filtered data	44.7635	9.5022	8.1759	68.1947	15.6426		0.41%	1.09	0.01%
2Cross correlation & Raw data	44.6567	9.0567	67.1801	103.817	51.423		5.99%	8.90	4.22%
2Cross correlation & Filtered data	44.5654	9.5147	140.161	69.7319	23.7819		8.54%	17.34	6.02%
2Cross correlation & Complex trace data	44.8114	8.707	23.8707	131.319	78.7259		0.20%	3.47	1.70%
Meteorage company	44.7359	9.6959		-	R	52.7798			
UK MetOffice	44.732	10.3622		R	-	52.7798			
3Maximum amplitude & Raw data	44.9422	10.3629	6.8609	32.3328	12.195		0.37%	1.08	0.01%
3Maximum amplitude & Filtered data	44.8585	10.6929	7.1674	7.1995	15.6771		0.36%	1.08	0.01%
3Zero Crossing & Filtered data	44.8991	10.5273	7.3861	18.5573	2.5154		0.30%	0.93	0.00%
3Zero Crossing & Smoothed filtered data	44.9221	10.4584	5.8362	24.1662	4.4059		0.26%	0.76	0.00%
3Cross correlation & Raw data	44.8729	10.7633	7.0969	2.5855	20.3595		0.33%	1.00	0.01%
3Cross correlation & Filtered data	44.865	10.7006	7.5608	6.2895	15.9373		0.32%	1.00	0.01%
3Cross correlation & Complex trace data	45.1866	8.5182	78.3419	179.7241	159.9938		2.00%	11.50	5.00%
Meteorage company	44.9197	10.5141		-	R	20.1609			
UK MetOffice	44.896	10.7672		R		20.1609			

The time difference extracted from cross correlation with any processed data is convenient to calculate, but the accuracy in these cases is unsatisfactory. Considering consistency and accuracy, the most accurate combination is measuring time differences from the amplitude maximum of raw data. The difficulty in programming this combination to measure arrival time differences automatically is that there are several maximum peaks in one lightning recording. The maxima may not be at the same peak in the recordings at different stations. It was fortunately found that the maximum in complex trace data is always located between the first peak and second peak in the raw data. As a result, the same peaks in the recording at different stations can be selected from the maxima or minima before the maximum in complex trace data. This method has been tested and examined for many cases, and was used for this PhD project.

4.3 Location Calculation Based on the Measured Time

4.3.1 Chi-square Value

The lightning location can be calculated in two ways once the arrival time differences are known. The forward thinking is to draw hyperbolas between the receivers based on the time differences, and then calculate the superposition of these hyperbolas. However, the earth is not perfectly spherical, and propagation of electromagnetic waves is complicated, which makes the mathematical procedure unrealistic. The inverse thinking is to find the location that matches the measured time differences.

The match degree of locations is determined by the chi-square value:

$$X_{chi} = \sum_{n=1}^{N} \left(\Delta t_n - \frac{\Delta d_n}{v} \right)^2 , \qquad (4.1)$$

where X_{chi} is the chi-square value, N is the number of receiver pairs, Δt_n are the measured time differences between receivers, Δd_n are the distance differences from the possible lightning location to the receivers, and v is the wave propagation velocity which

defaults to c, i.e. the speed of light, in many lightning detection systems. The chi-square value is some direct proportion of the Root Mean Square (RMS) value

$$X_{RMS} = \sqrt{\frac{X_{chi}}{N}}. \qquad (4.2)$$

The chi-square value is an indicator of the match degree between the measured time differences and the possible location. A smaller chi-square value means that this theoretical location is closer to the true location. While this chi-square value will never be zero, because the propagation speed is not identical to the speed of light (See Chapter 6), and due to the error of the extracted time difference. As a result, the theoretical location with the smallest chi-square value is the calculated location.

Actually, the calculation result should be an area rather than a certain accurate location because of the uncertainty and error in the time differences. In theory, there are N-1 independent time differences for N receivers. For easier understanding, These N-1 time differences are imagined to be a point in an N-1 dimensional space of all possible time differences, named the multi-dimension time difference model. The time differences of all geo-locations on earth make up an earth surface in this N-1 dimensional space. The point would be on this earth surface if the chi-square value is zero. However, the wave propagation velocity varies depending on different frequencies and different propagation paths. In addition, the time may have a certain level of error. As a result, the measured time differences will be stereoscopic rather than a point, which adds to the uncertainty in each direction from the measured point in this multi-dimension time difference model. Therefore, the calculation result should be an area, which may be achieved using the interferometry idea (See Chapter 7). In the case of current ATD calculations, the calculated location is the point on the Earth's surface that is closest to the measured point in the multi-dimension time difference model, and the distance between these two points is the square root of the minimum chi-square value.

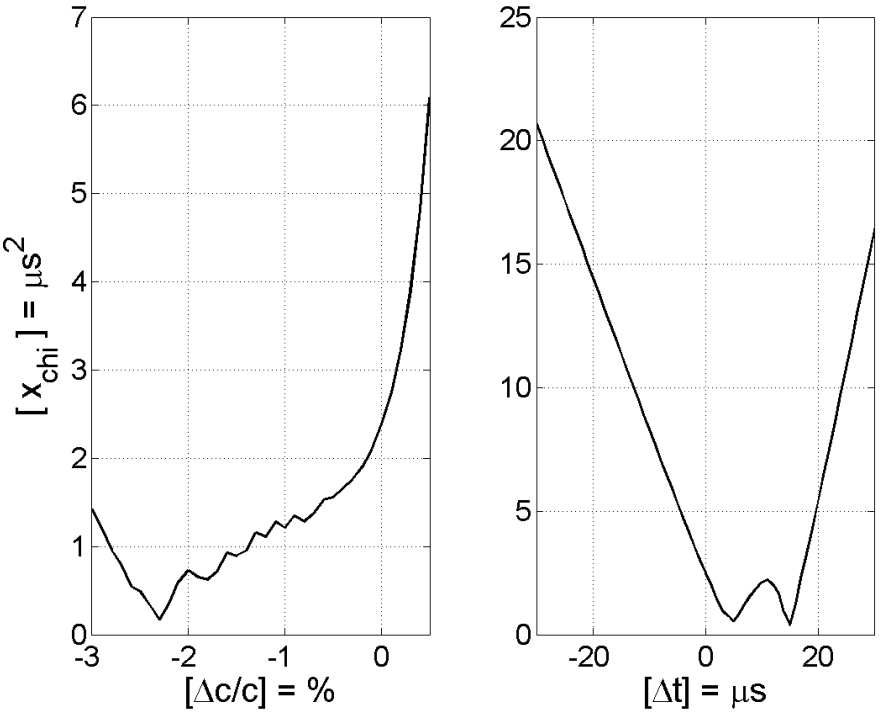

Figure 4.4 Chi-square sensitivity tests with a varying velocity (left) and time shift at the receiver in Bath (right).

In order to test the sensitivity of the chi-square value and minimize the distance between the measured point and the earth surface in the multi-dimension time difference model, the minimum chi-square value is calculated in different circumstances, such as different wave propagation velocities and different time accuracies of the receiver (Figure 4.4). It was found that the smallest minimum chi-square value is observed with a velocity smaller than c, and a delayed arrival time at one receiver. It illustrates that the wave propagation velocity for this network is not at the speed of light. This is also a possible reason for the smallest minimum chi-square value with an arrival time delay. Further study about the wave propagation velocity is described in Chapter 6. Overall, the chi-square value is a sensible and sensitive index for lightning location.

4.3.2 Determine Lightning location

The next step is to find the location that has the smallest chi-square value. There will be too many calculations if we search the entire map with certain accuracy. For example,

there will be one million times the calculations if we search the whole Europe to 0.01 degree accuracy in latitude and longitude. It is a waste of computational effect for a single lightning calculation. The idea of loops searching is shown in Figure 4.5.

Figure 4.5 Searching loops for lightning detection.

The basic idea of loops searching is to find the minimum value within a large area with a large step, and to repeat the same process in the surrounding area with a smaller step. The example in Figure 4.5 uses 4 loops with the step from 1° to 0.001°. The final location resolution is ~1 km. The benefit of using loops searching is to avoid the ambiguity of global and local minima. One example of the chi-square value distribution in different searching loops is presented in Figure 4.6. The same feature is observed here and in numbers of other examples even with higher resolution that there is only one minimum when searching loops. It indicates that it is sensible to calculate lightning location by minimization of the chi-square value directly based on the gradient descend technique, which decreases the amount of computational time and effort needed.

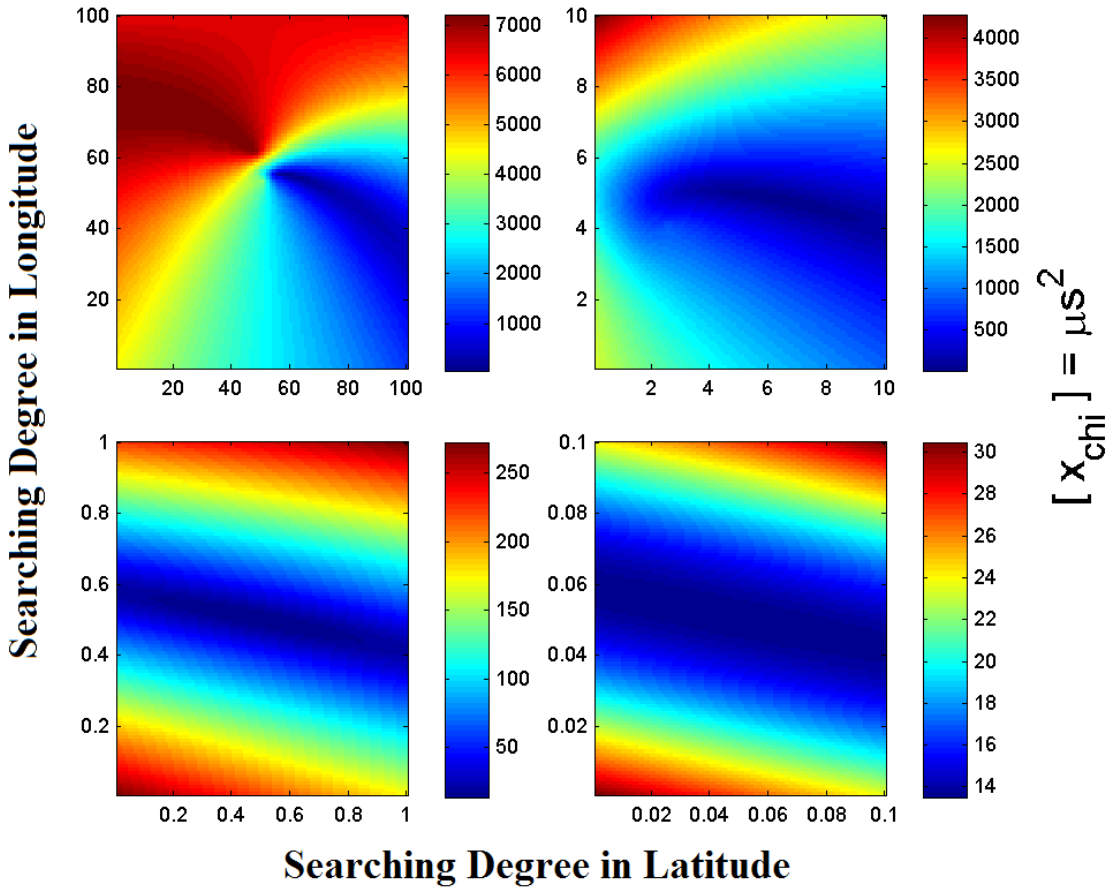

Figure 4.6 The chi-square value distribution in different searching loops with the searching unit from 1° to 0.001°.

4.4 Evaluation of the Result

The reliability of the result is as important as the result itself, and can determine the system error and identify areas of improvement. Results evaluation has two aspects: inside and outside (Table 4.1). Outside evaluation is the comparison of the result with other operational lightning detection systems, such as the MetOffice and Meteorage Company. Inside evaluation is rigorous self-assessment, which is the difference between the measured time differences and the time differences from the calculated location to the receivers.

The chi-square value and RMS value are two self-assessment methods. There are also several other equations that have the similar effect of result evaluation, such as the mean absolute percentage deviation:

$$P_{md} = \frac{1}{N}\sum_{n=1}^{N}\left|1 - \frac{\Delta \mathrm{d_n}}{\Delta t_n * c}\right|, \tag{4.3}$$

and the square percentage deviation:

$$P_{sd} = \sum_{n=1}^{N}(1 - \frac{\Delta \mathrm{d_n}}{\Delta t_n * c})^2, \tag{4.4}$$

and the distance between the theoretical location and the ideal true location:

$$\Delta X = v\sqrt{\sum_{n=1}^{N}\left(\frac{\Delta d_n}{v} - \Delta t_n\right)^2}\,. \tag{4.5}$$

These self-assessment equations can prove whether a result is reliable or not. Evaluation of some examples shows that the results of the lightning detection network are quite reliable (e.g. Table 4.1) and useful in determining the best time difference selection methods.

This developed experimental ATD lightning location program has been used as the fundamental algorithm for lightning analysis in this PhD project. The calculated results are precise even with only four receivers. Further research based on this program is described in the following Chapters.

Chapter 5 Lightning Sferics: Analysis of the Instantaneous Phase and Frequency Inferred from Complex Waveforms

5.1 Introduction

Ground-based lightning location systems are essentially based on received electromagnetic waves and subsequent signal processing [*e.g., Dowden et al., 2002; Holler et al., 2009; Bitzer et al., 2013; Rakov, 2013; Stock et al., 2014; Lyu et al., 2014; Nag et al., 2015; Wang et al., 2016; Sun et al., 2016*]. In the most commonly used lightning location method, Arrival Time Differences (ATD) are extracted by different signal processing techniques from the lightning waveforms recorded at different radio receiver stations [e.g. *Lee, 1986, 1990; Cummins et al., 1998, 2009*]. The different signal processing techniques used result in slightly different arrival times with different corresponding lightning locations [*Liu et al., 2016*]. Using a different time extraction point, e.g. the waveform peak or rising edge, and different data pre-processing, e.g. wide or narrow bandwidth or complex envelopes, can all introduce slightly varying time differences. As a result, a better understanding of the sferic, i.e. the received broadband lightning waveform, is a prerequisite for improving the accuracy of lightning location.

Much research into ionosphere perturbations and atmospheric chemistry uses broadband VLF waveforms, in particular lightning waveforms [e.g. *Cheng et al., 2007; Shao et al., 2013*]. The sferic is a broadband electromagnetic impulse generated by a lightning discharge, which propagates through the earth-ionosphere waveguide. The perturbations in the D-region caused by the variation of electron densities changes the received sferic in the time and frequency domains. A collection of average lightning waveforms at different distances, named a waveform bank, was introduced by Said *et al*. [*2010*]. This method offers an opportunity to characterize sferics and to estimate arrival time. This idea has

been adopted and is extended in this work to produce a new type of waveform bank for further analysis.

A time-dependent sferic signal is treated as an analytic signal, or complex trace, and the received signal is processed to determine the instantaneous phase and frequency at each sample in the time series [e.g. *Taner et al., 1979*]. This method will be applied to a new lightning waveform bank (<1000 km) produced from data collected by the long-baseline lightning receiver array described below. The timing accuracy of the instantaneous phase is compared with other methods using the speed of light as a reference. The derivative of the instantaneous phase is the instantaneous frequency, which is used here to study the relationship between the real frequency of the sferic and its spectrum. The observed instantaneous frequency changes in the complex waveform bank are discussed and related to the radio wave propagation with distance.

5.2 The Complex Waveform Bank

5.2.1 The Waveform Bank

Previous research associated with sferic waveform characteristics, including polarity estimation, cycle errors, and peak current, has shown that received lightning waveforms that originate from a certain storm cluster exhibit similar features [*Said et al., 2010, Figure 1*]. Thus, a small deviation of lightning waveform shape indicates propagation over similar distances. A representative waveform is calculated by averaging each of the lightning waveforms in one distance bin to reduce the noise in each average waveform and to acquire a more pure lightning waveform that includes subtle propagation effects. Comparing the representative waveforms at different distances is an effective method to study the propagation effects on lightning sferics.

Lightning locations are reported by the French lightning detection network, Meteorage, which covers south-western Europe and the western Mediterranean Sea. The electromagnetic waveforms of lightning discharges were recorded from ~21:00 UT 8th to ~03:00 UT on 9th August 2014 by four low-frequency radio receivers.

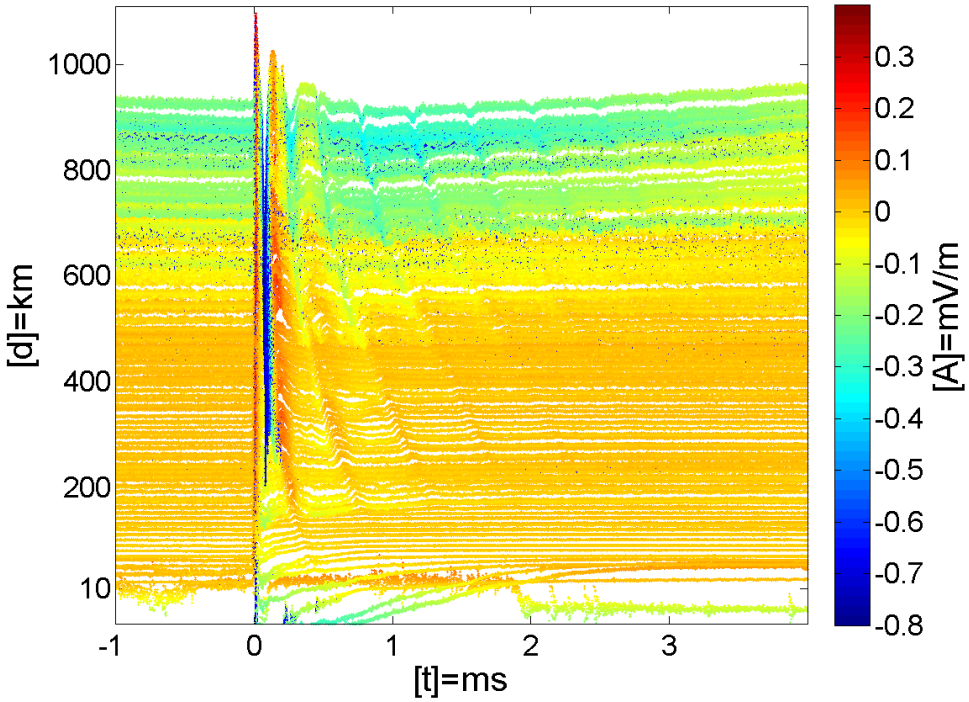

Figure 5.1 The average night-time waveforms of negative lightning discharges at distances from 10–1000 km. Each average waveform at a given distance was calculated from more than one hundred events. The time axis is referenced to t=0 corresponding to a propagation at the speed of light from the source to the receiver. A sequence of consecutive maxima resulting from the ionospheric reflections (or multi-hop sky waves) appear from ~100 km distance onwards, and the time differences between ground wave and sky waves are smaller for larger distances.

During the 13 hour long recording, more than 150,000 cloud-to-ground lightning stroke waveforms from a mesoscale convective system over central France were recorded by the four sensors with peak currents ranging from -4 kA to -40 kA, which were located 0–1000 km away from each radio receiver [*Liu et al., 2016*]. The lightning waveforms ranging from -1 ms to +4 ms around the occurrence of the lightning discharges were extracted from the digital recordings based on the lightning locations and time reported by Meteorage. The time t=0 of the lightning waveforms was referenced to the propagation time at the speed of light calculated from the great circle distance between the source and the receiver. This referencing procedure enables the calculation of one average waveform for each distance bin with a width of 10 km. Each distance bin consists of at least one

hundred lightning waveforms. The resulting 100 average waveforms comprise the lightning waveform bank, forming the basis for the subsequent data analysis (Figure 5.1). The difference between source currents and the interfering signals from the local noise environment, man-made noise and radio transmissions are thereby minimized. The ionosphere conditions are relative stable because all of these lightning waveforms propagated at night-time.

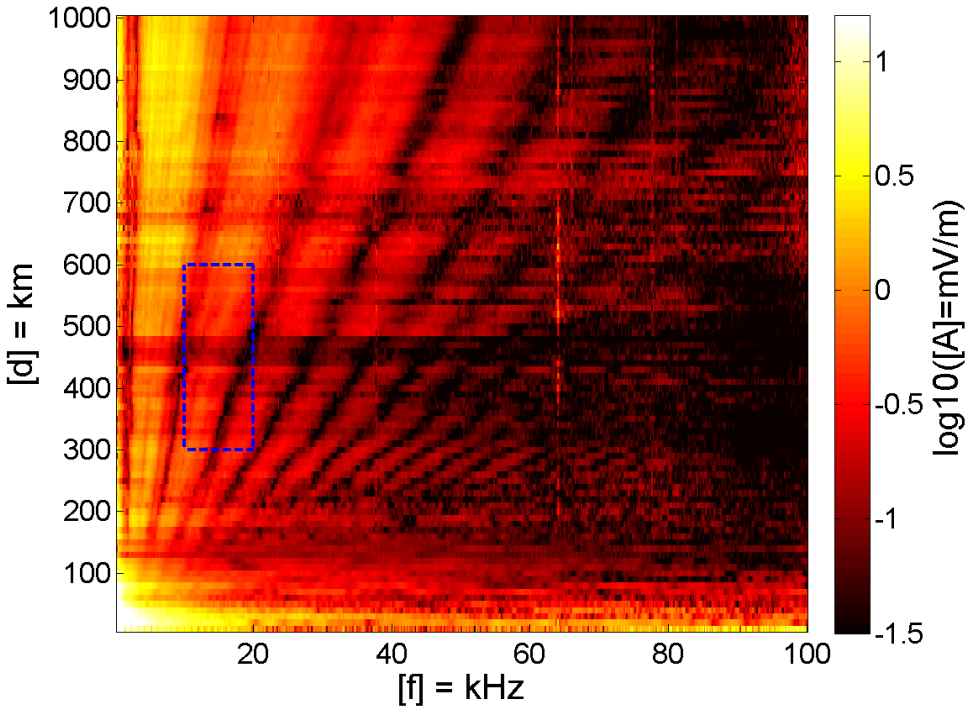

Figure 5.2 The spectra of the average waveforms. Interfering signals from the local noise environment, man-made noise and radio transmissions are minimized. The sequence of consecutive modal maxima (yellow and red) is separated by distinct minima (black) which are characteristic of the distance between the radio receiver and the lightning discharge. The area of the blue square is used for the analysis of the instantaneous frequencies (compare to Figure 5.8).

The waveform bank exhibits an initial pulse from the ground wave, and a sequence of subsequent maxima from ionospheric reflections or multi-hop sky waves. The first arrival sky wave can be observed after ~100 km propagation, and additional sky wave hops can be observed for longer distance propagation. The energy of the lightning signals

propagated along the ground path attenuate with distance due to ground conductivity, while the energy of lightning signals from the ionospheric reflections are attenuated by longer propagation distances and the ionospheric D-layer conductivity. The waveform bank shows distance-dependent arrival times of the ground wave and ionospheric reflections, which can be explained by ray theory [e.g. *Schonland et al., 1940; Carvalho et al., 2017; Qin et al., 2017*]. The waveform bank shows the ground wave arrival at 0 ms and the sky wave arrival at increasing time delays for shorter distances, which can be confirmed by theory using a flat-earth model and a spherical earth model..

A spectral waveform bank can be calculated by averaging the spectra of all waveforms at the same distance bin, or from the spectra of the average lightning waveforms at each distance bin, which produce same result (Figure 5.2). The spectral waveform bank exhibits a sequence of consecutive maxima in the frequency range up to 100 kHz. These consecutive relative maxima result from the constructive superposition of numerous wave propagation modes, named modal maxima in the following text. The modal maxima are separated from each other by distinct spectral minima that are characteristic for the distance between the lightning discharges and the radio receivers. These features of the spectral waveform bank result mainly from the lightning pulses and propagation effects, because averaging the waveforms eliminates the difference between source currents and most of the interfering noise. The spectral waveform bank is useful for understanding the propagation effects with distance, and can be used for theoretical modelling of radio wave propagation.

5.2.2 Complex Waveforms

The time dependent radio signal can be treated as an analytic signal or complex trace. This allows for the extraction of the envelope and instantaneous phase for each sample [*e.g. Taner et al., 1979; Liu et al., 2016*]. The complex trace can be obtained from the real valued recordings using the Hilbert transform. The Hilbert transform can be thought of as the convolution of the real signal with $1/(\pi t)$, where t is time. This convolution generates the Hilbert transform as an output of a linear time invariant system using the Cauchy principal value to avoid singularity. The Hilbert transform, $H(f(t))$, of a real valued time dependent function, $f(t)$, can also be understood as the effect of a phase shift

of the negative frequencies by +90° and positive frequencies by -90°, where using multiplication by an imaginary unit, j, to calculate the complex trace, $F(t)$, shifts the negative frequencies by another +90° and restores the positive frequencies.

In practice, the complex waveform can be calculated from the real signal by doubling the positive frequencies of $f(t)$and by eliminating the negative frequency of the real signal. This complex waveform is subsequently down converted by multiplying with a frequency shift operator, $e^{-j\Delta\omega t}$, that centres the spectrum at zero frequency. The frequency shift operator has in-phase and quadrature components, so this step can alternatively be used for obtaining a complex signal. The shift frequency, Δω, is normally set as the harmonic frequency which contains most of the energy of the target signal. For example, the shift frequency of a radio transmission is normally the centre frequency of its modulation. The shift frequency of lightning can be set at 10 kHz, as the return stroke deposits most of its energy around this frequency [*Fullekrug et al., 2013*]. The final complex waveform can be determined after applying a low-pass filter to the down converted signal in order to increase the signal to noise ratio:

$$F(t) = \Big(f(t) + jH\big(f(t)\big)\Big)\, e^{-j\Delta\omega t} = A(t)e^{j\varphi(t)} \qquad (5.1)$$

where $A(t)$ is the time dependent amplitude envelope, and $\varphi(t)$ is the time dependent instantaneous phase, i.e. $\varphi(t) = \tan^{-1}[\mathrm{Imag}(F(t))/\mathrm{Real}(F(t))]$.

Using this method, the complex waveform from 2–18 kHz of an average lightning signal at 300 km was calculated and is shown in Figure 5.3. This three-dimensional trace of a lightning waveform illustrates the amplitude envelope and instantaneous phase variation over time. In the beginning, the phase of the complex trace is chaotic and the amplitude is low when there is no lightning signal. The arrival of the ground wave and sky waves leads to large signals, which are well above the noise. These large signals result from a strong lightning discharge, so that the amplitude is increased and the phase is moved towards a specific value. In this example, the complex waveform rotates anticlockwise, which means that the instantaneous phase is decreasing during the pulse arrival. The signal returns to chaotic behaviour after the lightning event.

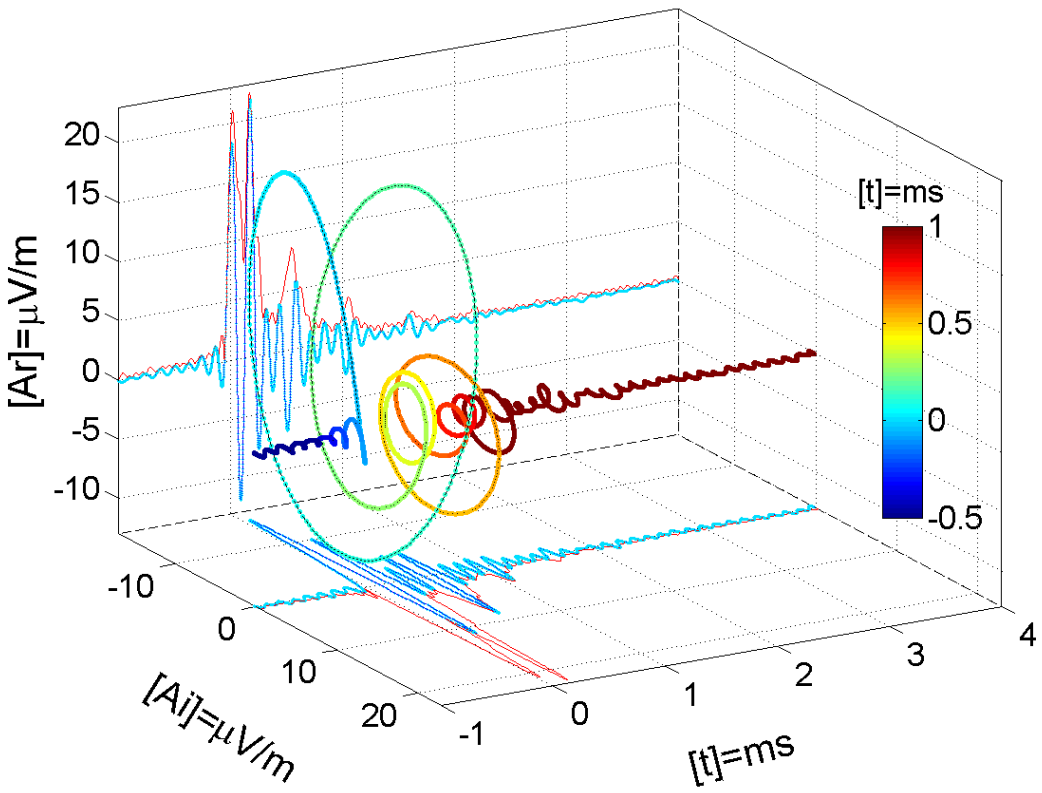

Figure 5.3. Isometric diagram of an average complex waveform of lightning at a distance of 300 km. The 3D trace of the complex lightning signal from 2 kHz to 18 kHz exhibits large amplitudes when the ground wave and sky waves are arriving. The rotation direction of the complex trace is anticlockwise, which means that the instantaneous frequency is smaller than the centre frequency. The blue lines show the real part, (A_r), and imaginary part, (A_i), of the complex lightning waveform. The thin red line is the amplitude envelope of the complex waveform.

Different information can be extracted from the complex waveform than from the real-valued signal, including the envelope of the complex trace and the instantaneous phase. The time differences calculated from the instantaneous phase between two lightning waveform peaks can be extracted by use of the transfer function calculated from the ratio between the two complex values at maximum amplitude. Normally, the time difference between two lightning waveforms is constrained by the sampling frequency. In order to achieve the sub-sample time difference $\delta t = \delta\varphi/\omega$, the two waveforms are time shifted first in order to superpose the amplitude peaks. The instantaneous phase difference $\delta\varphi$

can then be extracted from the transfer function of the peak samples in the two waveforms. The time difference inferred from the instantaneous phase achieves sub-sampling accuracy after taking into account cycle ambiguities, if any.

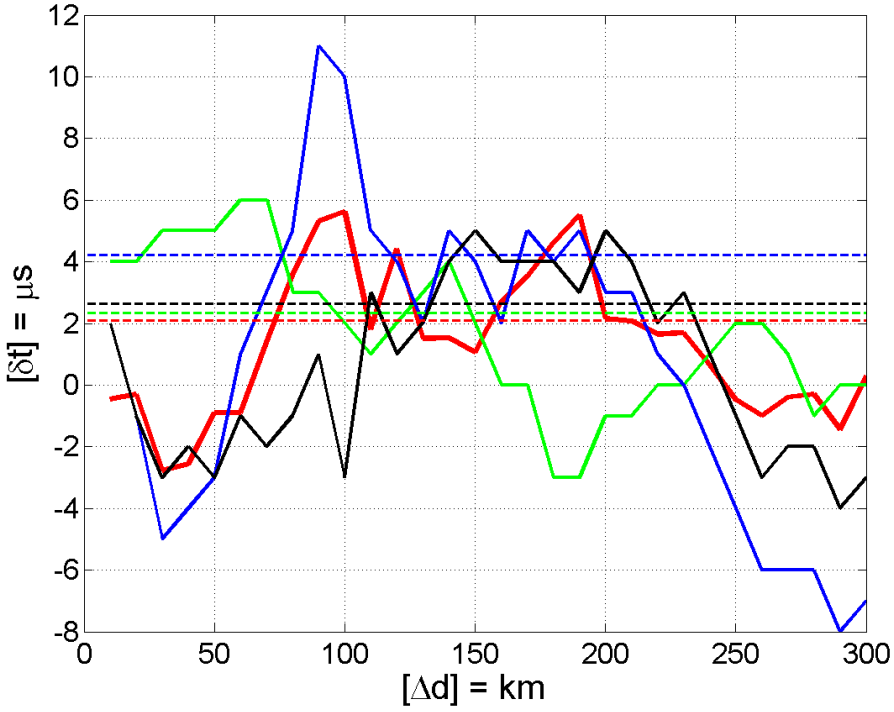

Figure 5.4. The time offsets between different propagation distances with respect to a speed of light propagation. The average lightning waveforms from 310 km to 600 km are compared with the average lightning waveform at 300 km distance. The time offset δt is the measured time differences Δt minus the supposed time differences with propagation velocity at speed of light Δd/c, and the distance differences Δd in this case is compared to lightning waveform at 300 km distance, i.e., d-300. By comparing different signal processing methods, the average value of the absolute time offset by using the instantaneous phase of the complex lightning waveform (red) is less than just using the amplitude envelope (blue) or using the amplitude of the real signal (black) or cross correlating lightning waveforms (green). The corresponding average values of the absolute time offset are shown by the dashed lines.

The propagation time delay relative to the speed of light using different signal processing methods can be compared by using the lightning waveform bank. The average lightning

waveforms from 310 km to 600 km are compared to the average waveform at 300 km using four different time extraction methods (Figure 5.4). The time offset δt is the measured time differences Δt minus the supposed time differences with propagation velocity at speed of light Δd/c, and the distance differences Δd in this case is compared to lightning waveform at 300 km distance, i.e., d-300. All these methods determine the time offset measured with reference to the propagation time between the source and the receiver at the speed of light. The first three methods extract time stamps by waveform cross correlation, and from the peak of the filtered data (5–15 kHz) and the envelope of the complex trace. The average values of the absolute time offsets over all distances differ from 10–300 km with respect to the speed of light using these three methods are ~2.33 μs,~2.63 μs and ~4.23 μs, respectively, with corresponding ranges of [-3 6] μs , [-4, 5] μs and [-8, 11] μs. The average value of the absolute time offset using the instantaneous phase is only ~2.08 μs with a corresponding range [-2.78, 5.62] μs (Figure 5.4). In the case of a lightning location system measuring time differences with a propagation velocity of the speed of light, the time accuracy is therefore slightly improved by calculating the instantaneous phase from the complex waveform.

5.3 Instantaneous Frequency

The different rotation directions of complex waveforms may indicate a different elevation angle of the incident lightning sferic [*Fullekrug et al., 2016, Figure 2, right*]. The rotation direction is the polarity of the derivative of the instantaneous phase in a complex waveform. This time dependent derivative, $f_i = d\varphi/dt$, is called the instantaneous frequency [*Taner et al., 1979*]. The instantaneous frequency indicates the phase change for each sample with reference to the centre frequency of the signal. The rotation direction is anticlockwise when the instantaneous frequency is smaller than the centre frequency and it is clockwise when the instantaneous frequency is larger than the centre frequency. A convenient way of computing the instantaneous frequency, f_i, from the complex trace, C, is to compute the derivative of the arctangent function:

$$f_i = \frac{1}{2\pi}\frac{d}{dt}tan^{-1}\left(\frac{Im(C)}{Re(C)}\right), \qquad (5.2)$$

which results in:

$$f_i = \frac{Re(C)\frac{d(Im(C))}{dt} - Im(C)\frac{d(Re(C))}{dt}}{2\pi(Re(C)^2 + Im(C)^2)}. \quad (5.3)$$

A signal that consists of two frequency components, f_1 and f_2, is analysed in order to explore the relationship between the instantaneous frequency and the two frequency components. Assuming that C_1 and C_2 are two single sinusoid complex signals, the instantaneous frequency of the superposed signal is:

$$f_i = \frac{1}{2\pi}\frac{d}{dt}tan^{-1}\left(\frac{Im(C_1) + Im(C_2)}{Re(C_1) + Re(C_2)}\right), \quad (5.4)$$

which results in:

$$f_i = \frac{1}{2\pi}\frac{d}{dt}tan^{-1}\left(\frac{A_1\sin\alpha + A_2\sin\beta}{A_1\cos\alpha + A_2\cos\beta}\right), \quad (5.5)$$

where A_1 and A_2 are the amplitudes of the two sinusoid signals, and α and β are the phases of the sinusoids C_1 and C_2. The derivatives of α and β are f_1 and f_2. The explicit calculation of the derivative in equation 5.5 yields:

$$f_i = \frac{(A_1\cos\alpha + A_2\cos\beta)(A_1 f_1\cos\alpha + A_2 f_2\cos\beta) + (A_1 f_1\sin\alpha + A_2 f_2\sin\beta)(A_1\sin\alpha + A_2\sin\beta)}{(A_1\cos\alpha + A_2\cos\beta)^2 + (A_1\sin\alpha + A_2\sin\beta)^2} \quad (5.6)$$

In order to simplify this result, we assume that $\alpha = \beta$ when the amplitude of the superposed signal is maximal. In this case, it follows that:

$$f_i = \frac{A_1 f_1 + A_2 f_2}{A_1 + A_2}. \quad (5.7)$$

Similarly, we assume that $\alpha = \pi + \beta$ when the amplitude of the superposed signal is minimal. In this case, it follows that:

$$f_i = \frac{A_1 f_1 - A_2 f_2}{A_1 - A_2}. \qquad (5.8)$$

Consequently, the instantaneous frequency of a signal consists of N frequency components is

$$f_i = \frac{1}{2\pi}\frac{d}{dt} tan^{-1}\left(\frac{\sum_j^N A_j \, sin\, \alpha_j}{\sum_j^N A_j \, cos\, \alpha_j}\right), \qquad (5.9)$$

Which results in

$$f_i = \frac{\left(\sum_j^N A_j f_j \cos\alpha_j\right)\left(\sum_j^N A_j \cos\alpha_j\right) + \left(\sum_j^N A_j \sin\alpha_j\right)\left(\sum_j^N A_j f_j \sin\alpha_j\right)}{2\pi\left(\left(\sum_j^N A_j \cos\alpha_j\right)^2 + \left(\sum_j^N A_j \sin\alpha_j\right)^2\right)}, \qquad (5.10)$$

Where A_j are the amplitudes of the sinusoid signals and α_j are the phases of these sinusoids The derivatives of α_j are the frequency of each sinusoids f_j. If the phases of each sinusoids are same, i.e., $\alpha_j = \alpha \forall j$, then

$$f_i = \frac{\sum_j^N A_j f_j}{\sum_j^N A_j}. \qquad (5.11)$$

These results show that the instantaneous frequency is equal to the amplitude-weighted frequency in the frequency domain when the amplitude of the complex signal is maximal. The instantaneous frequency may be singular when the amplitude difference is zero.

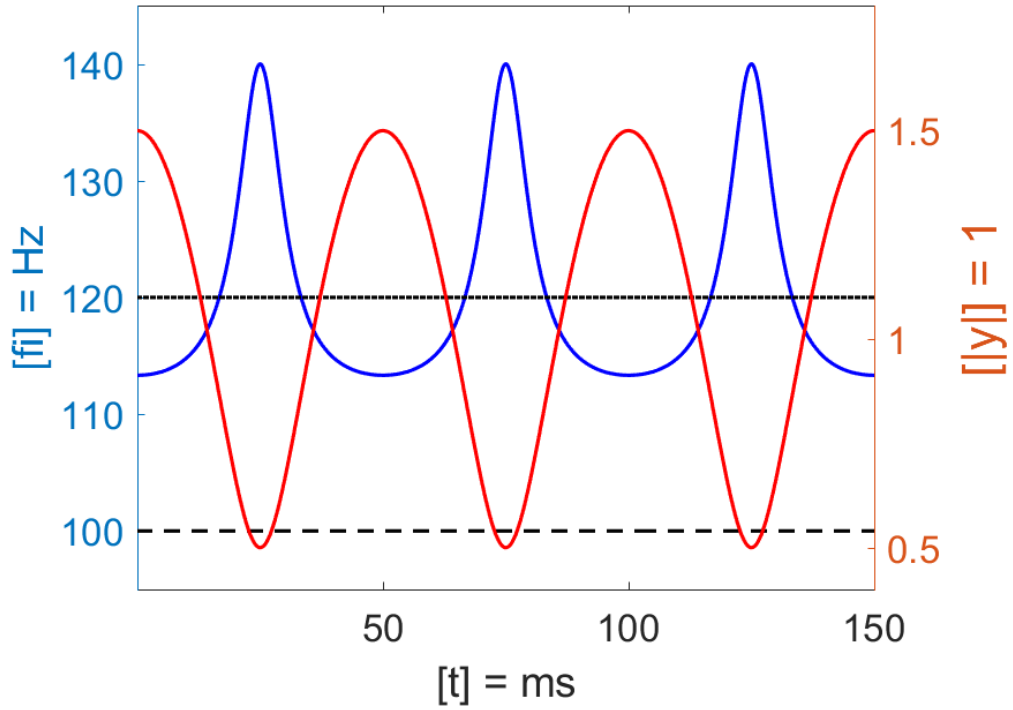

Figure 5.5 The instantaneous frequency of a simulated superposed signal that consists of two frequency components at 100 Hz and 120 Hz (black solid and dashed lines). The calculated instantaneous frequency of the averaged signal (blue line) is more stable, and is equal to the amplitude-weighted average value calculated by equation 5.7 when the amplitude is maximal (red line).

The instantaneous frequency of two frequency components is confirmed by simulating a superposed signal $y = sin(2\pi\times100t) + 2sin(2\pi\times120t)$ (Figure 5.5). The signal is down converted by 110 Hz to compute the complex waveform. The instantaneous frequency is calculated directly from the derivative of the arctangent function (equation 5.3). The instantaneous frequency of a single sinusoid signal is a real constant frequency. The instantaneous frequency of the superposed signal varies depending on the amplitude of the complex waveform. The instantaneous frequency is equal to the amplitude-weighted average value calculated by equation 5.7 when the amplitude is maximal. The instantaneous frequency is not within the range of the two frequency components, and is equal to the result calculated by equation 5.8 when the amplitude is minimal. This simulation result confirms that the instantaneous frequency represents the amplitude-weighted average of the true frequencies in each sample when the amplitude is maximal.

The instantaneous frequency provides no meaningful information about either of the two frequency components when the amplitude is minimal. Therefore, for a real wideband signal, such as lightning, the instantaneous frequency is only a reliable indicator of the true frequency spectrum when the amplitude is maximal.

5.4 Instantaneous Frequencies of Lightning Waveforms

The instantaneous frequency of the average lightning waveform at a distance of 300 km is calculated for different frequency bandwidths (Figure 5.6). At the beginning, the instantaneous frequency is chaotic due to the noise and large sensitivity of the instantaneous phase, and it is only relatively stable during the arrival of the lightning pulse, confirmed by the simulation result in the previous section. In order to emphasize the results during maximum amplitude, the amplitude weighted average instantaneous frequency was calculated by averaging n=20 samples of the dot product between the amplitudes and their instantaneous frequencies divided by the sum of all amplitudes. This amplitude-weighted average of the instantaneous frequency with empirically selected n smooths the original instantaneous frequency but remains most of the frequency variation. This amplitude-weighted average instantaneous frequency is likely to be of benefit for detailed monitoring of the frequency distribution during the lightning period.

The instantaneous frequency of the average lightning waveform propagated over 300 km calculated from 2–18 kHz (Figure 5.3) shows that the instantaneous frequency is smaller than the centre frequency of 10 kHz when the amplitude is at a maximum (Figure 5.6, top). This explains why the rotation direction of the complex waveform during the lightning period is anticlockwise. The result means that the median value of the amplitude-weighted instantaneous frequency from 2–18 kHz during the lightning period is below 10 kHz according to the theoretical analysis explained in the previous section. However, there are several modal maxima in the spectra within this frequency range (Figure 5.2). Each peak in the spectrum may vary differently during the lightning period. As a result, it is better to concentrate on one modal maximum in the spectrum, so that the small variations of each peak during the lightning period can be observed individually. The instantaneous frequency calculated from a narrowband frequency range around one

peak in the spectrum (See Figure 5.2, frequency range from 8.8–12.8 kHz) is much less variable (Figure 5.6, bottom). The instantaneous frequency around the lightning pulse is almost constant, indicating that the frequency distribution during the lightning period is stable.

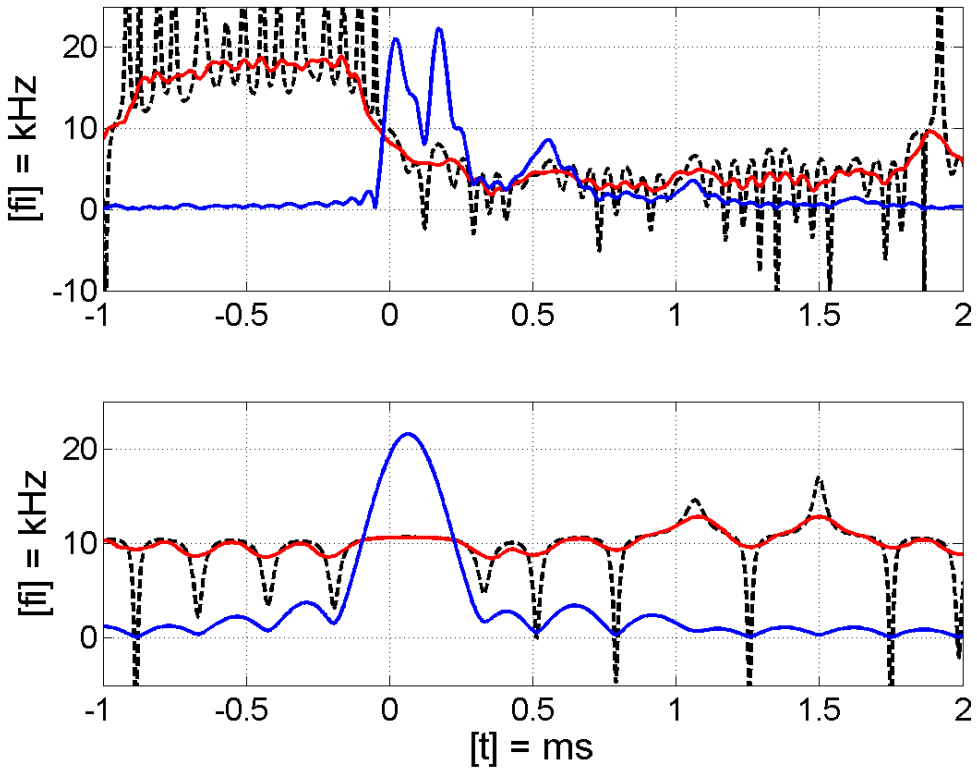

Figure 5.6 The instantaneous frequency (black dashed line) calculated from a lightning waveform with two frequency bandwidths, 2–18 kHz (top) and 8.8–12.8 kHz (bottom), confirms the theoretical result that the instantaneous frequency is more stable when the amplitude of the signal is maximal (blue line). The amplitude-weighted average instantaneous frequency (red line) smooths the original instantaneous frequency. The instantaneous frequency calculated from a 4 kHz bandwidth around one modal maximum in the spectrum is less variable than using a bandwidth from 2–18 kHz, which contains many modal maxima.

As a result, the instantaneous frequency at the maximum amplitude is selected to represent the median frequency during the lightning period. The instantaneous frequencies at the maximum amplitudes of the lightning waveforms from similar

distances are compared to determine the differences between individual events (Figure 5.7). As discussed above, a narrow frequency bandwidth of 4 kHz is chosen with a varying centre frequency, in order to constrain the target frequency range around the same modal maximum in the spectrum. These varying centre frequencies are selected from the maxima of the second modal peak, which always falls between 10–20 kHz in the spectrum, for example at 300 km, 350 km and 400 km distance. The instantaneous frequencies at the maximum amplitudes are calculated for all the waveforms recorded by one station, and the distribution of the instantaneous frequencies in the same distance bin shows a clearly peaked distribution (Figure 5.7). This indicates that the instantaneous frequencies within one distance bin are range limited. The centre frequencies associated with the main peaks of the distributions are clearly distance dependent as a result of radio wave propagation. In other words, the instantaneous frequency inferred from the average lightning waveform can be used to represent the source receiver distance.

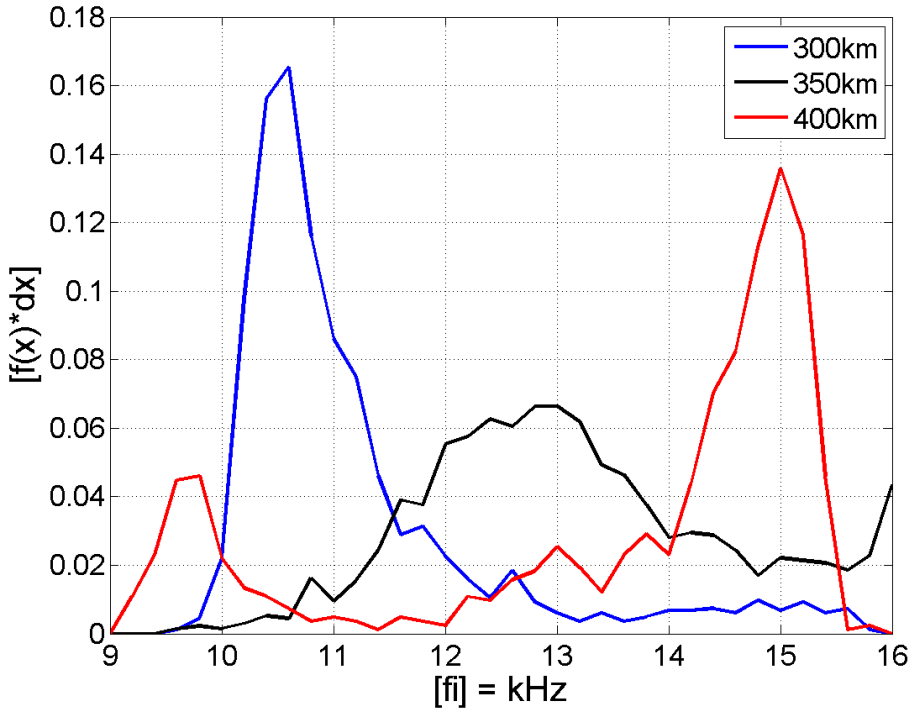

Figure 5.7 The distributions of the instantaneous frequencies at maximum amplitudes inferred from all the lightning waveforms recorded by one station at several distance bins are clearly peaked distributions.

This idea can be tested by extending the analysis to the average lightning waveforms from 300–600 km in each distance bin separated by 10 km in the frequency range 10–20 kHz (Figure 5.8). The calculated instantaneous frequencies are obviously distance dependent and closely follow the second modal maximum in the spectra. This excellent result strongly suggests that instantaneous frequency has a promising potential application for determining the lightning distance from a single radio receiver.

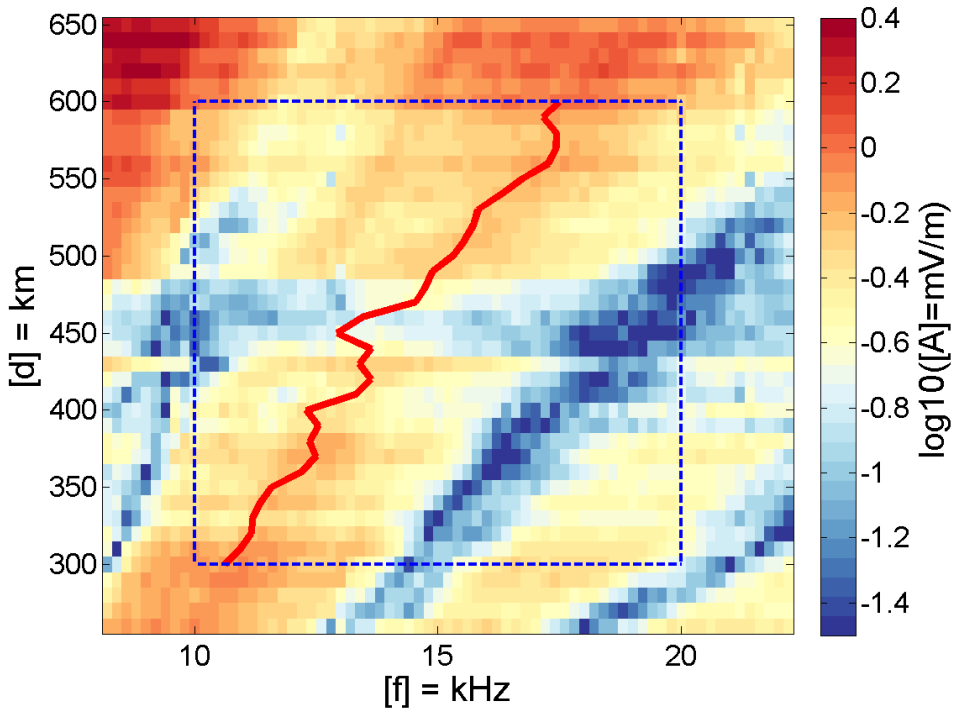

Figure 5.8 The instantaneous frequencies (red line) at maximum amplitudes of the average lightning waveforms at distances ranging from 300–600 km (blue square) follow the modal maximum in the spectra well.

5.5 Discussion and Conclusion

The lightning waveform bank produced for distances up to 1000 km with a spatial resolution of 10 km is well suited for use in studying long-baseline lightning location systems and electromagnetic wave propagation. For most lightning location systems, the baseline is smaller than 1000 km so we can simulate and examine a new location algorithm or new site deployment. For wave propagation and ionospheric research, this waveform bank is valuable as a reference for modelling [*e.g. Pasko and Fullekrug, 2011*].

In particular, spectra have been calculated across a lightning waveform bank, to reveal a sequence of consecutive modal maxima depending on distance and frequency. This waveform bank is generated from lightning recordings of a thunderstorm in Europe, which may not be identical to waveform banks calculated for other geographical areas and which limits the propagation distance less than 1000 km. However, the general method of producing the waveform bank and the spectral waveform bank is applicable to other recordings and longer distance than 1000 km in the future. In addition, this method is also applicable to study other types of lightning, such as, IC events.

To the best of our knowledge, the complex waveform bank analysis of lightning is used here for the first time, providing an opportunity to extract the instantaneous phase and instantaneous frequency. Determination of distance using the instantaneous frequency is just one potential application of this complex waveform bank. The instantaneous frequency may also, given more data, be determined by different arrival azimuths, elevation angle or different times of day. For example, it is observed that a different incident elevation angle indicates a different rotation direction in the complex waveform of the lightning, i.e., a different instantaneous frequency [*Fullekrug et al., 2016, Figure 2, right*]. By using the instantaneous frequency for distance determination, the lightning signal can be first approximated within <50 km, because the instantaneous frequency can vary, e.g. between 400 km and 450 km distance (Figure 5.8). This uncertainty is very likely due to the lack of data at these distances, which could be improved by collecting more data with longer recordings. On the other hand, the instantaneous frequency is calculated based on each lightning waveform that involves the interference from local noise environment of each station. It is proven that the distribution of instantaneous frequencies from lightning at similar distances shows a clearly peaked distribution if they are recorded at the same station (Figure 5.7). The distributions may differ slightly between different stations, most probably due to varying local radio environments and/or different propagation paths. As a result, determining distance using instantaneous frequency may be more accurate if the reference instantaneous frequencies are derived from each station separately.

In summary, this study has offered several results: (1) The average lightning waveforms from different distances exhibit a sequence of consecutive maxima resulting from

ionospheric reflections, which can be used for radio propagation studies, lightning modelling, lightning detection simulation, etc. (2) In the spectral waveform bank, the sequence of consecutive modal maxima is separated by distinct minima at different frequencies and distances. (3) Long-baseline lightning location can achieve sub-sampling time accuracy using the instantaneous phase of the complex lightning waveform. (4) The instantaneous frequency calculated from average lightning waveforms has been shown to be distance dependent, and therefore has the potential to be used for determination of lightning distance.

Chapter 6 Variable Phase Propagation Velocity for Long-baseline Lightning Receiver Array

6.1 Introduction

All lightning location techniques are based on recording radio waves that propagate from lightning discharges to the receivers. Radio wave propagation depends on numerous factors such as the frequency, ionospheric height, terrain, and ground conductivity [e.g., *Schonland et al., 1940; Barr et al., 2000*]. This natural variability results in uncertainties for the computed lightning locations. An improved understanding of the underlying physics of lightning location uncertainties enables novel opportunities toward improving the ATD method [*Cummins et al., 2010*]. Correcting timing errors caused by propagation effects are important for each lightning detection sensor in a network [*e.g. Honma et al., 1998; Schulz et al., 2016*]. There have been many studies of time delay and amplitude attenuation due to electromagnetic wave propagation over different ground conductivities [*e.g. Cooray et al., 1983; Caligaris et al., 2008; Cooray et al., 2009;*] and terrain [*Li et al., 2015; Li et al., 2016 (a,b)*]. These effects result in a wave propagation velocity that has direct influence on the determination of lightning locations, and might enable improvements to the geolocation accuracy of lightning discharges [e.g., *Jean et al., 1960*; *Steele and Chilton, 1964; Chapman et al., 1966; Dowden et al., 2002*].

Long range lightning location systems commonly use the group velocity, which is always less than or equal to the speed of light. The group velocity ($Vg=\delta\omega/\delta k$) is the velocity of a group of waves within an amplitude envelope. The phase velocity ($Vp=\omega/k$) determines the change of phase at a given location of one radio frequency component. For long-baseline lightning location systems (>400 km), the received radio waves are normally a mixture of ground wave and sky waves, i.e. ionosphere hops. The contribution of the sky

wave results in an elevation angle of the incident wave, which is seen by a receiver array as the slowness of the wave [e.g., *Fullekrug et al., 2015*]. The word 'slowness' is used in seismology, and it is suggested here to use the word 'phase propagation velocity' for radio waves. The phase propagation velocity is affected by the wave arrival elevation angle (θ) and the wave arrival velocity (*Vg*), which is influenced by the ground and ionospheric parameters. This phase propagation velocity ($Vg/cos\theta$) is meant to be the velocity as it appears to a receiver array, considering the elevation angle of the incident wave. For example, the phase propagation velocity will be infinite if the wave arrives with a ~90° elevation angle at the receiver array. The phase propagation velocity will be the group velocity if the wave arrives horizontally with a 0° elevation angle. This velocity with a given elevation angle is suitable for 2D lightning location calculation because the propagation distances are normally inferred from ground paths.

The scientific literature reports contradictory results on whether the phase velocity in Very Low Frequency (VLF) transmissions is larger or smaller than the speed of light in the Earth-ionosphere waveguide [e.g., *Jean et al*., 1960; *Steele and Chilton, 1964*]. To resolve this controversy, it would be helpful to investigate VLF transmissions with the aim of inferring the phase propagation velocity that results from the effects of sky and ground waves in a steady-state transmission. This contribution of sky waves and ground effects may also influence the performance of long-baseline lightning location systems, such as the UK MetOffice ATDnet [*Bennett et al., 2011*]. The experimental long-baseline lightning receiver array with >400 km receiver separation uses the frequency range from 5 kHz to 15 kHz, which contains a significant portion of the electromagnetic energy deposited by lightning return strokes [*Fullekrug, 2013b*]. A novel technique using variable phase propagation velocity is proposed here to mitigate the impact of sky waves and ground effects on the determination of lightning locations and to study the spatial variability of the phase propagation velocity in the given frequency range over central France.

An experimental long-baseline lightning receiver array was deployed in Western Europe (Chapter 3) and recorded electric field strengths continuously from 15:00 until 24:00 (UTC) on August 8th, 2014, when a mesoscale convective system developed over central France.

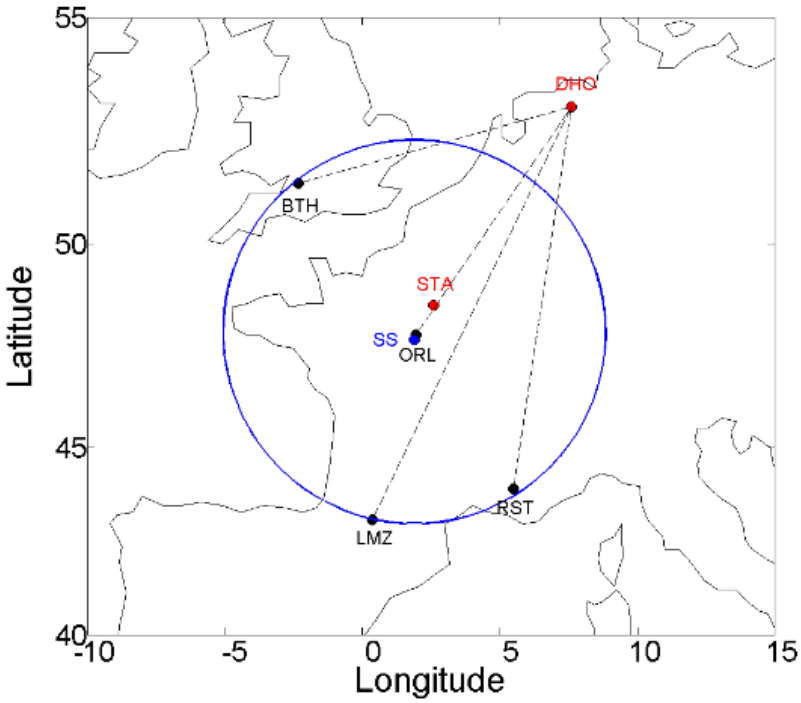

Figure 6.1 The geometry of the experiment. The locations of the two VLF transmitters (red dots) and the long-baseline (>400 km) radio receivers (black dots) used in this study. The circle (blue line) that determines the inside and outside of the receiver array is centred on the sweet spot (blue dot) of the receivers.

6.2 Phase Propagation Velocities of Radio Waves from VLF Communication Transmitters

Low frequency radio waves are a mixture of ground waves and sky waves such that the waves arrive at a radio receiver with a certain elevation angle [e.g., *Fullekrug et al., 2015*]. In order to assess the impact of the elevation angles of sky waves and ground effects, the phase propagation velocities of radio waves from well-known VLF submarine communication transmitters that operate near ~20 kHz were calculated for comparison with the previous conflicting results [e.g., *Jean et al., 1960*; *Steele and Chilton, 1964*]. The phase propagation velocities were inferred from the time delay of the radio signals received at different locations, and the corresponding distance differences between different propagation paths from the transmitters to the receivers. The main benefit from

studying VLF transmissions is their well-known transmission property [e.g., *Thomson, 2010*] and the locations of the radio transmitters [e.g., *Fullekrug et al*., *2015, supplement*].

In this study, transmissions from the French VLF transmitter in Sainte Assise (STA), operating at 20.9 kHz, and the German VLF transmitter (DHO) in Rhauderfehn, operating at 23.4 kHz, during a quiet period at night were used. These transmissions were chosen because their operating frequencies are close to the frequency range of the experimental lightning receiver array (5–15 kHz) and also because the transmitters are located inside and outside of the radio receiver array (Figure 6.1).

The time dependent radio signal was treated as an analytic signal, or complex trace. This allowed for the determination of the instantaneous phase at each sample in the time series (Section 5.2.2). The calculated complex transmission signal was down converted to the base current, and a low-pass filter was applied to extract the target frequency band, which is normally 150 Hz single sided bandwidth for VLF transmitters. The instantaneous phase was then inferred. Cyclic ambiguities occur when comparing the instantaneous phase between different recordings when the propagation path is longer than the wavelength of the radio wave. To avoid such ambiguities, the recorded waveforms were shifted by the propagation time from the transmitter to the receiver with an assumed propagation velocity. The shifted waveforms were calculated by multiplication with the time shift operator, $e^{-j\omega\Delta t}$, in the frequency domain, with Δt as the propagation time. To a first order approximation, the propagation time is $\Delta t = d/c$, where d is the propagation distance, and c is the assumed propagation velocity at the speed of light.

The phase propagation velocity is $v=d/t$, where d is distance and t is time. Assuming the velocities are the same for different propagation paths to a first order approximation, the velocity can be determined as $v=\Delta d/\Delta t$, where Δd is the differences in distance between two propagation paths, d_1-d_2, and Δt is the time difference that results from the wave propagation, $\Delta d/c + \delta t$. The phase propagation velocity, v, for one pair of receivers can then be inferred from:

$$v = \frac{\Delta d}{\frac{\Delta d}{c} + \delta t}, \qquad (6.1)$$

where $\delta t = \delta\varphi/\omega$ is the time residual calculated from the observed phase residual $\delta\varphi$ measured with respect to the speed of light after shifting the two down converted complex traces, and ω is the angular carrier frequency of the radio wave. The signs of these differences need to be consistent. The time residual δt of the shifted waveform between pairs of receivers will be zero if the radio waves propagate at exactly at the speed of light, i.e. v=c.

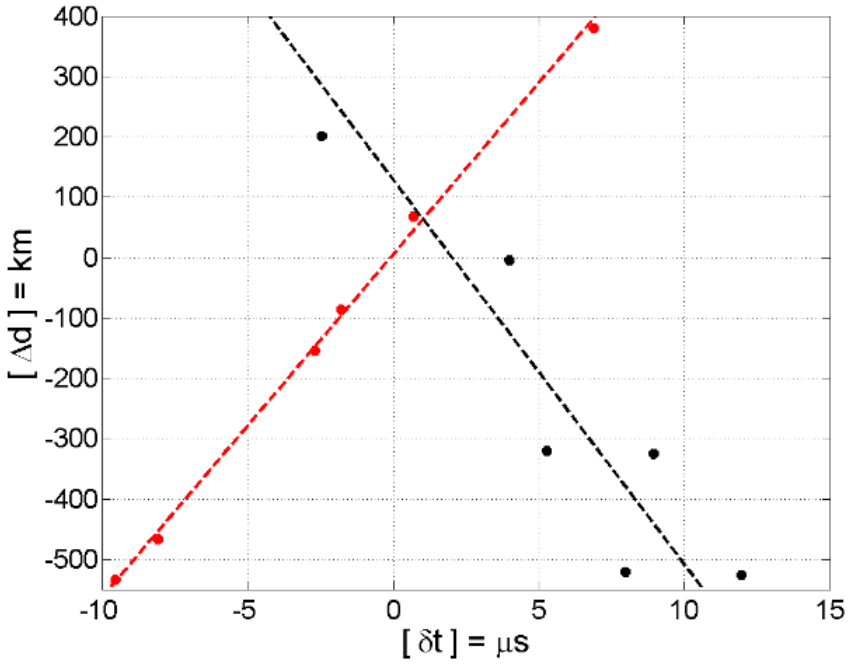

Figure 6.2 The measured phase velocities inferred from two VLF transmitters. The stable ratio of differences in distance and the measured time differences between the transmitters and the radio receiver pairs indicate a fixed phase propagation velocity that is larger than the speed of light for DHO (black) and smaller than the speed of light for STA (red).

The time residuals between pairs of receivers for the two transmitters depend on the differences in distance between the transmitters and the receivers (Figure 6.2). Equation 6.3 can be reformulated to determine the ratio between the distance and time differences $\Delta d/\delta t = v * c/(c - v)$. A fixed ratio between Δd and δt corresponds to a fixed velocity for the radio wave propagation. The slope of the linear relationship between Δd and δt showed that the averaged phase propagation velocities are practically constant for each of

the transmitters. The phase propagation velocities were ~0.64% faster and ~0.51% slower than the speed of light for the transmitters in Rhauderfehn (DHO) and Sainte Assise (STA), respectively.

This result highlights that it is possible for the phase propagation velocity of a radio wave to be smaller or larger than the speed of light. For example, a phase propagation velocity larger than the speed of light can occur when the radio wave arrives at an array of radio receivers with a certain elevation angle [e.g., *Fullekrug et al., 2015, Figure 2, right, Rost and Thomas, 2002, Figure 1*]. In this case, the radio waves from Rhauderfehn would have a larger phase propagation velocity, possibly because the radio waves arrived from larger elevation angles compared to the transmitter at Sainte Assise which is located inside the radio receiver network. The received VLF transmission consisted of ground and sky waves as a result of waveguide propagation effects. This result strongly suggests that the ground wave is more attenuated for Rhauderfehn than Sainte Assise, since it is located at a larger distance from the network (compare to Figure 6.1, and *Mezentsev and Fullekrug, JGR, 2013, Figure 8*). It follows that the phase propagation velocity depends on the location of the radiation source and the ground parameters along the propagation paths to the radio receivers. This result compares well with results previously reported in the scientific literature [e.g., *Jean et al., 1960*; *Steele and Chilton, 1964*]. Thus, small lightning location uncertainties, caused by the mixture of ground wave and sky waves as a result of waveguide propagation effects, can be introduced if a fixed value for the wave propagation velocity is used in an ATD lightning location system.

6.3 Lightning Location Method and Simulation

The long-baseline lightning receiver array reported here uses an ATD approach in the frequency range 5–15 kHz. This frequency range was chosen because the return stroke deposits most of its energy there, such that the phase is well determined. The signatures from lightning discharges were identified in the recordings and the time differences between pairs of radio signals were determined to calculate the best possible lightning location. In theory, the lightning location is the intersection between the hyperbolas of constant differences in distance that define possible lightning locations. The hyperbola for

each pair of receivers can be determined from the differences in distance between two receivers by multiplication of the measured time of arrival differences with a pre-determined fixed wave propagation velocity [*Dowden et al., 2002*].

The arrival time of the lightning return stroke signal is defined by the first peak, i.e. the nearest local maximum that precedes the absolute maximum in the complex trace in the filtered data. Thus, the time differences between stations are taken as the difference between the corresponding arrival times of the return stroke. This method was used as it has been found to be the best compromise between location accuracy and computational effort. Using the first peak as the arrival time should, in theory, exclude the effect of the sky waves in the transient lightning signal. In practice, it was found that there are still some effects due to the digital filtering. For example, the average distance from the lightning to the receivers was about ~560 km over the recorded 9 hours. The time delay between the ground wave and sky wave was about 95 μs, making a simplified assumption that the ground was flat and the ionosphere was at 90 km in height. The rise time of the return stroke was ~5 μs and the decay time to the half-peak value was 70 to 80 μs [*Rakov, 2013*]. The narrow-band filter broadened the two separate impulses in time such that they overlapped slightly and the peak from the ground wave contained some contribution from the sky wave.

In practice, the ATD method finds the closest match between the measured time differences and the time differences associated with the best possible lightning location. This closest match was determined here by minimizing the Root Mean Square (RMS) value:

$$X_{RMS} = \sqrt{\frac{1}{N}\sum_{n=1}^{N}\left(\Delta t_n - \frac{\Delta d_n}{v}\right)^2}, \qquad (6.2)$$

where N is the number of receiver pairs, Δt_n are the measured time differences between receivers, Δd_n are the differences in distance from the best possible lightning location to the receivers, and v is the wave propagation velocity which defaults to the speed of light in many lightning detection systems.

The wave propagation velocity used in equation 6.2 influences the determination of the lightning locations. As a result, different lightning locations and their corresponding RMS values for several lightning events were calculated for different velocities. For example, one typical lightning discharge occurred inside the lightning receiver array in southern France [43.6929^{o}N 0.6077^{o}E] at 18:01:31 and 189486 μs on 8th August, 2014. The propagation velocity varied in steps of 0.01% within ±0.5% of the speed of light. The variation in the lightning location and RMS value demonstrates the importance of the propagation velocity in the lightning receiver array (Figure 6.3, inset).

The lightning location shifted gradually from northwest to southeast with increasing propagation velocity. The velocity with the minimum RMS value was 0.17% slower than the speed of light. The distance between the location with the minimum RMS value and the location calculated with the speed of light was ~700 m. This suggests that a fixed wave propagation velocity can introduce hundreds to thousands of metres difference in the determined lightning location if the radio waves from lightning discharges do not propagate at the speed of light.

6.4 Lightning Locations Inferred from Variable Phase Propagation Velocity

Phase propagation velocities of VLF radio waves are slightly different from the speed of light, as demonstrated by the observed phase propagation velocities of the VLF transmissions for submarine communication. In order to reduce the location uncertainty caused by the use of a fixed velocity, a variable phase propagation velocity was implemented in the lightning receiver array. This step is based on the idea that the phase propagation velocities for different wave propagation paths vary as a result of sky wave contributions and ground effects. The calculated locations with variable phase propagation velocities were possibly closer to the real lightning location because real wave propagation is more complex than light travelling through a vacuum. The lightning locations inferred from variable phase propagation velocities and fixed velocities were compared for many events.

At least three independent time differences are necessary to enable the unique determination of three independent parameters, i.e. latitude, longitude, and the phase propagation velocity. This calculated phase propagation velocity represents an averaged phase propagation velocity for the 5–15 kHz frequency range along the propagation paths from that particular lightning location to all the radio receivers. The phase propagation velocity calculated from the optimization of the RMS function in equation 6.2 needs to be constrained because the propagation velocity cannot be largely different from the speed of light even if it differs slightly from the speed of light. The phase propagation velocities inferred from the radio waves of lightning discharges were calculated using the data recorded from 18:00 to 19:00 (UTC) on 8th August 2014. About ~68% ($\pm 1\,\sigma$) of the calculated phase propagation velocities did not exceed ±1.5% of the speed of light. Thus, results with a phase propagation velocity outside this range were considered to be questionable, possibly as a result of interference, such that these phase propagation velocities were not used in further analysis. More than 80% of the calculated phase propagation velocities were slower than the speed of light, possibly because most of the contribution from sky waves was mitigated by the time difference selection method described in Section 4. The lightning locations inferred from fixed velocities and variable phase propagation velocities in France were roughly similar on a large scale (Figure 6.3).

In order to assess the performance of this novel lightning location method, the locations calculated by the variable phase propagation velocity and the fixed velocity were compared to the lightning locations reported by the commercial lightning location system ATDnet of the UK MetOffice (Figure 6.4). ATDnet is the first lightning detection network used in Europe [*Lee, 1986; Lewis, 1960*]. It has more radio receivers, and the receivers are more evenly distributed across Europe than the experimental lightning receiver array investigated here, such that the results of ATDnet can be taken as ground truth. The distances between the lightning locations inferred from variable phase propagation velocities and the lightning locations reported by ATDnet were smaller than the distances between the locations inferred from the speed of light and the locations reported by ATDnet. The average improvement of the distances to ATDnet locations was ~890 m, and the most likely improvement of the distances was ~1.06 km. A similar result was inferred from a comparison to the locations reported by the lightning location system Meteorage. Using variable phase propagation velocities the calculated results were ~0.78

km closer to Meteorage locations. Meteorage uses shorter distances between receivers such that the contributions of sky waves to the observed radio waves are negligible compared to long-baseline lightning detection networks. The improvement of the lightning locations by ~0.89–1.06 km therefore indicates that the use of variable phase propagation velocities for lightning location mitigates the effect of sky wave contributions and ground effects.

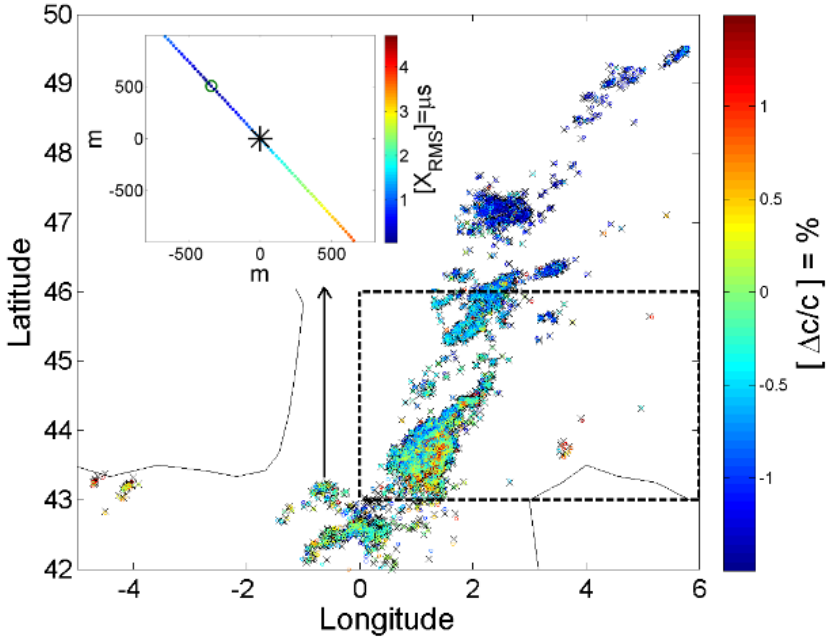

Figure 6.3 The lightning locations inferred from variable phase propagation velocities. The lightning locations inferred from a variable phase propagation velocity (coloured circles) were compared to locations inferred from a fixed velocity (grey crosses) during one hour of recording. The deviations from propagation at the speed of light exhibited a smooth spatial change (colour). The thunderstorm moved north-eastwards where numerous lightning discharges occurred, which were used to map the phase propagation velocity (dashed area). (inset) The calculated lightning location moved from northwest to southeast when the propagation velocity varied from 0.995c to 1.005c, where the colour indicates the RMS value of the time differences. The location calculated with the speed of light (cross) was 700 m away from the location with the minimum RMS (circle).

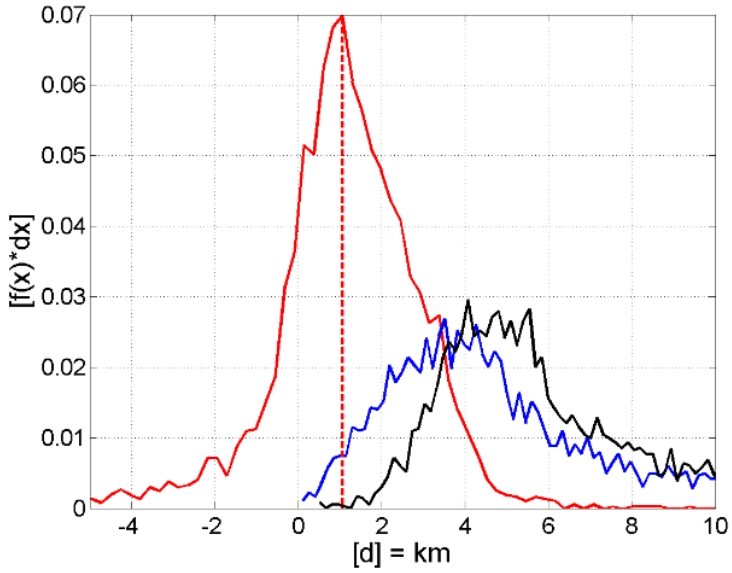

Figure 6.4 The comparison between the lightning locations inferred from variable phase propagation velocities and ATDnet locations reported by the UK MetOffice. The lightning locations inferred from the variable velocity (blue line) and fixed velocity (black line) were compared with lightning locations reported by the UK MetOffice. The comparison indicates an improvement of the average location accuracy by ~890 m (red line) when using the variable phase propagation velocity.

6.5 Velocity Map

The calculated phase propagation velocities in the given frequency range were very similar in neighbouring areas, and exhibited a distinct smooth change over larger areas (Figure 6.3). This observation led to the idea of creating a velocity map to characterize the mitigation of sky wave contributions and ground effects over a larger area. The velocity map uses one representative phase propagation velocity over a small area if the observed phase propagation velocities in this area fit a normal distribution well.

Radio signals from more than thirty thousand lightning discharges were recorded within ~9 hours in an area extending from 0°–6°E and from 43°–46°N on 8th August, 2014. The area of interest was divided into grid cells of 0.5° in latitude and longitude for analysis. Note that the grid cells were not square in distance because the latitudes are not great

circles. This grid cell size was chosen as a trade-off between spatial resolution and getting large enough sample populations of lightning discharges in individual cells.

The statistical stability of the phase propagation velocities in a grid cell was tested before calculation of the velocity map. The velocity distributions in two example grid cells fitted different normal distributions well (Figure 6.5, top). The mean velocities for these two grid cells were 0.9965c and 1.0033c, with standard deviations of 0.0044c and 0.0042c, respectively. The mean velocities therefore differed significantly from the speed of light. The distributions within the example grid cells demonstrated that the mean phase propagation velocity appropriately represents the distributions of phase propagation velocities in a small region.

The mean phase propagation velocities for each individual grid cell were different (Figure 6.5, bottom). A few grid cells (shown in white) contained fewer than forty events – too few to support a statistically meaningful result. For two grid cells with poor statistical distributions, i.e., grid cells from 44°–44.5° N, 5.5°–6° E and 44.5°–45° N, 1.5°–2° E, the median phase propagation velocities were unusually small and large, respectively, and were hence excluded from further analysis. For most grid cells, the phase propagation velocities were smaller than the speed of light by ~0.1–1%. There were also some locations that showed a mean phase propagation velocity larger than the speed of light. This observation indicates that these radio waves did not arrive from the horizon at zero elevation angles, similar to the radio transmissions described in Section 3.

Assuming that the mean phase propagation velocity for each grid cell represents the phase propagation velocity in the given frequency range for the centre location, contour lines can be drawn between the centres to produce a smoothed velocity map (Figure 6.6, top). The phase propagation velocities in the two invalid grid cells are replaced by the mean values of their surrounding grid cells. The velocities of the grid cells with too few samples are filled by the median value of all the other phase propagation velocities. The final map shows a smooth variation of the phase propagation velocities across the studied area.

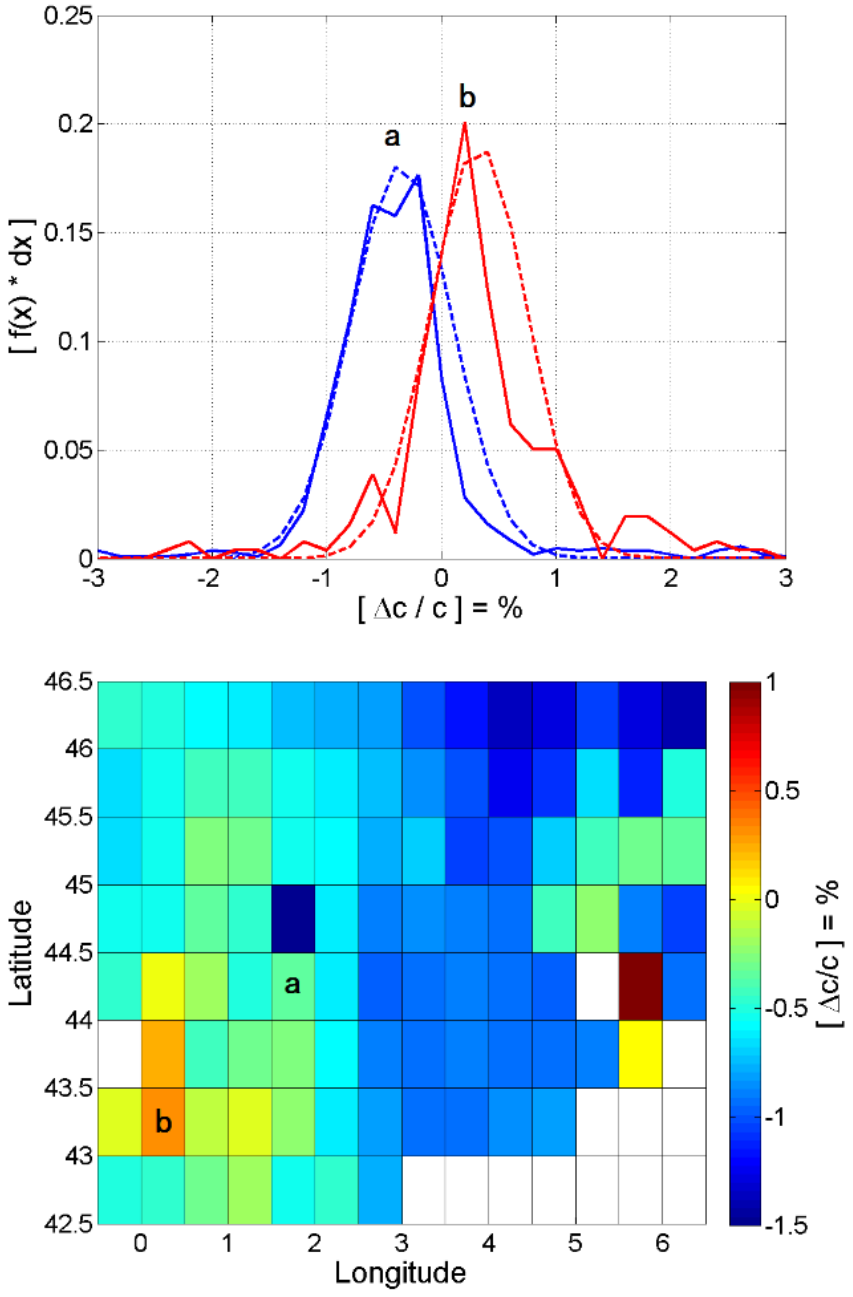

Figure 6.5 The velocity map and the distributions in two grid cells of the map. (top) The velocity distributions (solid lines) of two sample grid cells compare well to normal distributions with small standard deviations (dashed lines). One grid cell extends from 44°–44.5° N and 1.5°–2° E (blue line) and the second grid cell extends from 43°–43.5° N and 0°–0.5° E (red line). (bottom) The velocity map is composed of individual grid cells that exhibit a smooth spatial gradient. The white grid cells have fewer than 40 lightning discharges and are therefore not shown.

6.6 Discussion and Conclusion

A comparison of the inferred lightning locations with the lightning locations reported by ATDnet and Meteorage as ground truth strongly suggests that the lightning locations inferred from the variable phase propagation velocity are more accurate than the locations inferred from the fixed velocity in this VLF long-baseline lightning receiver array. This increase in accuracy is attributed to the ability of the variable phase propagation velocity to mitigate the influence of sky waves and ground effects on the calculation of the lightning location. It is interesting to note that ATDnet uses a fixed velocity for the calculation of their lightning locations. It therefore appears plausible that these lightning locations could also be improved by use of variable velocities to mitigate sky wave contributions, but perhaps to a smaller degree because ATDnet uses more radio receivers. For more resource intensive short-baseline lightning location networks that use mainly ground waves to determine lightning locations, variable velocities could only mitigate wave propagation effects associated with variations of the ground conductivity and terrain. The velocities inferred from the calculated velocity map are applicable to be integrated into this novel method for improving location accuracy. For example, these velocities can be used as the weight or the constraint by using the variable phase propagation velocity, which can deduce the computation time and improve the location accuracy.

The velocity map shows a smooth spatial variation of the phase propagation velocities from radio waves of lightning discharges in central and southern France. This velocity map represents the propagation velocities of radio waves from lightning discharges as they appear to the lightning receiver array. The map of phase propagation velocities therefore reflects the average impact of sky waves and ground waves on the calculation of lightning locations as a result of the network configuration, i.e., the different propagation paths between the lightning locations and the radio receivers. It is conceivable that the map of phase propagation velocities is a combined product of ground wave propagation influenced by the ground conductivity and sky wave propagation influenced by ionospheric conductivity.

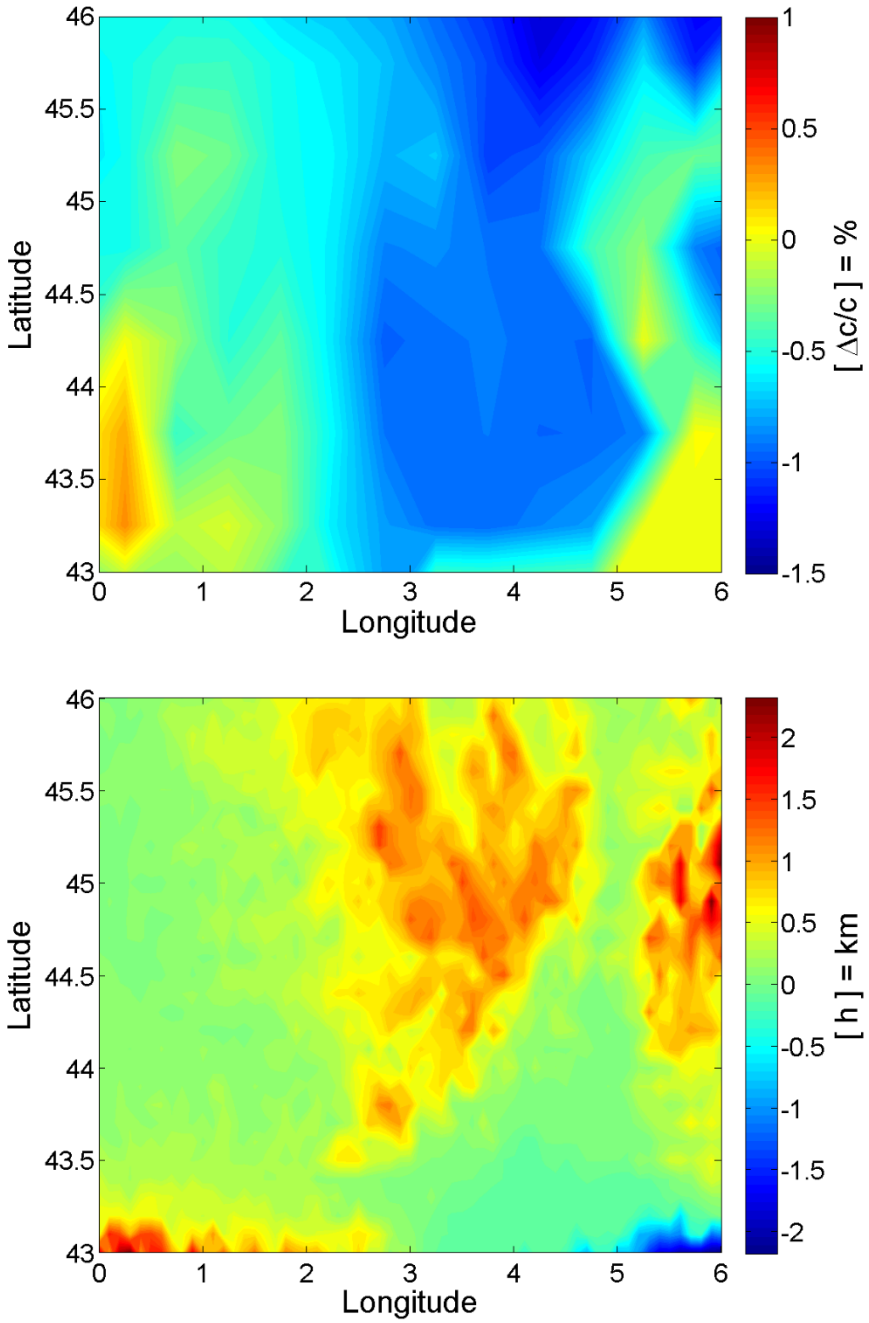

Figure 6.6 Comparison of the final velocity map with a map of the topographic elevation. (top) The final velocity map is calculated from the interpolated contours of the individual grid cells, and exhibits a smooth spatial change. (bottom) The topographic elevation map shows the Massif Central in the centre of France, and exhibits a similar pattern when compared to the final velocity map. The area of high elevation represents mountains and the area of negative elevation is the seabed of the Mediterranean south of France.

In this case, a phase propagation velocity map could be derived using a denser network of radio receivers and longer recordings to reflect other geophysical properties such as the topography and ground conductivities [*ITU-R, 2015*]. To elucidate this speculative possibility, the map of phase propagation velocities was compared to a terrain elevation map in France (Figure 6.6, bottom). Interestingly, the phase propagation velocities of lightning discharges at higher altitudes were smaller than at lower altitudes. For example, the phase propagation velocities over the mountainous area of the Massif Central were slightly slower than the speed of light, possibly because the mountain peaks disturb radio wave propagation. This result seems to confirm recent modelling work that suggests the time delay of lightning radiated electromagnetic fields can be significantly affected by the presence of mountainous terrain [*Li et al., 2016 a, b*]. The phase propagation velocity in the flatlands can occasionally exceed the speed of light, which indicates the arrival of the radio wave from an elevation angle. This result might possibly be due to the elevation profile or the dispersion caused by the ground conductivity profile along the propagation path, and needs further research. Note that the phase propagation velocity is inferred from differential measurements between receiver pairs, therefore the expectation is that the geophysical property around the source might not be a dominant factor, which possibly explains why the correlation is poor in some grid cells. Nevertheless, it is also possible that the properties of the propagation path near the source have a larger effect on the total phase delay than the properties far away from the source. This is suggested, for example, by the Sommerfeld-Norton attenuation function over a flat earth [*e.g. Galejs, 1972, Figure 9.3*] with a potential similar effect for inhomogeneous conductivity of the earth [*e.g. King, 1966*]. It therefore appears promising to compare various phase propagation velocity maps inferred from other lightning detection networks to identify the influence of geographic features on VLF radio wave propagation [Barr *et al., 2000*].

The relationship between the phase propagation velocity and ionospheric conditions is another promising area for future research. The observed phase propagation velocities of the transmissions were different when thunderstorms occurred along the propagation path. These ionospheric conditions also changed with time, e.g., the diurnal variability discussed in [*Schonland et al., 1940*]. The studied thunderstorm propagated eastward over 9 hours from day to night. As a result, the characteristics of the wave propagation in different ionospheric conditions may be revealed by analysing the calculated phase

propagation velocities at different times of day (Figure 6.7). It was observed that the phase propagation velocities inferred from DHO increased from day time to night time, and the velocity variation mainly occurred during the day-night terminator across the receiver network. Variation in the phase propagation velocity was dominated by the change in sky waves, because the ground conductivity remained the same regardless of time. As a result, it is confirmed that variation in ionospheric conditions will result in a different phase propagation velocity.

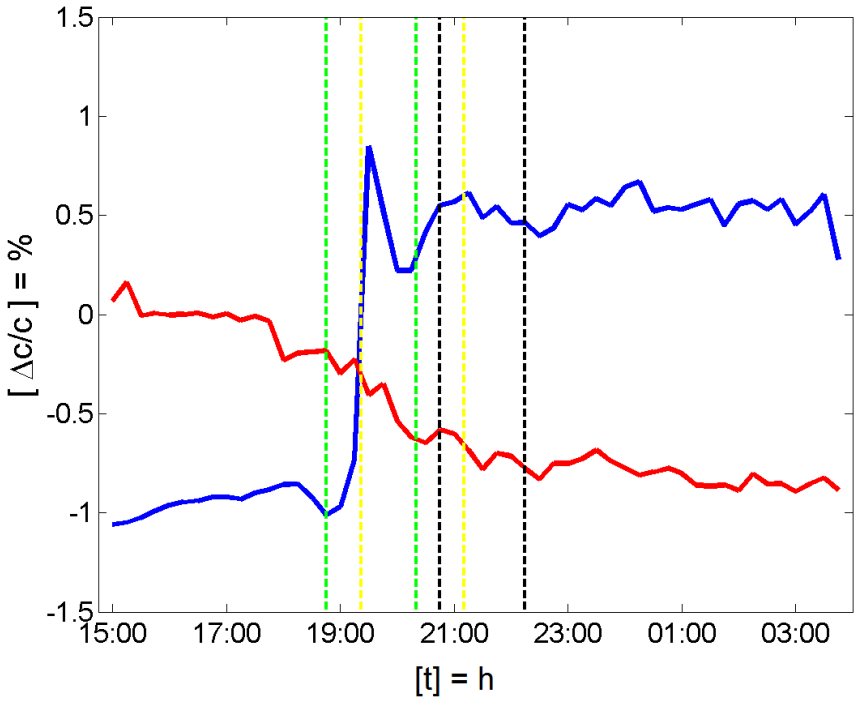

Figure 6.7. Time monitoring of the phase propagation velocities of two VLF transmissions. Green, yellow and black lines indicate the time of the network covered by civil (green), nautical (yellow) and astronomical (black) twilight. The phase propagation velocity of STA (red) is decreasing during the civil twilight passing network, while the velocity of DHO (blue) is increasing.

In summary, this study enabled several results. (1) The phase propagation velocities inferred from radio waves emitted by VLF transmitters can be smaller or larger than the speed of light. (2) Simulations show that lightning locations calculated with different phase propagation velocities can cause deviations of the lightning location by hundreds to

thousands of metres when compared to the location inferred using the speed of light. (3) A long-baseline lightning receiver array that uses variable phase propagation velocities can improve the lightning location accuracy by ~0.89–1.06 km when compared to lightning locations inferred from an array with more radio receivers. (4) As a result of the network configuration, the phase propagation velocities were mapped over central and southern France to summarize the impact of sky waves and ground effects on the calculation of lightning locations. (5) Phase propagation velocities also vary with different ionospheric conditions, e.g. day—night differences.

Chapter 7 Application of Interferometry Technique in a VLF Long-baseline Lightning Receiver Array

7.1 Introduction

The basic ATD algorithm calculates lightning location based on the difference in two time stamps between recordings, and has been very efficient and popular because of limited data communication in the past. In order to investigate more lightning information, nowadays, the interferometry technique can be used due to the increasing capability of big data telecommunication and computational resources. This technique takes advantage of the whole lightning waveform rather than a few samples.

The narrowband interferometer reconstructs the development of lightning discharges using a single station with a pair of antennas [*e.g. Richard and Auffray, 1985; Rhodes et al., 1994; Shao et al., 1995*]. Broadband interferometers, e.g. 40–350 MHz, 20–80 MHz, have subsequently been developed quickly [*e.g. Shao et al., 1996; Ushio et al., 1997; Morimoto et al., 2005; Stock et al., 2014*]. Three dimensional location of lightning sources is achieved with synchronised observations of electric field changes between a few nearby, i.e. ~10 km, sets of broadband interferometers. This broadband interferometry technique was firstly applied in VHF and developed to LF from near-field recordings [*e.g. Stock et al., 2014; Lyu et al., 2014*]. Different radiation sources associated with different lightning processes are located within different frequency ranges, which fits the research about lightning electromagnetic signatures.

For the long-baseline lightning receiver array, the features of received lightning waveforms vary depending on the propagation distance, and most of the weak sources attenuated during a long distance wave propagation. While, the interferometry technique is superior to utilize diminutive differences between recordings for nearby events.

Therefore, the greater the distance between receivers, the more difficult it is to locate sources using the interferometry technique. To resolve this problem, methods to apply the interferometry technique to a long-baseline lightning receiver array are discussed in this work.

The data recorded by an experimental long-baseline (>400 km) receiver array deployed in Western Europe is used for this research. Three possible methods using the interferometry technique are discussed: treating the whole lightning waveform as one signal and shifting the lightning waveforms to each map pixel detect the coincident signal (Section 2), cross-correlating recordings within each short time window to detect coherent sources (Section 3), and calculating lightning locations for each sample using instantaneous phase to specify a lightning area (Section 4). The interferometry techniques described here represent a method of using more samples and information from the original recordings rather than just a time stamp, which may differ from the previous research into interferometers. Different information, e.g. coherent weak sources and lightning location for each sample, can be retrieved using these interferometric methods with the long-baseline receiver array.

7.2 2D Lightning Mapping Calculation

The benefit of developing the interferometry technique is to use the whole lightning waveform from the original recording rather than just a time stamp for calculation of time differences. This section proposes the idea of treating the whole lightning waveform as one signal and shifting the lightning waveforms to each map pixel to detect the coincident signal for a 2D lightning map. The waveforms are shifted by the propagation time from the receivers to each pixel of the earth map with an assumed propagation velocity of the speed of light. The shifted lightning waveforms overlap if the lightning occurs at this pixel. The average amplitude of these overlapping waveforms is maximal if the amplitudes are uniform for all receivers, and their phases are coherent in the ideal case. Conversely, the average amplitude of other pixels is relatively low and the phases are unrelated, because the lightning pulses recorded at different receivers are eliminated, or at

least reduced, because they do not coincide in time. The average amplitude is used as a reference for the electromagnetic energy.

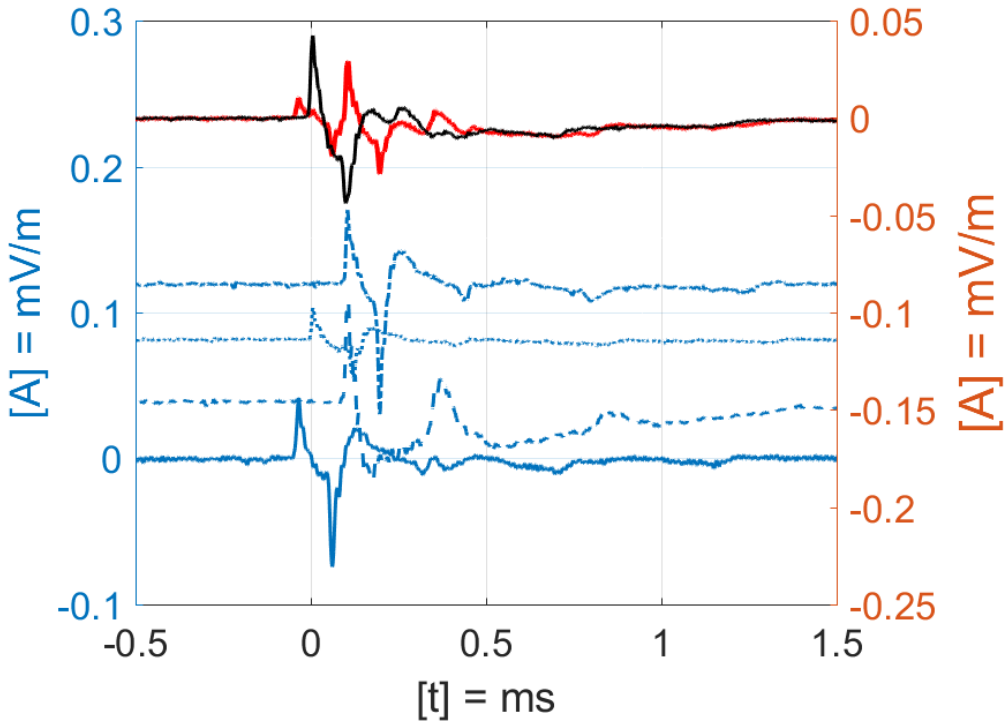

Figure 7.1 The waveforms shifted to an incorrect lightning location pixel (blue lines). The average amplitude of shifted waveforms (red line) present a lower maximum with time delay compared to the average amplitude inferred from the correct lightning location pixel (black line).

These average amplitudes at different pixels make up an electromagnetic energy map at each time period, and form a movie presenting the electromagnetic energy distribution variation with time. Ideally, the radio transmitters can also be located because of the coherent transmission signal, even if the amplitude is much smaller than lightning signal. This ideally uses entire recordings, suitable for lightning and electromagnetic energy monitoring in a certain area. The average waveforms at different distances can be used for theoretical simulation (Section 5.2.1). The simulated lightning recordings at different receivers are selected according to the distance from the assumed lightning location to the receivers, and are separated by the corresponding propagation time. The assumed lightning for this simulation was randomly selected at [47°N 0°E]. In the pixel including

the correct location, all the waveforms are perfectly overlapped and the average amplitude presents an outstanding maximum at the assumed lightning time (Figure 7.1, black line). For comparison, the waveforms shifted to the pixel centred at [47°N 0.5°E] appear with certain time offsets (Figure 7.1, blue lines). The average amplitude of this pixel presents a lower maximum with a time delay (Figure 7.1, red line). This example illustrates that the average amplitude inferred from the correct lightning location pixel can be distinguished from the average amplitude of other pixels.

The average amplitude of waveforms normally exhibits several maxima and a period of large amplitude. This is because the originally recorded lightning sferic waveform contains many peaks due to the effects of wave propagation and instrument filters. In theory, electromagnetic waves are emitted by the lightning discharge, which occurs with a short duration and large amplitude. To simplify the modelling, we assume that the lightning emitted waves are a pulsed signal. Therefore, the received lightning waveform can be understood as the response to the input of a pulsed signal: the Impulse Response (IR). The IR can be calculated by the division between the spectrum of the received lightning waveform and the spectrum of the pulsed input signal, $IR = \mathcal{F}(y_{out}(t))/\mathcal{F}(y_{in}(t))$. Consequently, the input signal can be calculated by the inverse IR with a known received signal and known IR: $y_{in} = \mathcal{F}^{-1}(\mathcal{F}(y_{out}(t))/IR)$.

The features of received lightning waveforms vary depending on the propagation distance according to the average waveform bank (Chapter 5). The impulse responses are calculated based on the average waveforms and hence varies with distance. As a result, the inverse IR can be used for distance estimation (Figure 7.2). The first 0.5 millisecond of the lightning waveform contains most of the information of the lightning, so this is set as the output signal (Figure 7.2, top, red line). The input signal is assumed to be the pulsed signal with a unity peak at '0' time, which can be retrieved by the inverse IR at the corresponding distance (Figure 7.2, middle). The inferred input signal with the inverse IR at an inappropriate distance (e.g. 50 km longer) presents a much smaller peak and a noisy background (Figure 7.2, bottom). The peak amplitudes of the inferred input signals with the inverse IR at different distances are compared (Figure 7.3). It illustrates that the peak amplitude of the inferred input signal decreases with the inverse IR at larger distances from the actual distance.

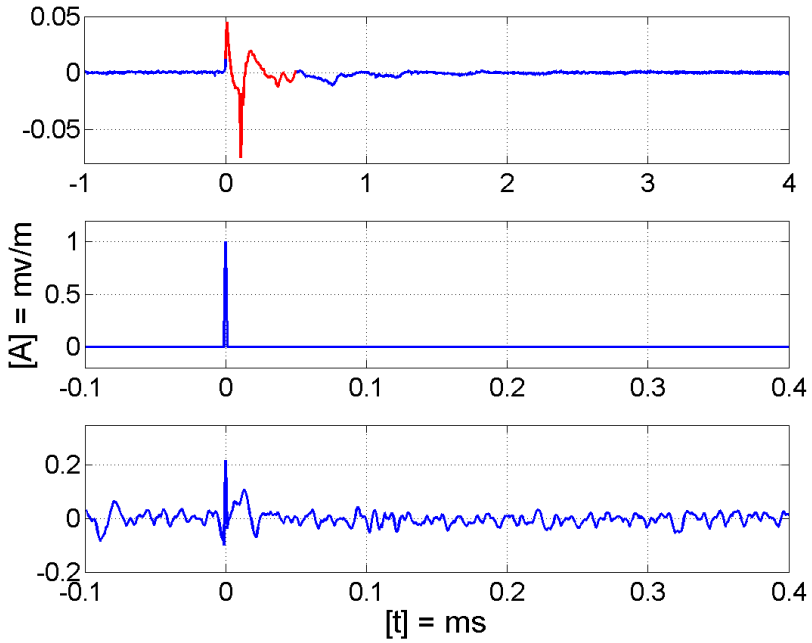

Figure 7.2 Lightning signal analysis with inverse impulse response. (top) the received lightning waveform from a distance of 510 km, (middle) the inferred input signal with the inverse IR at 510 km, (bottom) the inferred input signal with the inverse IR at 560 km.

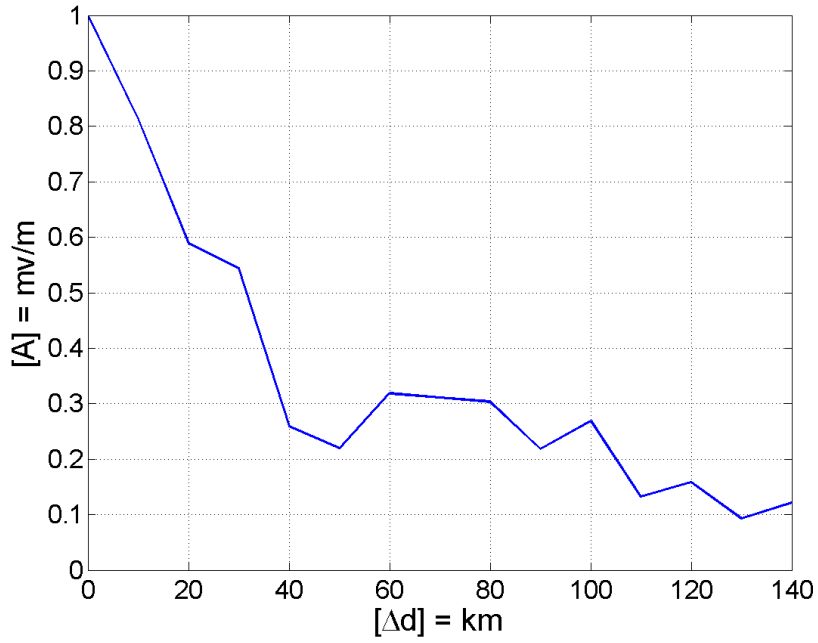

Figure 7.3 The peak amplitude of the inferred input signals with the inverse IR at different distances.

The inverse IR method can be applied to the shifted waveforms to improve the average amplitude result in Figure 7.1. The average amplitude of the inferred input signal for the correct lightning location pixel is a unity impulse. The average amplitudes for other pixels decrease with a further distance to the correct lightning location pixel. As a result, the correct lightning location pixel is observed on this lightning map. It shows that this lightning mapping idea works for this simulation and is the subject for further study using real data.

7.3 Interferometric-ATD Calculation

The generalized cross-correlation algorithm is popular for use with interferometry in the broadband signal in VHF and LF [*e.g. Stock et al., 2014; Lyu et al., 2014*]. The cross-correlation algorithm calculates the similarity between two signals as a function of the displacement of one relative to the other, and can be used to detect coherent radio sources. More sources associated with weak lightning processes are located for a better understanding of lightning physics from near-field recordings. Here, a similar analysis of cross-correlation is applied to the recordings from a long-baseline receiver array. This method is developed in order to detect weaker lightning sources.

The cross-correlations between recordings from each pair of stations are calculated from a 5 ms time window in steps of 2.5 ms. The window length is selected to be slightly larger than the maximum time difference between each pair of receivers, to involve all of the possible time intervals and to cover the least noise. The step length is selected to be half of the window length, in order to avoid omission and repetition. For each time window, a coherent source is identified when the maximum normalized cross-correlation coefficient of each receiver pair is larger than 0.35. This threshold is empirically selected from the distribution of the maximum normalized cross-correlation coefficient distribution, and it is much larger than coefficient inferred from uncorrelated signal by at least 0.05 from comparison.

The cross-correlation coefficient is calculated between each pair of receivers at each time window. Numerous coherent sources are detected from 1-second recordings by this method (Figure 7.4). Normally, the arrival angle of the incident wave is calculated for

VHF interferometer. However, the incident waves to different receivers are entirely different in this case, due to the long distances between each receiver. As a result, the determination of the incident wave elevation angle is not available in this case. The ATD approach is used to calculate the lightning location from the measured time differences. Since the lightning is always far from the receivers, the altitude of these sources cannot be calculated, so it is not possible to define the detailed lightning process of each coherent source. Nevertheless, many of these sources are from weak signals in the original recordings. Most of the locations calculated from the measured time differences of these coherent sources are in central France, where a mesoscale convective system developed at the time of recording. Much fewer events were reported by the lightning location system Meteorage during this second, possibly due to the high amplitude threshold in the pure ATD method. It is also possibly that the fewer coherent events are identified when more stations are used. Nevertheless, it is still promising to apply this interferometric-ATD calculation for more coherent lightning sources.

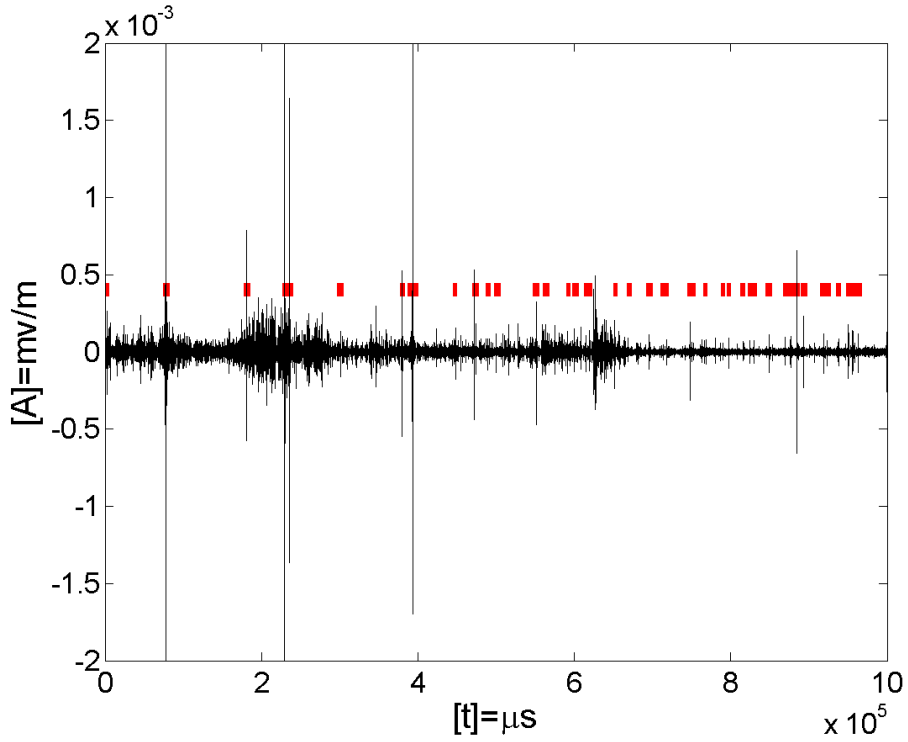

Figure 7.4 The coherent sources (red) determined by the cross-correlation of 1-second data (black) recoded using different receivers at 17:59:49 on 08-08-2014.

7.4 Lightning Location Calculation for Each Sample

Due to the complication of electromagnetic wave propagation over long distances, the measured arrival time differences do not exactly fit the arrival time differences for one specific lightning location. As a result, most lightning location systems report an area using error ellipses, which are normally calculated by the differences between the measured arrival time differences and theoretical time differences from the calculated location.

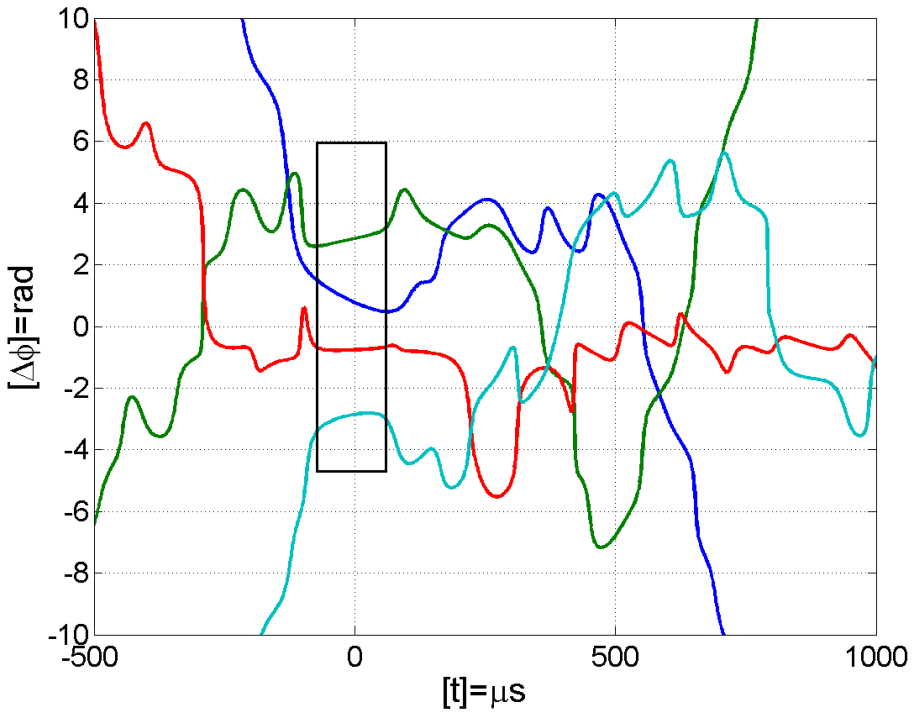

Figure 7.5 The instantaneous phase differences between different receivers of a lightning recording at 18:00:04 on 08-08-2014. The instantaneous phase differences are stable during the lightning arrival time (black square). The time axis is referenced to t=0 corresponding to the peak of the complex envelope.

To calculate this lightning area, a method of calculating the lightning location from each sample is proposed. It is assumed that the actual lightning strike point is within the range of all calculated valid locations for each sample. The instantaneous phase is extracted to achieve subsampling time accuracy for calculating one location for each sample (Chapter

5). In order to retrieve the correct corresponding samples, the lightning waveforms are shifted to ensure that the maximum amplitude of the complex trace from 5–15 kHz is superposed at t=0. The instantaneous phase differences are calculated between the shifted lightning waveform (Figure 7.5). The calculated unwrapped phase at t=0 is constrained to be within $-\pi$ to π in order to avoid cycle ambiguity between waveforms. The instantaneous phase differences are relatively stable during the lightning amplitude peaks, and the derived time differences can be used for calculation of the lightning locations in each sample.

The derived time difference Δt is calculated from the instantaneous phase difference $\Delta\varphi$, and the number of the whole cycle is inferred from shifting the waveform by *n cycles*, i.e. $\Delta t = \left(\frac{\Delta\varphi}{\pi} + n\right) * \frac{1}{f_c}$, where f_c is the centre frequency, e.g. 10 kHz, and $1/f_c$ is the full cycle length. The lightning location is then calculated for each sample based on these derived time differences (Figure 7.6). These locations are calculated using a fixed wave propagation velocity, and also using a variable phase propagation velocity for comparison [*Liu et al., 2016*]. The calculated locations make up a lightning trace, but some of them are unreliable because of the noisy instantaneous phase when the signal to noise ratio (SNR) is low. Valid sample locations are empirically selected by the root mean square (RMS) value (< 27.5 μs) for location inferred with a fixed wave propagation velocity, and the propagation velocity deviation from the speed of light $(\Delta c/c)$ within ±1.5 % [*Liu et al., 2016*] for locations inferred with a variable phase propagation velocity. The instantaneous phase differences of these valid samples may be stable (Figure 7.5). There are 65 sample locations that fit both strict criteria. It is speculated that this 65-μs location trace may be the actual lightning movement. The circle consisting of these 65 locations is the most likely area of lightning occurrence, and this area is smaller when the calculation uses the variable phase propagation velocity. Overall, the lightning locations can be calculated for each sample with the instantaneous phase, and the calculated corresponding lightning area is smaller when using a variable phase propagation velocity for many examples.

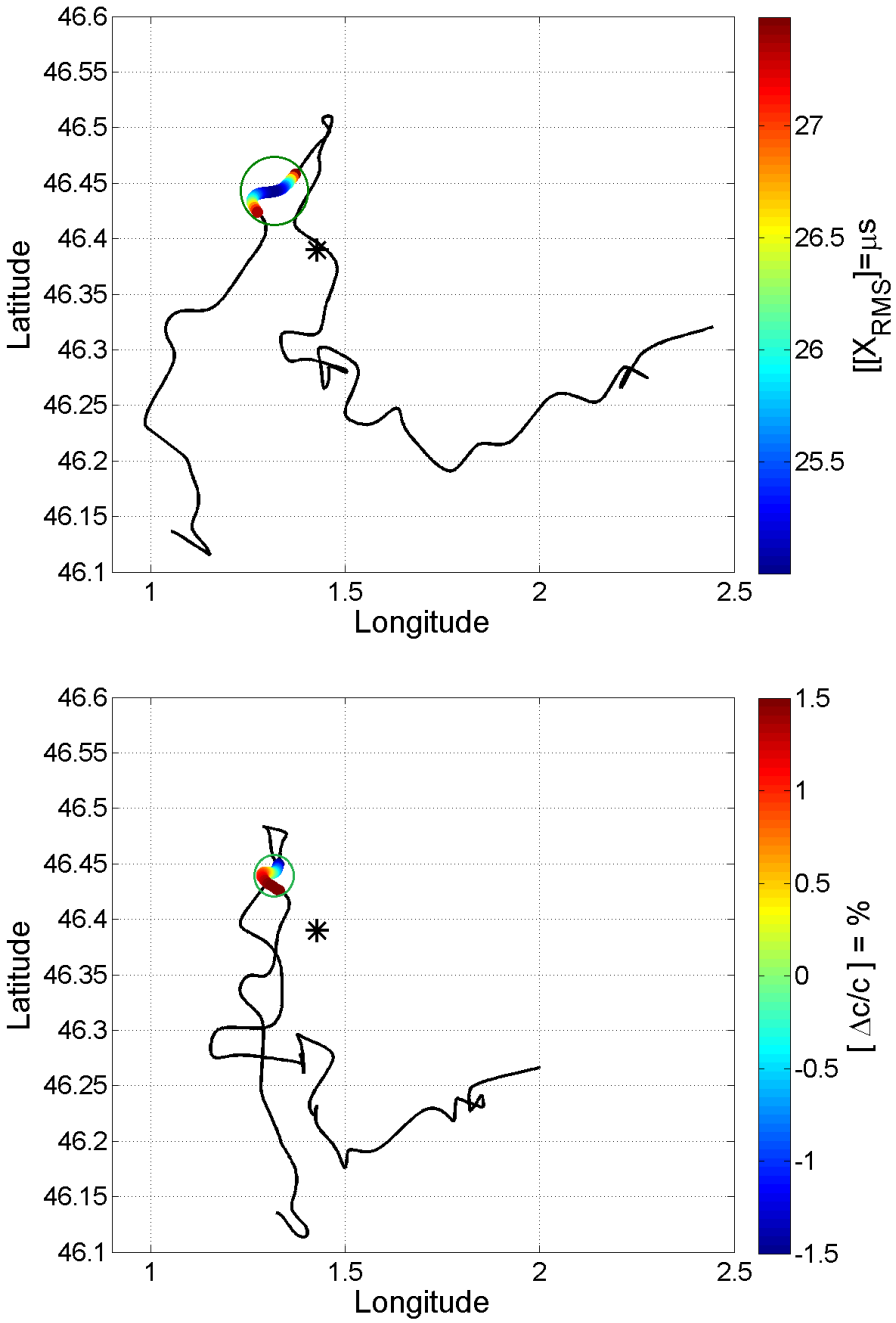

Figure 7.6 Lightning locations calculated for each sample (black line) with a fixed velocity at the speed of light (top) and a variable phase propagation velocity (bottom). 65 sample sources (colour dots) are selected depending on the strict constraint conditions, RMS and calculated phase propagation velocity, which constitute the most likely area of lightning occurrence (green circle). The calculated locations are very closed to the lightning location reported by Meteorage (black star).

7.5 Discussion and Conclusion

The whole lightning waveform is treated as one signal and shifted to each pixel of the earth map for lightning and electromagnetic energy monitoring. The average waveforms at different distances are used in a simulation with the inverse IR. The inferred input signal differs significantly when using the inverse IR at correct or incorrect distances, which can be used for distance determination. The result inferred from the shifted waveforms to the appropriate and inappropriate lightning location pixels is different. As a result, there is potential for creating a 2D lightning mapping algorithm for local area lightning monitoring by shifting recording to each pixel of the earth map. However, this idea may not be applicable to individual waveforms. The distance determination of inverse IR may not perform well for real lightning waveforms, because the SNR of real recordings that are not averaged is relatively low. It is suggested to improve the SNR before applying the inverse IR. For example, the lightning waveform can be filtered by the bandwidth that consists of most lightning energy inferred from the average waveforms.

The generalized cross-correlation algorithm can be used for a long-baseline receiver array. The coherent sources are identified by cross-correlation calculation in each short time window. Many weak lightning radiation sources can be found using this method. The combination of time shifting and cross-correlation algorithm has been attempted in a shorter time window. The recordings were shifted to an approximate location, and the maximum cross-correlation coefficient was calculated in order to detect weaker coherent sources. However, the whole cross-correlation coefficient increases with shorter recordings, and it may introduce numerous spurious coherent sources due to inappropriate selection criteria. It is expected that more and weaker lightning sources can be located using a proper identification mechanism by this method, which is worth further analysis.

The lightning location area was determined by the locations calculated for each sample, assuming that the actual lightning strike point lies within the range of all these valid sample locations. Each location was calculated by the instantaneous phase differences between recordings. The most reliable locations within one lightning were selected based on the criteria for the RMS value and $\Delta c/c$, which may describe the propagation of a

lightning discharge. The circle around these sample locations was determined as the most likely area of lightning occurrence. The stable instantaneous phase differences during the lightning amplitude maxima are the key element for the calculation. Further analysis is suggested into the physical meaning of the location for each sample and the calculated lightning location area.

In summary, this study enables the use of the interferometry technique with a VLF long-baseline receiver array. Three methods, 2D lightning mapping, cross-correlation with a short time window, and lightning location for each sample, are proposed here in order to take advantage of the greater number of samples and phase information from recordings. It is expected that long-range lightning locations can be improved in the future by the use of interferometry technique.

Chapter 8 Conclusions

8.1 Summary

This thesis has investigated VLF electromagnetic waves to mitigate the interference from long distance wave propagation in two aspects: research regarding lightning sferics, and the wave propagation velocity. In addition, the interferometry technique has been preliminarily applied to an experimental long-baseline lightning receiver array in order to take advantage of the greater number of samples and information from the original recording. The results accomplished can be summarised as follows:

- An ATD programme has been developed as the fundamental algorithm of an experimental long-baseline lightning receiver array deployed in Western Europe.

- A waveform bank has been produced consisting of the average lightning waveforms from different distances. The waveform bank exhibits a sequence of consecutive maxima resulting from ionospheric reflections, which can be used for radio propagation studies, lightning modelling, lightning detection simulation, etc.

- In the spectral waveform bank, the sequence of consecutive modal maxima is separated by distinct minima at different frequencies and distances.

- Long-baseline lightning location can achieve sub-sampling time accuracy by using the instantaneous phase of the complex lightning waveform.

- The instantaneous frequency calculated from average lightning waveforms has been shown to be distance dependent, and it therefore has the potential to be used for lightning distance determination.

- Phase propagation velocities inferred from radio waves emitted by VLF transmitters can be smaller or larger than the speed of light.

- Simulations show that lightning locations calculated using different phase propagation velocities can cause deviations of the lightning location by hundreds to thousands of metres when compared to the locations inferred from the speed of light.

- A long-baseline lightning receiver array that uses variable phase propagation velocities can improve the lightning location accuracy by ~0.89–1.06 km when compared to lightning locations inferred from an array with more radio receivers.

- As a result of the network configuration, the phase propagation velocities have been mapped over central and southern France to summarize the impact of sky waves and ground effects on the calculation of lightning locations.

- Phase propagation velocities also vary with different ionospheric conditions, e.g. day—night differences.

- The whole lightning waveform is treated as one signal and shifted to each pixel of the earth map for lightning and electromagnetic energy monitoring using the inverse impulse response.

- The generalized cross-correlation algorithm has been used with a long-baseline receiver array to detect weak coherent sources.

- The lightning location area is determined by the locations calculated for each sample by the instantaneous phase differences between recordings.

8.2 Further Work

Some of the outcomes from this research, such as the complex waveform bank and velocity map, were generated from lightning recordings of a thunderstorm in Europe, which may not be identical to the results for other geographical areas. However, the general methods of generating these results are applicable to other locations. It is expected that using this algorithm with more data, will lead to greater knowledge about

lightning wave propagation characteristics. Similarly, many promising methods, such as lightning location calculation using the instantaneous phase, lightning distance determination using the instantaneous frequency, and using a variable phase propagation velocity, can be tested with other long-baseline lightning location systems.

The determination of distances using the instantaneous frequency is just one potential application of the complex waveform bank. The instantaneous frequency may also, given more data, be determined by different arrival azimuths or different times of day. For example, a different incident elevation angle indicates a different rotation direction in the complex waveform of the lightning, i.e., a different instantaneous frequency [*Fullekrug et al., 2016, Figure 2*]. By using the instantaneous frequency for distance determination, the lightning signal can be first approximated within <50 km, because the instantaneous frequency can vary, e.g. between 400 km and 450 km distance (Figure 5.8). This uncertainty is very likely due to the lack of data at these distances, which could be improved by collecting more data with longer recordings. The distribution of instantaneous frequencies from lightning at similar distances shows a clearly peaked distribution if they are recorded at the same station (Figure 5.7). The distributions may differ slightly between different stations, most probably due to varying local radio environments and/or different propagation paths. As a result, determining distances using instantaneous frequency may be more accurate if the instantaneous frequencies are derived from each station separately.

As discussed in Section 6.6, the inferred phase propagation velocity appears to have high correlation with geographic features near the source. However, the phase propagation velocity is inferred from differential measurements between receiver pairs, therefore the expectation is that geophysical properties around the source might not be a dominant factor. It is suggested to compare various phase propagation velocity maps inferred from other lightning location networks to identify the influence of other geographic features on VLF radio wave propagation.

The three proposed methods for applying interferometric techniques with a VLF long-baseline receiver array are feasible to use more samples and information from the original recording. It is speculated that a combination of these methods may work well, so that a

lightning location pixel can be inferred by shifting the waveforms. Weaker lightning sources can be detected by the cross-correlation algorithm, and the location area of these lightning sources can be calculated by inferring a location from each sample. However, the correlation between the lightning processes and the result inferred with these methods has not been analysed. Further analysis is strongly suggested into the long-baseline interferometric technique.

Bibliography

Abarca, S. F., K. L. Corbosiero, and T. J. Galarneau Jr. (2010), An evaluation of the Worldwide Lightning Location Network (WWLLN) using the National Lightning Detection Network (NLDN) as ground truth, J. Geophys. Res., 115, D18206, doi:10.1029/2009JD013411.

Akita, M., S. Yoshida, Y. Nakamura, T. Morimoto, T. Ushio, Z. Kawasaki, and D. Wang (2011), Effects of charge distribution in thunderstorms on lightning propagation paths in Darwin, Australia, J. Atmos. Sci., 68(4), 719–726. doi: 10.1175/2010JAS3597.1

Anderson, R. Spectacular Video of Earth from Orbit, September 20, 2011, [online], available from: http://blogs.agu.org/martianchronicles/2011/09/20/spectacular-video-of-earth-from-orbit/ [accessed on 15 Aug 2017]

Barr, R., Jones, D. L., and Rodger, C. J. (2000), ELF and VLF radio waves. Journal of Atmospheric and Solar-Terrestrial Physics, 62(17), 1689-1718, doi: 10.1016/S1364-6826(00)00121-8.

Bennett, A. J., Gaffard, C., Nash, J., Callaghan, G. and Atkinson, N. C. (2011), The effect of modal interference on VLF long-range lightning location networks using the waveform correlation technique. J. Atmos. Oceanic Technol., 28, 993–1006. doi: http://dx.doi.org/10.1175/2011JTECHA1527.1.

Berger, K.: Blitzstorm-Parameter von Aufwartsblitzen. Bull. Schweiz. Elektrotech. Ver. 69, 1978, pp. 353-360.

Betz, H. D., K. Schmidt, and W. P. Oettinger (2009), LINET—An international VLF/LF lightning detection network in Europe, in Lightning: Principles, Instruments and Applications, pp. 115–140, Springer, Dordrecht, Netherlands.

Bitzer P. M., H. J. Christian, M. Stewart, J. Burchfield, S. Podgorny, D. Corredor, J. Hall, E. Kuznetsov, and V. Franklin (2013), Characterization and applications of VLF/LF source locations from lightning using the Huntsville Alabama Marx Meter Array, J. Geophys. Res. Atmos., 118,3120–3138, doi:10.1002/jgrd.50271.

Caligaris, C., Delfino, F., and Procopio, R. (2008), Cooray–Rubinstein formula for the evaluation of lightning radial electric fields: Derivation and implementation in the time domain. Electromagnetic Compatibility, IEEE Transactions on 50(1): 194-197. doi: 10.1109/TEMC.2007.913226.

Carvalho, F. L., M. A. Uman, D. M. Jordan, J. D. Hill, S. A. Cummer, D. A. Kotovsky, and R. C. Moore (2017), Triggered lightning sky waves, return stroke modeling, and ionosphere effective height, J. Geophys. Res. Atmos., 122, 3507–3527,

Chapman F. W., Jones D. Llanwyn, Todd J. D. W., Challinor R. A., (1966), Observations on the propagation constant of the earth ionosphere waveguide in the frequency band 8 c/s to 16 kc/s, Radio Science, 1, doi: 10.1002/rds19661111273.

Chen M.T. Lu and Y. Du, (2011), Performance of TOA/DF Lightning Location Network in China — Site errors and detection efficiency, 2011 7th Asia-Pacific International Conference on Lightning, Chengdu, pp. 48-54. doi: 10.1109/APL.2011.6111072

Cheng, Z., S. A. Cummer, H.-T. Su, and R.-R. Hsu (2007), Broadband very low frequency measurement of D region ionospheric perturbations caused by lightning electromagnetic pulses, J. Geophys. Res., 112, A06318, doi:10.1029/2006JA011840.

Christian, H.J., and McCook, M.A. (1998), Lightning detection from space: A lightning primer, NASA office.

Christian, H. J., et al., (2003), Global frequency and distribution of lightning as observed from space by the Optical Transient Detector, J. Geophys. Res., 108(D1), 4005, doi:10.1029/2002JD002347.

Cooper, M.A. (1980), Lightning Injuries: Prognostic Signals for Death. Ann. Emerg. Med.,9, pp. 134-138. Doi: 10.1016/S0196-0644(80)80268-X

Cooray, V., and S. Lundquist (1983), Effects of propagation on the rise times and the initial peaks of radiation fields from return strokes, Radio Sci., 18(3), 409–415, doi:10.1029/RS018i003p00409.

Cooray, V. (2009), Propagation effects due to finitely conducting ground on lightning-generated magnetic fields evaluated using Sommerfeld's integrals. Electromagnetic Compatibility, IEEE Transactions on 51(3): 526-531. doi: 10.1109/TEMC.2009.2019759.

Cummins, K. L., M. J. Murphy, E. A. Bardo, W. L. Hiscox, R. B. Pyle, and A. E. Pifer (1998), A Combined TOA/MDF Technology Upgrade of the U.S. National Lightning Detection Network, J. Geophys. Res., 103(D8), 9035–9044, doi:10.1029/98JD00153.

Cummins, K., and M. Murphy (2009), An overview of lightning locating systems: History, techniques, and data uses, with an in-depth look at the US NLDN, IEEE Trans. Electromag. Compat., 51(3), 499–518, doi:10.1109/TEMC.2009.2023450.

Cummins K.L., M.J. Murphy, J.A. Cramer, W. Scheftic, N. Demetriades, A. Nag, (2010), Location accuracy improvements using propagation corrections: A case study of the U.S. National Lightning Detection Network, preprints, 21st International Lightning Detection Conference, Orlando, FL.

Cummer, S. A., Y. Zhai, W. Hu, D. M. Smith, L. I. Lopez, and M. A. Stanley (2005), Measurements and implications of the relationship between lightning and terrestrial gamma ray flashes, Geophys. Res. Lett., 32, L08811, doi:10.1029/2005GL022778.

Cummer, S. A., G. Lu, M. S. Briggs, V. Connaughton, S. Xiong, G. J. Fishman, and J. R. Dwyer (2011), The lightning–TGF relationship on microsecond timescales, Geophys. Res. Lett., 38, L14810, doi:10.1029/2011GL048099.

Demetriades NWS, Murphy MJ, Cramer JA (2010), Validation of Vaisala's Global Lightning Dataset (GLD360) over the continental United States. Preprints, 29th Conference Hurricanes and Tropical Meteorology, 10–14 May, Tucson, AZ, 6 p

Diendorfer. G., Pichler. H. and Mair. M. (2009), Some Parameters of Negative Upward-Initiated Lightning to the Gaisberg Tower (2000–2007), IEEE Transactions on Electromagnetic Compatibility, 51: 443-452, doi: 10.1109/TEMC.2009.2021616.

Dowden, R. L., Brundell, J. B., Rodger, C. J. (2002), VLF lightning location by time of group arrival (TOGA) at multiple sites. Journal of Atmospheric and Solar-Terrestrial Physics 64(7): 817-830. doi:10.1016/S1364-6826(02)00085-8.

Enno, S., G. Anderson, and J. Sugier. (2016), ATDnet Detection Efficiency and Cloud Lightning Detection Characteristics from Comparison with the HyLMA during HyMeX SOP1. J. Atmos. Oceanic Technol., 33, 1899–1911, doi:10.1175/JTECH-D-15-0256.1

Finke U (2007) Statistics of the optical lightning radiation source derived from satellite observations. In: AGU – Fall Meeting 2007, Dec, 10–14, 2007, San-Francisco, CA, eos. Trans. AGU, 88(52), Fall Meet. Suppl., Abstract AE41A-01

Fowler, D., et al., (2013), The global nitrogen cycle in the twenty-first century, Phil Trans R Soc B 368: 20130164, doi: 10.1098/rstb.2013.0164

Füllekrug, M. and S. Constable (2000), Global triangulation of intense lightning discharges, Geophysical Research Letters 27(3): 333-336, doi: 10.1029/1999GL003684.

Füllekrug, M., Mareev, E. and Rycroft, M. (2006), Sprites, elves and intense lightning discharges, Springer Science & Business Media, doi: 10.1007/1-4020-4629-4.

Füllekrug, M. (2010), Wideband digital low-frequency radio receiver, Meas. Sci. Technol., 21 (015901), 1–9, doi:10.1088/0957-0233/21/ 1/015901.

Fullekrug, M., et al. (2013), Electron acceleration above thunderclouds. Environmental Research Letters, 8 (3), 035027, doi: 10.1088/1748-9326/8/3/035027.

Füllekrug, M., A. Mezentsev, R. Watson, S. Gaffet, I. Astin, and A. Evans (2014), Array analysis of electromagnetic radiation from radio transmitters for submarine communication, Geophys. Res. Lett., 41, 9143–9149, doi:10.1002/2014GL062126.

Füllekrug, M., A. Mezentsev, R. Watson, S. Gaffet, I. Astin, N. Smith, and A. Evans (2015), Map of low-frequency electromagnetic noise in the sky. Geophys. Res. Lett., 42, 4648–4653. doi: 10.1002/2015GL064142.

Füllekrug, M., Z. Liu, K. Koh, A. Mezentsev, S. Pedeboy, S. Soula, S.-E. Enno, J. Sugier, and M. J. Rycroft (2016), Mapping lightning in the sky with a mini array, Geophys. Res. Lett., 43, 10,448–10,454, doi:10.1002/2016GL070737.

Galejs, J. (1972). Terrestrial Propagation of Long Electromagnetic Waves: International Series of Monographs in Electromagnetic Waves (Vol. 16). Pergamon Press.

Goodman, S. J., R. J. Blakeslee, W. J. Koshak, D. Mach, J. Bailey, D. Buechler, L. Carey, C. Schultz, M. Bateman, E. McCaul Jr., G. Stano (2013), The GOES-R Geostationary Lightning Mapper (GLM). Atmos. Res., 125- 126, 34-49. doi: 10.1016/j.atmosres.2013.01.006.

Holle, R.L., and P.E. Lopez. (1993), Overview of real-time lightning detection systems and their meteorological uses. NOAA Technical memorandum ERL NSSL-102. National Severe Storms Laboratory, Norman, OK, pp 68.

Höller, H., Betz, H.-D., Schmidt, K., Calheiros, R. V., May, P., Houngninou, E., and Scialom, G. (2009), Lightning characteristics observed by a VLF/LF lightning detection network (LINET) in Brazil, Australia, Africa and Germany, Atmos. Chem. Phys., 9, 7795-7824, doi: 10.5194/acp-9-7795-2009.

Honma, N., F. Suzuki, Y. Miyake, M. Ishii, and S. Hidayat (1998), Propagation effect on field waveforms in relation to time-of-arrival technique in lightning location, J. Geophys. Res., 103(D12), 14141–14145, doi:10.1029/97JD02625.

Horner, F. (1954), The accuracy of the location of sources of atmospherics by radio direction-finding, Proc IEEE 101: 383-390, doi: 10.1049/pi-3.1954.0091.

Horner, F. (1957), Very-low-frequency propagation and direction-finding, Proc IEEE 104: 73-80, doi: 10.1049/pi-b-1.1957.0118.

Hutchins, M. L., R. H. Holzworth, J. B. Brundell, and C. J. Rodger (2012a), Relative detection efficiency of the World Wide Lightning Location Network, Radio Sci., 47, RS6005, doi:10.1029/2012RS005049.

Hutchins, M.L., R. H. Holzworth, C. J. Rodger and J. B. Brundell (2012b), Far field power of lightning strokes as measured by the World Wide Lightning Location Network, JTech (J. Atmos. and Ocean. Tech. (AMS), V.29,1102-1110, doi: 10.1175/JTECH-D-11-00174.1

Ibrahim, W.I., Ghazali, M.R. (2012), Measurements of Electric and Magnetic Fields due to Lightning Strokes Based on Single-station Detection. APACE 2012 Melaka, Malaysia, 2012, doi: 10.1109/APACE.2012.6457674

International Telecommunication Union (ITU), (2015) Recommendation ITU-R P.832-2, World Atlas of Ground Conductivities

Japan Aerospace Exploration Agency, (2013), Global Lightning and sprIte MeasurementS on JEM-EF (JEM-GLIMS) obtained its first observation data, January 31, 2013

Jean, A. G., W. L. Taylor, and J. R. Wait (1960), VLF phase characteristics deduced from atmospheric wave forms, J. Geophys. Res., 65(3), 907–912, doi:10.1029/JZ065i003p00907.

King, R. J., S. W. Maley, J. R. Wait, (1966) Ground-wave propagation along three section mixed paths, Proc. Inst. Elec. Eng., 1135, 747–751, doi: 10.1049/piee.1966.0121.

Krider, E. P., R. Carl Noggle, and Martin A. Uman (1976), A Gated, Wideband Magnetic Direction Finder for Lightning Return Strokes. J. Appl. Meteor., 15, 301–306. doi: 10.1175/1520-0450(1976)015<0301:AGWMDF>2.0.CO;2.

Lee, A. (1986), An experimental study of the remote location of lightning flashes using a VLF arrival time difference technique, Q. J. Roy. Meteor. Soc., 112, 203–229, doi:10.1002/qj.49711247112.

Lee, A.C. (1990), Bias Elimination and Scatter in Lightning Location by the VLF Arrival Time Difference Technique. J. Atmos. Oceanic Technol., 7, 719–733, doi: 10.1175/1520-0426(1990)007<0719:BEASIL>2.0.CO;2

Levine, J.S., Augustsson, T.R., Anderson, I.C. and Hoeel, J.M. (1984), Tropospheric Sources of NOx: Lightning and Biology. Atmos. Environ. 18, pp. 1797-1804. Doi: 10.1016/0004-6981(84)90355-X

Lewis, E. A., R. B. Harvey, and J. E. Rasmussen (1960), Hyperbolic direction finding with sferics of transatlantic origin, J. Geophys. Res., 65(7), 1879–1905, doi:10.1029/JZ065i007p01879.

Li, D., A. Mohammad, F. Rachidi, M. Rubinstein, M. Paolone, D. Pavanello, S. Metz, Q. Zhang, and Z. Wang (2015), On Lightning Electromagnetic Field Propagation along an Irregular Terrain, IEEE Transactions on Electromagnetic Compatibility, 99(1), doi: 10.1109/TEMC.2015.2483018

Li, D., M. Azadifar, F. Rachidi, M. Rubinstein, G. Diendorfer, K. Sheshyekani, Q. Zhang, and Z. Wang (2016a), Analysis of lightning electromagnetic field propagation in mountainous terrain and its effects on ToA-based lightning location systems, J. Geophys. Res. Atmos., 121, doi:10.1002/2015JD024234.

Li, D., F. Rachidi, M. Rubinstein, G. Diendorfer, Z. Wang (2016b) , Location accuracy evaluation of ToA-based lightning location systems over mountainous terrain, In 24th International Lightning Detection Conference (ILDC).

Liu, Z., K. L. Koh, A. Mezentsev, S.-E. Enno, J. Sugier, and M. Füllekrug (2016), Variable phase propagation velocity for long-range lightning location system, Radio Sci., 51, 1806–1815, doi:10.1002/2016RS006058.

Lyu, F., S. A. Cummer, R. Solanki, J. Weinert, L. McTague, A. Katko, J. Barrett, L. Zigoneanu, Y. Xie, and W. Wang (2014), A low-frequency near-field interferometric-TOA 3-D Lightning Mapping Array, Geophys. Res. Lett., 41, 7777–7784, doi:10.1002/2014GL061963.

Mallick, S. et al (2013), Calibration of the ENTLN against rocket-triggered lightning data, 2013 International Symposium on Lightning Protection (XII SIPDA), Belo Horizonte, 2013, pp. 39-46. doi: 10.1109/SIPDA.2013.6729186

Mallick, S., V. A. Rakov, T. Ngin, W. R. Gamerota, J. T. Pilkey, J. D. Hill, M. A. Uman, D. M. Jordan, A. Nag, and R. K. Said (2014), Evaluation of the GLD360 performance characteristics using rocket-and-wire triggered lightning data, Geophys. Res. Lett., 41, 3636–3642, doi:10.1002/2014GL059920.

Mardiana, R., Z.-I Kawasaki, T Morimoto (2002), Three-dimensional lightning observations of cloud-to-ground flashes using broadband interferometers. Journal of Atmospheric and Solar-Terrestrial Physics 64(1): 91-103. doi:10.1016/S1364-6826(01)00099-2.

Mazur, V., E. Williams, R. Boldi, L. Maier, and D. E. Proctor (1997), Initial comparison of lightning mapping with operational time-of-arrival and interferometric systems, J. Geophys. Res., 102(D10), 11071–11085, doi:10.1029/97JD00174.

Mezentsev, A., and M. Füllekrug (2013), Mapping the radio sky with an interferometric network of low-frequency radio receivers, J. Geophys. Res., 118, 8390–8398, doi:10.1002/jgrd.50671.

Morimoto, T., Kawasaki, Z., Ushio, T., (2005) Lightning observations and consideration of positive charge distribution inside thunderclouds using VHF broadband digital interferometry, Atmospheric Research, Volume 76, Issue 1, 2005, pp. 445-454, doi: 10.1016/j.atmosres.2004.11.024

Nag, A., et al. (2011), Evaluation of U.S. National Lightning Detection Network performance characteristics using rocket-triggered lightning data acquired in 2004–2009, J. Geophys. Res., 116, D02123, doi:10.1029/2010JD014929.

Nag, A, Murphy, MJ, Schulz, W, and Cummins, KL (2015), Lightning locating systems: Insights on characteristics and validation techniques. Earth and Space Science, 2, 65–93. doi: 10.1002/2014EA000051.

Noxon, J. F. (1976), Atmospheric nitrogen fixation by lightning. Geophys. Res. Lett., 3: 463–465. doi:10.1029/GL003i008p00463

Oetzel, G.N., and Pierce, (1969), E.T. VHF technique for locating lightning. Radio Sci. 4, pp. 199-201. Doi: 10.1029/RS004i003p00199

Ortega, P. (2007) A Three Magnetic direction finder Network for a Local Warning Device. Journal of Lightning Research, 2, pp. 18-27

Orville, R. E. (1991), Calibration of a magnetic direction finding network using measured triggered lightning return stroke peak currents, J. Geophys. Res., 96(D9), 17135–17142, doi:10.1029/91JD00611.

Orville, R.E. (2008), Development of the National Lightning Detection Network. Bull. Amer. Meteor. Soc., 89, 180–190, https://doi.org/10.1175/BAMS-89-2-180

Pasko, V.P. and Fullekrug, M. (2011), Waveforms of Nighttime Atmospherics as a Measure of the Lower Ionospheric Electron Density Profiles over UK and France on August 31, 2008', paper presented to 30th URSI General Assembly (No. GHE2-7), Istanbul, Turkey, 13-20 August, viewed 24 July 2017, http://www.ursi.org/proceedings/procGA11/ursi/GHE2-7.pdf

Qin, Z., M. Chen, B. Zhu, and Y. Du (2017), An improved ray theory and transfer matrix method-based model for lightning electromagnetic pulses propagating in Earth-ionosphere waveguide and its applications, J. Geophys. Res. Atmos., 122, 712–727, doi:10.1002/2016JD025599.

Rakov, V. A. (1999,). Lightning electric and magnetic fields. In Proc. 13th Int. Zurich Symp. on Electromagnetic Compatibility, Zurich, Switzerland, 16-18 Feb, 1999, pp. 561-566.

Rakov, V. A., D. E. Crawford, K. J. Rambo, G. H. Schnetzer, M. A. Uman, and R. Thottappillil (2001), M-component mode of charge transfer to ground in lightning discharges, J. Geophys. Res., 106(D19), 22817–22831, doi:10.1029/2000JD000243.

Rakov, V. A. and M. A. Uman (2003), Lightning: physics and effects, Cambridge University Press. doi:10.1256/wea.168/03.

Rakov, V. A. (2008), Lightning electromagnetic environment: From continuing-current fields to X-rays, in Intl. Conf. on Grounding and Earthing & 3rd Intl. Conf. on Lightning Phys. and Effects, Florianopolis, Brazil.

Rakov, V. (2013), Electromagnetic methods of lightning detection, Surveys in Geophysics 34(6): 731-753. doi:10.1007/s10712-013-9251-1.

Rhodes, C. T., X. M. Shao, P. R. Krehbiel, R. J. Thomas, and C. O. Hayenga (1994), Observations of lightning phenomena using radio interferometry, J. Geophys. Res., 99(D6), 13059–13082, doi:10.1029/94JD00318.

Richard, P., and G. Auffray (1985), VHF-UHF interferometric measurements, applications to lightning discharge mapping, Radio Sci., 20(2), 171–192, doi:10.1029/RS020i002p00171.

Richard, P., A. Delannoy, G. Labaune, and P. Laroche (1986), Results of spatial and temporal characterization of the VHF-UHF radiation of lightning, J. Geophys. Res., 91(D1), 1248–1260, doi:10.1029/JD091iD01p01248.

Richard, P., Soulage, A., Laroche, P., and Appel, J. (1988), The SAFIR lightning monitoring and warning system, application to aerospace activities. In Proc. Int. Aerospace and Ground Conf. on Lightning and Stastic Electricity. Oklahoma City, Oklahoma, Apr 1988, pp. 383-390.

Rison, W., R. J. Thomas, P. R. Krehbiel, T. Hamlin, and J. Harlin (1999), A GPS-based three-dimensional lightning mapping system: Initial observations in central New Mexico, Geophys. Res. Lett., 26, 3573–3576, doi:10.1029/1999GL010856.

Rison, W., Krehbiel, P. R., Stock, M. G., Edens, H. E., Shao, X. M., Thomas, R. J., Stanley, M. A., Zhang, Y. (2016), Observations of narrow bipolar events reveal how lightning is initiated in thunderstorms, Nat Commun 7. doi:10.1038/ncomms10721.

Rodger, C. J., J. B. Brundell, R. L. Dowden, and N. R. Thomson (2004), Location accuracy of long distance VLF lightning location network. Ann. Geophys., 22, 747-758. doi:10.5194/angeo-22-747-2004

Rodger, C. J., J. B. Brundell, and R. L. Dowden (2005), Location accuracy of VLF World Wide Lightning Location (WWLL) network: Post-algorithm upgrade. Ann. Geophys., 23, 277-290. doi: 10.5194/angeo-23-277-2005

Rost, S., and C. Thomas (2002), Array seismology: Methods and applications, Rev. Geophys., 40 (3), 2(1)-2(27), doi:10.1029/2000RG000100.

Said, R. K., U. S. Inan, and K. L. Cummins (2010), Long-range lightning geolocation using a VLF radio atmospheric waveform bank, J. Geophys. Res., 115, D23108, doi:10.1029/2010JD013863.

Schimmel, M, and H. Paulssen, (1997), Noise reduction and detection of weak, coherent signals through phase-weighted stacks. Geophys. J. Int., 130: 497–505. doi: 10.1111/j.1365-246X.1997.tb05664.x

Schonland, B. F. J., J. S. Elder, D. B. Hodges, W. E. Phillips, J. W. van Wyk (1940), The wave form of atmospherics at night. Proc. R. Soc. Lond. A 1940 176 180-202. doi: 10.1098/rspa.1940.0085.

Schonland, B.F.J. (1964), The Flight of Thunderbolts, 2nd Ed. Oxford Univ. Press, London and New York

Schulz, W., G. Diendorfer, S. Pedeboy, and D. R. Poelman (2016), The European lightning location system EUCLID – Part 1: Performance analysis and validation, Nat. Hazards Earth Syst. Sci., 16, 595-605, doi:10.5194/nhess-16-595-2016.

Shao, X. M., P. R. Krehbiel, R. J. Thomas, and W. Rison (1995), Radio interferometric observations of cloud-to-ground lightning phenomena in Florida, J. Geophys. Res., 100(D2), 2749–2783, doi:10.1029/94JD01943.

Shao, X., D. Holden, and C. Rhodes (1996), Broad band radio interferometry for lightning observations, Geophys. Res. Lett., 23(15), 1917–1920, doi: 10.1029/96GL00474

Shao, X. M., Lay, E. H., & Jacobson, A. R. (2013). Reduction of electron density in the night-time lower ionosphere in response to a thunderstorm. Nature Geoscience, 6(1), 29-33. doi:10.1038/ngeo1668

Sonnadara, D.U.J., Fernando, I.M.K., Namasivayam, S., Ariyaratne, T.R., Jayaratne, K.P.S.C.and Bandara, K.R.A. (1999), The role of site selection on localizing ground flashes in an automated lightning detection network. IPSL, Proc. 15th Tech. Sess., Sri Lanka, 1999

Sonnadara, D.U.J., Edirisinghe, C.M. and Fernando, I.M.K. (2001), Performance Comparison between the Magnetic Direction Finding Technique and the Time of Arrival Technique. Proceedings of the Technical Sessions. 17, pp. 30-36.

Soula, S., Iacovella, F., van der Velde, O., Montanyà, J., Füllekrug, M., Farges, T., Bór, J., Georgis, J.-F., NaitAmor, S. and Martin, J.-M., (2014), Multi-instrumental analysis of large sprite events and their producing storm in southern France. Atmospheric Research 135: 415-431. doi:10.1016/j.atmosres.2012.10.004.

Steele, F. K., and C. J. Chilton (1964), Measurement of the phase velocity of VLF propagation in the earth-ionosphere waveguide, Radio Sci. J. Res. NBS 68D, No. 12, 1269–1273. doi: 10.6028/jres.068D.131.

Stock, M. G., M. Akita, P. R. Krehbiel, W. Rison, H. E. Edens, Z. Kawasaki, and M. A. Stanley (2014), Continuous broadband digital interferometry of lightning using a generalized cross-correlation algorithm, J. Geophys. Res. Atmos., 119, 3134-3165, doi:10.1002/2013JD020217.

Stock, M., et al. (2015). Near-field Interferometric Imaging of Lightning. Abstract AE31B-0425 presented at 2015 Fall Meeting, AGU, San Francisco, Calif., 16 Dec.

Sun, Z., X. Qie, M. Liu, D. Cao, and D. Wang (2013), Lightning VHF radiation location system based on short-baseline TDOA technique—Validation in rocket-triggered lightning, Atmos. Res., 129, 58–66.doi: 10.1016/j.atmosres.2012.11.010

Sun, Z., X. Qie, M. Liu, R. Jiang, Z. Wang, and H. Zhang (2016), Characteristics of a negative lightning with multiple-ground terminations observed by a VHF lightning location system, J. Geophys. Res. Atmos., 121, 413–426, doi:10.1002/2015JD023702.

Taner, M. T., F. Koehler, R. E. Sheriff (1979), Complex seismic trace analysis. Geophysics 44(6): 1041-1063. doi: 10.1190/1.1440994.

Thomas, R. J., P. R. Krehbiel, W. Rison, S. J. Hunyady, W. P. Winn, T. Hamlin, and J. Harlin (2004), Accuracy of the Lightning Mapping Array, J. Geophys. Res., 109, D14207, doi:10.1029/2004JD004549.

Thomson, N. (2010), Daytime tropical D region parameters from short path VLF phase and amplitude, J. Geophys. Res., 115, A09313, 1-11, doi:10.1029/2010JA015355

Uman, M.A.(1971), Understanding Lightning, BEK Technical Publication, Pittsburgh, Pennsylvania

Uman, M.A. (1974), The Earth and Its Atmosphere as a Leaky Spherical Capacitor. Am. J. Phys. 42, pp. 1033-1035. Doi: 10.1119/1.1987924

Ushio, T., Z. Kawasaki, Y. Ohta, and K. Matsuura (1997), Broadband interferometric measurement of rocket triggered lightning in Japan, Geophys. Res. Lett., 24(22), 2769–2772, doi: 10.1029/97GL02953

Wang, Y., X. Qie, D. Wang, M. Liu, D. Su, Z. Wang, D. Liu, Z. Wu, Z. Sun, Y. Tian (2016), Beijing Lightning Network (BLNET) and the observation on preliminary breakdown processes, Atmos. Res. 171: 121-132. doi:10.1016/j.atmosres.2015.12.012

Zhu Y. et al (2017), Evaluation of ENTLN performance characteristics based on the ground-truth natural and rocket-triggered lightning data acquired in Florida, J. Geophys. Res. Atmos., 122, doi:10.1002/2017JD027270.